HOKKAIDO UNIVERSITY

| | |
|---|---|
| Title | Construction of Hematite-based Photoelectrochemical Cells for Visible Light Water Splitting |
| Author(s) | 于, 卿 |
| Degree Grantor | 北海道大学 |
| Degree Name | 博士(理学) |
| Dissertation Number | 甲第12501号 |
| Issue Date | 2016-12-26 |
| DOI | https://doi.org/10.14943/doctoral.k12501 |
| Doc URL | https://hdl.handle.net/2115/64471 |
| Type | doctoral thesis |
| File Information | Qing_Yu.pdf |

Hokkaido University Collection of Scholarly and Academic Papers : HUSCAP




# Construction of Hematite-based Photoelectrochemical Cells for Visible Light Water Splitting

（ヘマタイト系光電気化学セルの構築および可視光照射下における水分解に関する研究）

**Qing Yu**

**Graduate School of Chemical Sciences and Engineering**

**Hokkaido University**

**2016**

# CONTENTS

**Contents** I

**Abstract** 1

**Chapter 1 Introduction** 3

1.1 General background of photoelectrochemical water splitting 3

1.2 A brief overview of hematite photoanodes and current approaches to improve the photoelectrochemical activity 8

1.2.1 A brief overview of hematite photoanodes 8

1.2.2 Current approaches to improve the performances of hematite photoanodes 10

1.3 P-type iron-based photocathodes 16

1.4 Motivation of this thesis 17

References 22

**Chapter 2 Hematite Homojunctions without Foreign Element Doping** 28

2.1 Introduction 28

2.2 Experiments 30

2.2.1 Pulsed laser deposition and preparation of photoelectrodes 30

2.2.2 Characterization 33

2.2.3 Photoelectrochemical Properties 34

2.2.4 Water Splitting 34

2.3 Results and discussion 34

2.3.1 Characterization of high-vacancy $Fe_2O_3$ (HV-$Fe_2O_3$) and low-vacancy $Fe_2O_3$ (LV-$Fe_2O_3$). 34

2.3.2 Preparation and photoelectrochemical performances of hematite homojunction photoanodes (HV/LV-$Fe_2O_3$) 42

2.3.3 Mechanism discussion 47

2.3.4 Long-time water splitting performance of hematite homojunction photoanodes (HV/LV-$Fe_2O_3$) 51

2.4 Conclusions 53

References 55

**Chapter 3 Hematite Films Decorated with Nanostructured Ferric Oxyhydroxide** 59

3.1 Introduction 59

3.2 Experiments 61

3.2.1 Preparation of FeOOH decorated hematite photoanodes 61

3.2.2 Characterization 62

3.2.3 Photoelectrochemical properties 62

3.2.4 Water splitting 63

3.3 Results and discussion 63

3.3.1 Characterization of FeOOH cocatalyst 63

3.3.2 Photoelectrochemical performances of $Fe_2O_3$/FeOOH photoanodes 73

3.4 Conclusions 83

References 85

**Chapter 4 p-Type $LaFeO_3$ photocathodes and construction of p-$LaFeO_3$/n-$Fe_2O_3$ photocell** 88

4.1 Introduction 88

4.2 Experiments 91

4.2.1 Preparation of p-$LaFeO_3$ photocathodes 91

4.2.2 Characterization 92

4.2.3 Photoelectrochemical Properties 92

4.2.4 Water Splitting 92

4.3 Photoelectrochemical performances for the $LaFeO_3$ photocathodes 93

4.4 p-$LaFeO_3$/n-$Fe_2O_3$ photocell for water splitting 101

4.5 Conclusions 115

References 117

**Chapter 5 General conclusions and future prospects** 120

6.1 General conclusions 120

6.2 Future prospects 123

**Acknowledgement** 125

# Abstract

Photoelectrochemical (PEC) water splitting has been widely researched since 1970s as it is a promising method for solar energy conversion. Among the various semiconductors, iron-based photoelectrodes such as hematite have been extensively studied because of its visible light responsibility, earth abundant property, non-toxic and high stability. However, hematite has a very short lifetime of excited state carrier and hole diffusion length that significantly limits its efficiency in charge separation and collection as a PEC anode. And overall solar water splitting using PEC devices are still faced with great challenges due to lack of p-type photocathodes.

In order to improve the photo-to-electricity efficiency, three strategies are proposed in this work. Firstly, as high recombination (<0.1 s) is existed in most hematite photoanodes, forming junctions are commonly used ways to improve the charge separation efficiency in photoelectrodes via constructing a large magnitude of interfacial electric field in it. The construction of homojunction in hematite can be realized by self-doping method. Secondly, as the water oxidation rate (> 1s) on electrodes is much slower than the charge recombination rate (< 0.1 s), cocatalysts are needed to load on the surface of hematite to increase the charge transfer kinetics between the electrode/electrolyte interfaces. Finally, as $LaFeO_3$ has a perovskite structure, the nearly 180º B-O-B atom chains inside the $ABO_3$ structure could offer an ideal three-dimensional transportation channel for photo-excited carriers, and make it a promising candidate for photoelectrochemical water reduction.

In chapter 1, general background about photoelectrochemistry and a simple overview of iron-based photoelectrodes is introduced.

In chapter 2, bilayer self-doped hematite homojunctions were fabricated for superior PEC activities with higher electron/hole separation efficiency. Hematite layers with different Fermi Levels were successfully fabricated by controlling the oxygen vacancy densities in them and then combined into junctions. Due to the formation of homojunction inside the hematite electrodes, high charge separation efficiency were realized via constructing a large magnitude of interfacial electric field in it. And the high

oxygen vacancy layer was protected by the formation and the outer low-vacancy-layer. By designing of homojunction, photocurrent density increased to nearly 5 times with lower onset potential and higher stability.

Chapter 3 focused on nanostructured FeO(OH) decorated hematite as well as the charge transfer properties between electrode/electrolyte interfaces. After the decoration of FeO(OH), the onset potential decreased 140 mV while the photocurrent density improved nearly 4 times under AM 1.5 G illumination. It is proved that the high reaction area for the nanostructured morphology and high electrocatalytic activity of FeO(OH) increased the amount of photogenerated holes involved in the water oxidation reaction and accelerated the kinetics of water splitting. As a result, we demonstrated that the nanostructured FeO(OH) has great potential for application in PEC water oxidation as cocatalysts.

In chapter 4, hematite photoanode was connected with a p-type $LaFeO_3$ photocathode into a tandem cell for overall water splitting under visible light. After systematically studied the relationship between the area of electrodes and the PEC performances of n-$Fe_2O_3$/p-$LaFeO_3$ tandem cells, it is proved that the activity of this photocell is mainly determined by the activity of p-$LaFeO_3$ photocathode. Finally, an all-iron-based n-$Fe_2O_3$/p-$LaFeO_3$ tandem cell was obtained with high activity ($H_2$=11.5 μmol/h; $O_2$=5.7 μmol/h) for more than 120 hours.

In summary (Chapter 5), this thesis carried out a systematic study on constructing new hematite-based photoelectrochemical cells for visible light water splitting. By controlling the oxygen vacancy densities in hematite, the Fermi level of them can be tuned and further made into homojunctions. The formation of homojunction facilitated the efficient charge separation within the electrode. While decoration of FeO(OH) nanosheet cocatalyst improved the charge transfer kinetics at the electrode/electrolyte interface. The designing of $Fe_2O_3$/$LaFeO_3$ tandem cell demonstrated that the p-type photocathodes limited the whole performance of the photocell. This study opened up a perspective strategy towards obtaining efficient, highly-stable and low cost hematite-based PEC water splitting systems in the future research.

# Chapter 1 Introduction

## 1.1 General background of photoelectrochemical water splitting.

The problems of energy and environment issues have come into human's eyesight just in recent decades. Utilizing solar energy efficiently could help lessen the emergent energy and environmental crisis, as the solar light shining on the surface of the Earth ($1.3*10^5$ TW) surpasses the temporary global human energy consumption ($1.6*10^1$ TW in 2010) [1] by as high as four orders of magnitude. Solar water splitting offers a promising and environment-friendly pathway for hydrogen generation, and has been widely researched all over the world for decades.[2-4]

Photoelectrochemical water splitting is widely studied for solar water splitting in recent years. By only using a small piece of films, pure water splitting can be realized with high efficiency, long stability and good reproducibility. Besides, the electrodes can be easily replaced to a new one while the solution can be reused.

As electrons are the major donor carriers in n-type semiconductors, the Fermi levels of n-type semiconductors positioned close to their conduction band (Figure 1.1 a). As the Fermi level is higher than that of electrolyte, when n-type semiconductor contact with electrolyte, the band bending will upward until their Fermi level equaled. Under light irradiation, the band bending will be reduced due to the charge separation of n-type semiconductors under illumination. The Fermi levels of p-type semiconductors positioned close to their valence band （Figure 1.1 b）. When they contact with

electrolyte, the band bending will downward until their Fermi level equaled. Under light irradiation, the band bending will also be reduced due to the charge separation of semiconductors under illumination.

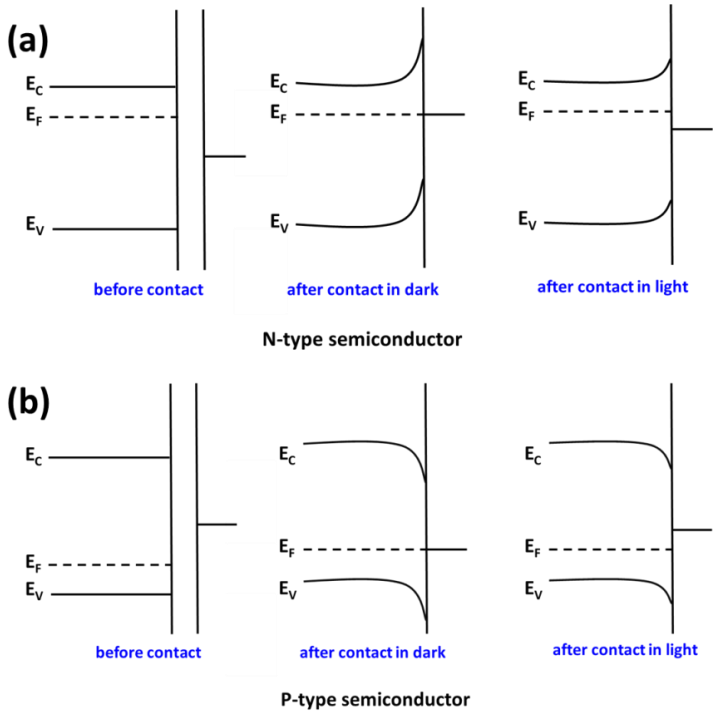



**Figure 1.1** band energy diagrams for n-type semiconductor (a) and p-type semiconductor (b) at different conditions. The conditions from left to right are before contact with electrolyte; contact with electrolyte in dark and contact with electrolyte under light illumination.

The n-type semiconductors are usually used as photoanodes in the photoelectrochemical cells for water oxidation. The holes will accumulate on the surface of the electrode while electrons will transfer through the substrate to the counter electrode for water reduction. Thus, water oxidation reaction is usually occurred on the surface of photoanode as shown in Figure 1.2 a. The valence band of the n-type

photoanode needs to be more positive than the water oxidation potential. Otherwise, more electricity is needed. Similarly, p-type semiconductors are usually functioned as the photocathode, in which the electrons will accumulate on the surface of electrodes and evolved in the water reduction reaction as shown in Figure 1.2 b. The conduction band of the p-type photocathode needs to be more negative than the water reduction potential.

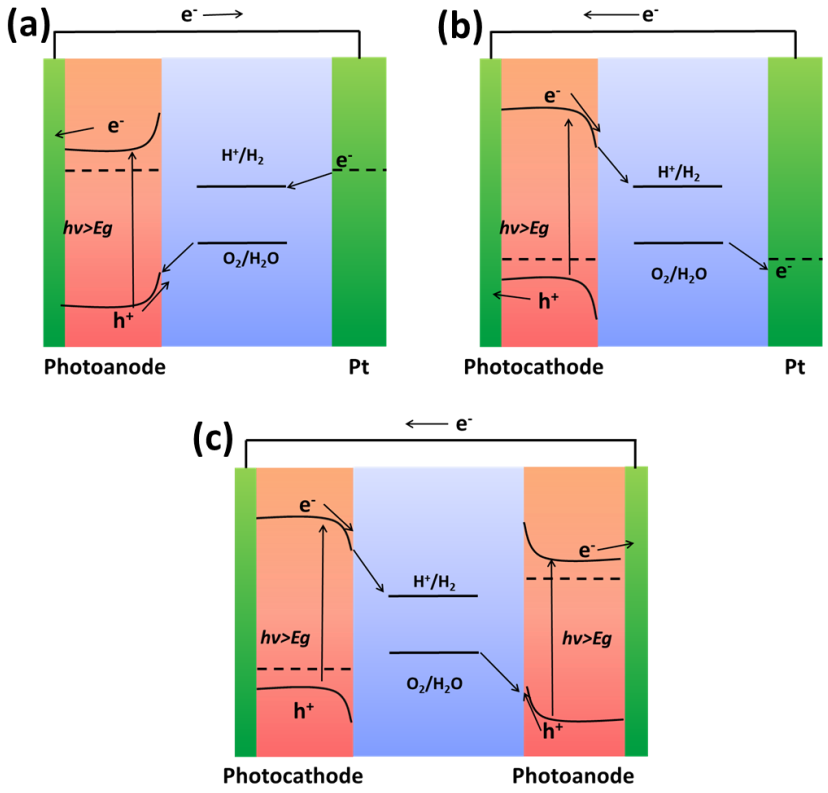



**Figure 1.2** PEC water splitting using (a) a photoanode, (b) photocathode, and (c) photoanode and photocathode in tandem configuration.

N-type photoanodes and p-type photocathodes can be accompanied in one photocell. When both of the two photoelectrodes are irradiated by the light, the electrodes in this system will accumulate on the surface of p-type material for water reduction, while

holes will accumulate on the surface of n-type material for water oxidation. In this kind of tandem configuration, the maximum photocurrent and the working potential of the photoelectrodes are theoretically determined by the intersection of the steady current-potential curves of the respective photoelectrodes.[2]

The first photoelectrochemical cell was developed by Fujishima and Honda in 1972 [5].They used n-$TiO_2$ anode for electrochemical water splitting by shining light on it. However an efficiency of merely 0.1% was estimated in their experiment. After their work, approaches to solving water splitting problems have been concentrated on exploring new materials for both anodic and cathodic processes. N-type semiconductors such as $TiO_2$,[5] $WO_3$,[6] $BiVO_4$,[7] ZnO[8] and $Fe_2O_3$[9-13] were used as photoanodes and p-type semiconductors such as $CaFe_2O_4$,[14] $Cu_2O$,[15] CuZnSeS[16] and $Fe_2TiO_5$[17] were considered to be used as photocathodes.

The ultimate goal of these efforts is an efficient photoelectrolysis cell design that can simultaneously drive, in an unassisted fashion, both the hydrogen evolution and water oxidation reactions. To achieve this gold, several requirements need to fulfill for the photoelectrodes. Firstly, the band gap of semiconductor cannot be too large (<2.8 eV) in order to absorb visible light which consist the majority of the solar light or too narrow to drive the water splitting reaction (theoretically >1.23 eV, practically >2 eV considering the over-potential). The band gaps for commonly used semiconductors can be referred in Figure 1.3. Secondly, the top of the valence band position for an n-type semiconductor (or the bottom of the conduction band position for a p-type

semiconductor) should be high enough to drive the water oxidation (or reduction) reaction. Thirdly, the materials are required to be stable under water splitting conditions and the elements in it need to be earth abundant considering future application in industry. Finally, appropriate methods are required to guarantee the stability and low cost of the photoelectrodes. However, to date no single semiconducting material has been found to meet all of these requirements.[18] And construction of tandem cells by combining p-type photocathode and n-type photoanode is needed for unbiased photoelectrochemical water splitting.

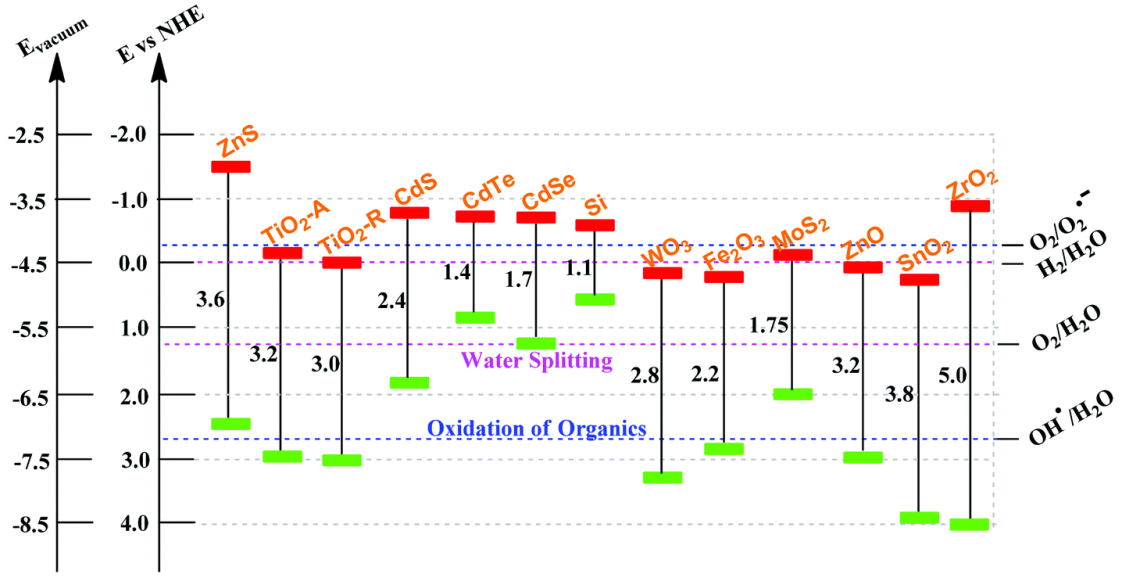



**Figure 1.3** Band gap energy, VB and CB for a range of semiconductors on a potential scale (V) versus the normal hydrogen electrode (NHE). Reference [19]

From above requirements for solar water splitting, $Fe_2O_3$, $WO_3$, and $BiVO_4$ are considered to be good candidates as photoanodes for overall solar water splitting. And $Fe_2O_3$ is thought to be the one of the most promising candidates for water oxidation due to its suitable band gap, enough positive valence band position, earth abundance and

high durability. Although Si is a good choice of photocathode, the stability is very low which limited the durability of the whole tandem cells.[20] And new choices of p-type photocathodes still need to be explored.

## 1.2 N-type hematite photoanodes.

### 1.2.1 A brief overview of hematite photoanodes.

Hematite is an n-type semiconductor in which electrons are carriers. The band gap ranges from 2.0 eV to 2.2 eV, which is suitable to absorb visible light. Normally, pure hematite powders show a red color while the color of hematite films changes from yellow to red depending on its thickness. Besides, the theoretical solar-to-hydrogen conversion efficiency (by ligand field theory and SCF-Xa calculations) of single crystalline hematite is very high, around 14-17% (based on the lower heating value of hydrogen), which means that it can attribute to a photocurrent of 11-14mA/cm$^2$.[21] As the crystalline of hematite plays an important role for photoelectrochemical activity, the morphology of hematite (crystal directions and porosity) plays an important role in order to achieve high PEC water splitting activities.

Till now, various methods were developed to prepare hematite with different morphologies. Park and his coauthors obtained hematite nanotubes with (110) lattice plane which has a photocurrent density about 1.5 mA/cm$^2$ at 1.2 V vs. RHE.[11] Mullins and his coworkers prepared hematite thin films with a preferred (104)

orientation by a reactive ballistic deposition method and get a photocurrent about 0.7 $mA/cm^2$ at 1.2 V vs. RHE.[12] The Choi's group prepared a transparent nanocrystalline hematite electrodes by anodic electrodeposition and improved the short circuit photocurrent to two times (0.52 $mA/cm^2$) by changing the pH of the electrodepostion solutions.[13]

As far as I know, the most exciting result for pure hematite photoanodes is realized by Dr. Grätzel and his coworkers. They synthesized nanostructured hematite and proved that with increasingly small dimensions the photocurrent will be improved since the electron-hole recombination rate is suppressed.[9] Based on this theory, they obtained hematite nanoparticle aggregates by atmospheric pressure chemical vapor deposition (APCVD).[10] By increasing the amount of these nanostructured hematite, the electrodes achieved a high photocurrent which was nearly 2 $mA/cm^2$ which may have a photon-to-current efficiency approaching the theoretical limit.

Although many efforts have been developed to improve the photoelectrocatalytic oxygen evolution activities of pure hematite photoanodes in the past years, the gases evolution rates and efficiencies are still far from practical application due to some initial disadvantages of this material. Firstly, both the lifetime of the excited state carriers and the hole diffusion length (~2 to 4 nm) are very short (~1 ps)[22-24]. This significantly limits the efficiency of hematite in charge separation and collection (to oxidize water) as a PEC anode. Secondly, as the position of the conduction band of hematite lies below the potential of hydrogen evolution, an external bias is required for

photoelectrocatalysis hydrogen evolution at the cathode. These intrinsic limitations of hematite bring about a much lower solar-to-hydrogen (STH) efficiency compared to the theoretical value.

In order to overcome aforementioned limitations of hematite, various strategies have developed to decrease the over potential and increase the photocurrent density. Doping is a popular method to improving the optical absorption, the donor density, and the electrical conductivity. Construction of junctions is an effective method to increase the charge separation and reduce the electron-hole recombination in the material. Cocatalyst decoration will enhance the charge transfer kinetics between the electrode/electrolyte interfaces, and lower the charge recombination at the interfaces. Taking advantages of the SPR effect is widely used to widen the light absorption range especially in the visible light region.

### 1.2.2 Current approaches to improve the performances of hematite photoanodes.

(1) Element doping in hematite.

In order to address the limitations of hematite, a series of unique elements have been doped into hematite. Dopants either metal or nonmetal elements have been extensively researched because they played important roles in improving the optical absorption coefficient, the donor density, electrical conductivity, and the flat band potential of pure hematite.[25-26] Li and his coworkers prepared a Ti doped hematite by a chemical method.[27] The onset potential is decreased and the photocurrent density increased

from 0.8 mA/cm$^2$ to 2.6 mA/cm$^2$. Sn doped hematite was also prepared by them.[28] The Sn doped hematite nanowire show a high photocurrent density as well, about 1.8 mA/cm$^2$. Other than popular Ti and Sn for hematite doping, Pt[29] and P[30] doping is also found to be an effective way to improve the photoelectrocatalytic water oxidation efficiency according to previous literatures.

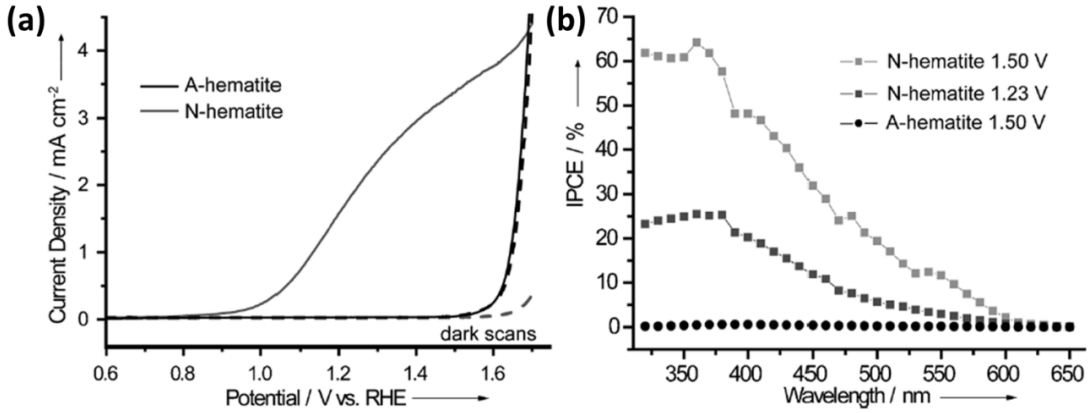



**Figure 1.4** a) Linear sweep voltage curves collected for A-hematite (black lines) and N-hematite (gray lines), at a scan rate of 10 mV/s, in a NaOH electrolyte solution (1m, pH 13.6) under illumination by simulated solar light of 100 mW/cm$^2$ and in the dark. b) Corresponding IPCE spectra for A-hematite and N-hematite, collected at potentials of 1.23 and 1.50 V vs. RHE. Reference [32].

Another way of doping for hematite is called "self-doping". Namely oxygen vacancies (VO) are created artificially by some unique treatment. The $Fe^{2+}$ sites in hematite could significantly increase the conductivity of the material through a polaron hopping mechanism.[31] Ling and his coworkers obtained self-doped hematite nanowire arrays through thermal decomposition of β-FeOOH in an oxygen-deficient atmosphere ($N_2$+air).[32] Although oxygen-vacancy-introduction is an effective method

to increase the photocurrent density of photoelectrodes, it should be highly emphasized that water splitting activity and Faradaic efficiency should be tested and calculated to exclude that the increased current is due to the oxidation of oxygen vacancies in materials. The gases of hydrogen and oxygen generated need to be 2:1, and the higher of oxygen faradaic efficiency the better. In addition, stability is also an important factor to judge whether oxygen vacancy is consumed in oxidation reaction on the photoanodes.

(2) Cocatalysts decoration.

As is commonly known, cocatalysts play an important role in photocatalysis by lower the redox overpotential at the respective active sites. Metal nanoparticles such as Pt are considered as good cocatalyst for water reduction due to its low overpotential for hydrogen evolution.[33] Most of the water oxidation reaction cocatalysts come from electrocatalytic water oxidation electrodes, for which have many kinds of choices to choose.[34] A series of materials have been tried to deposit on the surface of photoanodes, including $IrO_2$[35], cobalt phosphate (Co-pi)[36], nickel oxide[37], nickel oxyhydroxide[38], cobalt oxide[39] and $MnO_x$[40]. Among them, there are still a lot of studies concentrating on iron-based cocatalyst such as FeOOH[41], $NiFeO_x$[42], NiFeOOH[43] *et al.* in recent years due to their high stability and earth abundance. Hu and his coworkers prepared an optically transparent iron nickel oxide catalyst and loaded it on nanostructured hematite photoanode as cocatalyst as shown in Figure 1.5.[44] The low amount of catalyst decoration combined with its high activity at low

over-potential lead to significant improvement on the onset potential for PEC oxygen evolution. The onset potential decreased nearly 200 mV compared with pure hematite photoanode. And the photocurrent density at 1.2 V vs. RHE almost doubles to reach ~0.4 mA/cm$^2$.

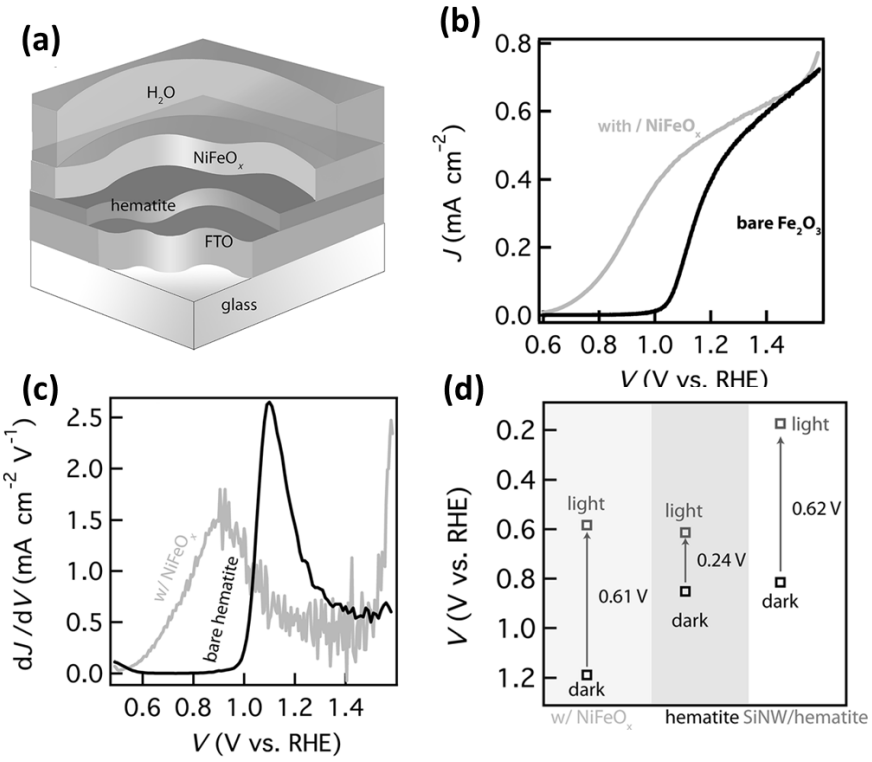



**Figure 1.5** a) Schematic perspective view of the modification; b) Photocurrent-density-voltage plot. c) First-order derivative of the photocurrent density as a function of voltage; d) Graph showing the significant difference observed between the measured photovoltages generated by bare hematite and hematite decorated with NiFeOx. Reference [44]

(3) Constructing junctions between two semiconductors.

Constructing bilayer junctions offers an effective way to improve the photoelectrochemical performances of photoelectrodes. The large magnitude of

interfacial electric field formed between different layers will realize high charge separation efficiency.[45] In fact, studies about bilayer junctions (either homogenous junction or heterogeneous junction) based on hematite are quite limited because the formation of junction between two semiconductors is more difficulty than just contacting them together. The crystal structures between the two layers need to match well so that the bending band of the two layers will be connected together. As a result, forming homojunction for hematite is much easier than heterojunction.

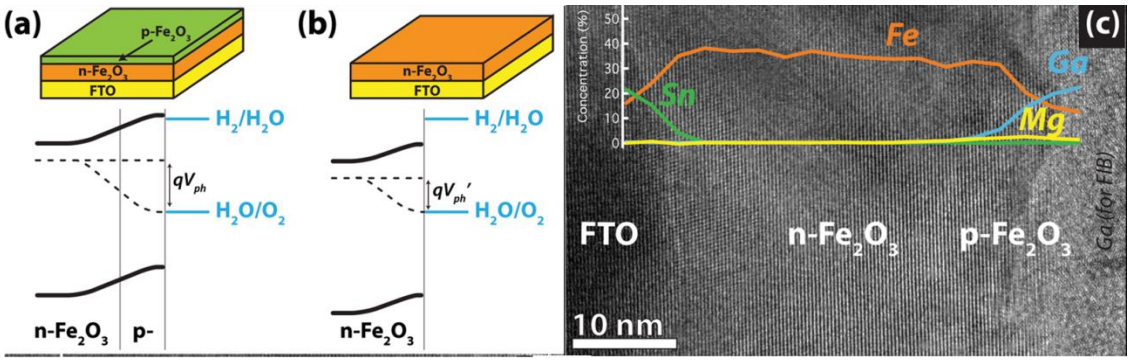



**Figure 1.6** (a) Energy diagrams of hematite with a p-type coating. The introduction of a p-type layer creates a built in field that does not depend on surface adsorptions, allowing for the measurement of a more substantial photovoltage ($V_{ph}$). (b) In comparison, although a built-in field can also be achieved on n-type hematite, its depth and magnitude are sensitive to the nature of the electrolyte. (c) Cross-sectional TEM of the n−p junction. Reference [46].

Wang and his coworkers prepared a p-type Mg-doped hematite layer on the surface of hematite by atomic layer deposition as shown in Figure 1.6.[46] By forming the homojunction between Mg-doped hematite and hematite, the photovoltages was enlarged. Wu and his coauthors loaded p-type NiO nanoparticles on the surface of

hematite films.[47] By loading NiO on the surface, not only holes from hematite are more easily accumulate on the surface via the p–n junction, but also barrier for oxygen evolution reaction is decreased.

(4) Surface plasmonic resonance and resonant light trapping.

Metals play an important role in photoelectrochemical water splitting. The suface plasmonic resonance effect of some precious metal can help improve the light absorption of semiconductors.[48] As the hole diffusion length in hematite is very short, the thickness of hematite are limited to one hundred nanometer. Due to the limited thickness, the light absorption for the hematite films is not adequate. In the case of low overall light absorption, plasmonic metal nanoparticles can be used to capture the light that cannot be absorbed by the thin films. Warren and his coworkers discussed the influence of plasmonic Au nanoparticles on the photoactivity of hematite electrodes.[49] And a relative enhancement in the water splitting efficiency at photon frequencies corresponding to the plasmon resonance in gold was observed especially at higher potentials.

Another method to enhance the activity of hematite photoanode is taking advantages of the resonant light trapping (Figure 1.7). Rothschild proposed a new strategy to overcome the limitations of hematite by means of resonant light trapping in ultrathin films designed as optical cavities.[50] The photoelectrochemical water splitting increased several times using metal substrates and this amplifies that the intensity closes to the surface wherein photo-generated minority charge carriers (holes) can reach the

surface and oxidize water before recombination taking place.

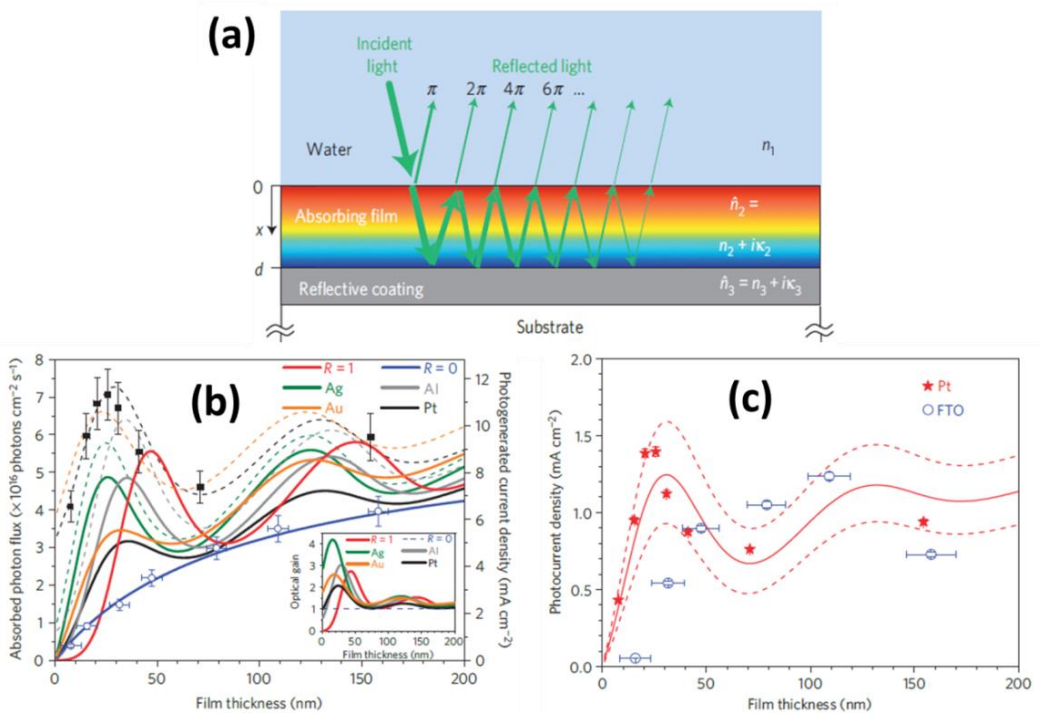



**Figure 1.7** (a) Schematic illustration of the light propagation in a quarter-wave absorbing film on a back-reflector substrate. (b) Sunlight absorption in hematite films on back-reflector substrates. (c) Photocurrent density, measured at 1.4 V RHE as a function of film thickness for Ti-doped hematite films. Reference [50].

## 1.3 P-type iron-based photocathodes.

Compared with the n-type photoanodes, researches about p-type photocathodes are relatively limited. One is due to the limited choice of p-type semiconductor. Another is the low photocurrent density of the p-type semiconductors. As the transportation of holes is much slower than electrons, the recombination of carriers in p-type semiconductors will be increased.[51] Initial p-type semiconductors such as $Cu_2O$,[15] $CuRhO_2$[52] have been studied for photoelectrochemical hydrogen evolution. Besides,

doping is another popular method to obtain p-type semiconductors, such as Cr doped $TiO_2$,[53] Cr doped $SrTiO_3$[54] and Rh doped $SrTiO_3$[55]. Although some of these materials such as $Cu_2O$[15] show a high photocurrent density to several $mA/cm^2$, the stability of them are very poor (< 1 hour) that it cannot be considered as a promising candidate for PEC water reduction. Iron-based p-type semiconductors such as $CaFe_2O_4$,[14] Mg[46] or Zn[56] doped $Fe_2O_3$ are preferable candidates considering the highly stable property in aqueous solutions under water reduction conditions.

$CaFe_2O_4$ is a promising candidate for photoelectrocatalytic water reduction. It is an initial p-type semiconductor with a band gap of 1.9 eV, which is suitable to absorb visible light. The conduction band edge of $CaFe_2O_4$ is -0.6 V vs. NHE while the valence band edge is +1.3 V vs NHE, which are suitable for water splitting.[57] Previous study proved that p-type $CaFe_2O_4$ can be used as a photocathode[14]. However, as its performance as photocathodes is limited, it is commonly introduced as a surface layer to form a p-n junction photoanode[58] to improve the water oxidation activity of the photoanodes.

## 1.4 Photoelectrochemical tandem cells.

Up to date, complete solar water splitting by PEC without externally applied bias were very limited. The reported examples for photoanodes in tandem cell are mainly concentrated on $WO_3$, $Fe_2O_3$, and $BiVO_4$ as they have visible-light responsibility, high stability and solar-to-electricity efficiency. These photoanodes were usually combined

with Si photocathodes or other solar cells for overall photoelectrochemical water splitting. $WO_3$/DSC (dye sensitized solar cell) tandem device ($\eta_{STH}$=3.10%),[59] $Fe_2O_3$/DSC tandem device ($\eta_{STH}$=1.17%),[59] Co-Pi/W:$BiVO_4$ with a 2-jn a-Si solar cell ($\eta_{STH}$=4.90%)[60], $NiFeO_x$-$Fe_2O_3$/a-Si (Figure 1.8)[61] were the most interesting examples for unbiased solar water splitting till now. And the solar to hydrogen efficiency is still far from requirement for application in industry. The main challenges are the lack of p-type photocathodes with larger carrier densities and low onset potentials. And both the photoanode and photocathode need to possess earth abundant element, non-toxic and high durability. All-iron-based tandem cells are promising candidates to fulfill all the above requirements.

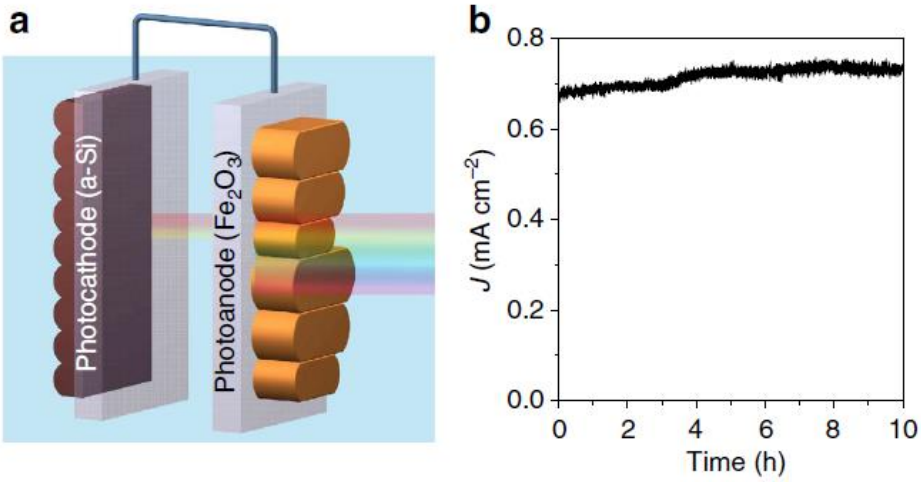



**Figure 1.8** (a) Schematics of overall unassisted water splitting by haematite photoanode (right) and amorphous Si photocathode (left) in a tandem configuration. (b) Photocurrent during the first 10 h. Reference [61].

## 1. 5 Motivation of this thesis.

Photoelectrochemical (PEC) water splitting has been widely researched since

1970s as it is a promising method for solar energy conversion. Among the various semiconductors, iron-based photoelectrodes such as hematite have been extensively studied because of its visible light responsibility, earth abundant property, non-toxic and high stability. However, hematite has a very short lifetime of excited state carrier and hole diffusion length that significantly limits its efficiency in charge separation and collection as a PEC anode. And overall solar water splitting using PEC devices are still faced with great challenges due to lack of p-type photocathodes. In this thesis, n-$Fe_2O_3$ photoanodes and p-$LaFeO_3$ photocathdoes were researched systematically and a new photocell, $Fe_2O_3$/$LaFeO_3$ tandem cell, was designed for the first time. In order to enhance the efficiency and stability of this tandem cell, hematite homojunction with FeO(OH) nanosheet cocatalyst were fabricated to improve the charge separation efficiency in the electrode and the charge transfer kinetics at the electrode/electrolyte interface. And $LaFeO_3$ was investigated as a new photocathode due to its perovskite structure.

In chapter 2, hematite homojunction was prepared to improve the charge separation efficiency of the electrode. As introduced previously, the short hole diffusion time and lifetime in hematite is one of the biggest challenges to obtain high performance. Forming junctions inside the electrode is an effective way to improve the charge separation in hematite. Although previous studies have proved that self-doping is an effective way to improve the PEC performances by changing the light absorption or increasing the hole densities, these artificial dopants (oxygen vacancies) on the surface

is easily consumed during the water oxidation process. In order to stabilize the artificial oxygen vacancies, hematite homojunction photoanode was designed with high-vacancy-layers inside and normal-vacancy-layers outside. By forming a homojunction inside the hematite electrodes, high charge separation efficiency were realized via constructing a large magnitude of interfacial electric field in it. What's more, the artificial oxygen vacancies inside the electrode were protected by the homojunction and normal hematite layer outside. The homojunction obtained were the first example of hematite homojunction without foreign element doping. And we offered a new approach for stabilizing artificial oxygen vacancies that has never been studied before.

In chapter 3, FeO(OH) nanosheet was decorated on the surface of hematite to improve the charge transfer kinetics at the electrode/electrolyte interface. Despite the charge separation efficiency is improved by forming homojunctions as discussed in Chapter 2, the performance of hematite is still far from required due to the high charge transfer barrier between the hematite/electrolyte interface. As a result, the second strategy to get well developed photoanodes was modifying FeO(OH) nanosheet cocatalysts on the surface to improve the charge transfer efficiency. FeO(OH) is a new choice of cocatalyst for water oxidation in recent years from 2012. Although FeO(OH) are proved to be a good cocatalyst for water oxidation on some photoanodes such as $BiVO_4$ and Si, they were usually grown parallel to the surface of the photoanodes which decreased reaction area of electrodes. However, this situation changed if we load FeO(OH) on the surface of hematite and nanostructured FeO(OH) were obtained on

hematite due to the similar Fe-O bond between them. Finally, nanostructured FeO(OH) can act as a cocatalyst to improve charge transfer kinetics and superior PEC performances of hematite photoanode were obtained. In this work, FeO(OH) were obtained in form of nanosheets for the first time. And a FeO(OH)/$Fe_2O_3$ photoanode were developed as a new photoanode for water oxidation.

In chapter 4, p-$LaFeO_3$/n-$Fe_2O_3$ tandem cell were designed for overall PEC water splitting. By forming homojunction and loading nanostructured FeO(OH) cocatalyst, hematite photoanodes are well designed. To further improve the light absorption efficiency of the whole hematite-based photocell, a new p-type $LaFeO_3$ thin film was prepared as photocathodes for PEC water reduction. As choices for initial p-type semiconductors are limited, studies of photocathodes are much fewer than n-type photoanodes. And they are still faced with problems such as low efficiency and stability. As $LaFeO_3$ has a perovskite structure, the nearly 180$^o$ B-O-B atom chains inside the $ABO_3$ structure could offer an ideal three-dimensional transportation channel for photo-excited carriers. Base on this theory, $LaFeO_3$ thin films were prepared by pulsed laser deposition and used as photocathodes for the first time for water reduction. By combining p-type $LaFeO_3$ photocathodes with hematite photoanodes, p-$LaFeO_3$/n-$Fe_2O_3$ tandem cell were obtained. And we offered the first example of an all-iron-based tandem cell for solar hydrogen conversion.

## References

[1] BP Statistical Review of World Energy June 2013, BP Statistical Review of World Energy, BP p.l.c, 1 St James's Square, London, SW1Y 4PD, UK.

[2] M. G. Walter, E. L. Warren, J. R. McKone, S. W. Boettcher, Q. Mi, E. A. Santori Chem. Rew. 2010, 110, 6446.

[3] T. Hisatomi, J. Kubota, K. Domen, Chem. Soc. Rev.

[4] D. A. Wheeler, G. Wang, Y. Ling, Y. Li, J. Z. Zhang, Energy Environ. Sci., 2012, 5, 6682.

[5] A. Fujishima and K. Honda, Nature, 1972, 238, 37–38.

[6] R. H. Coridan, M. Shaner, C. Wiggenhorm, B. S. Brunschwig, N. S. Lewis, J. Phys. Chem. C 2013, 117, 6949-6957.

[7] S. J. Hong, S. Lee, J. S. Jang, J. S. Lee, Energy Environ. Soc. 2011, 4, 1781-1787.

[8] Y. Zheng, X. Tao, L. Wang, H. Xu, Q. Hou, W. Zhou, J. Chen, Chem. Mater. 2010, 22, 928-934.

[9] S. D. Tilley, M. Cornuz, K. Sivula, M. Grätzel, Angew. Chem. Int. Ed. 2010, 49, 6405-6408.

[10] S. C. Warren, K. Voitchovsky, H. Dotan, C. M. Leroy, M. Cornuz, F. Stellacci, C. Hebert, A. Rothschild, M. Gratzel Nat. Mater. 2013, 12, 842-849.

[11] A. Mao, K. Shin, J. Kim, D. Wang, G. Han, J. Park, ACS Appl. Mater. Interfaces, 2011, 3, 1852-1858.

[12] N. T. Hahn, H. Ye, D. W. Flaherty, A. J. Bard, C. B. Mullins, ACS Nano, 2010, 4, 1977-1986.

[13] R. L. Spray, K. S. Choi, Chem. Mater., 2009, 21, 3701–3709.

[14] S. Ida, K. Yamada, T. Matsunaga, H. Hagiwara, Y. Matsumoto, T. Ishihara, J. Am. Chem. Soc. 2010, 132, 17342-17345.

[15] P. Wang, Y. Tang, X. Wen, R. Amal, Y. Ng, ACS Appl. Mater. Inter. 2015, 7, 19887-19893.

[16] Y. Zhang, S. Ouyang, Q. Yu, P. Li, J. Ye, Chem. Commun. 2015, 51, 14057.

[17] Q. Liu, J. He, T. Yao, Z. Sun, W. Cheng, S. He, Y. Xie, Y. Peng, H. Cheng, Y Sun, Y. Jiang, F. Hu, Z. Xie, W. Yan, Z. Pan, Z. Wu, S. Wei, Nat. Comm. 2014, 5, 5122.

[18] M. Gratzel, Nature 2001, 414, 338– 344.

[19] W. Wu, C. Jiang, W. A. L. Roy, Nanoscale, 2015, 7, 38-58.

[20] B. Seger, T. Pedersen, A. B. Laursen, P. C. K. Vesborg, O. Hansen, I. Chorkendorff, J. Am. Chem. Soc. 2013, 135, 1057−1064.

[21] L. A. Marusak, R. Messier, W. B. White, J. Phys. Chem. Solids 1980, 41, 981-984.

[22] N. J. Cherepy, D. B. Liston, J. A. Lovejoy, H. Deng and J. Z. Zhang, J. Phys. Chem. B, 1998, 102, 770–776.

[23] A. G. Joly, J. R. Williams, S. A. Chambers, G. Xiong, W. P. Hess and D. M. Laman, J. Appl. Phys., 2006, 99, 053521.

[24] J. H. Kennedy and J. K. W. Frese, J. Electrochem. Soc., 1978, 125, 709–714.

[25] K. Sivula, R. Zboril, F. Le Formal, R. Robert, A. Weidenkaff, J. Tucek, J. Frydrych, M. Gratzel, J. Am. Chem. Soc. 2010, 132, 7436–7444.

[26] J. A. Glasscock, P. R. F. Barnes, I. C. Plumb, N. Savvides, J. Phys. Chem. C 2007, 111, 16477-16488.

[27] G. Wang, Y. Ling, D. A. Wheeler, K. E. N. George, K. Horsley, C. Heske, J. Z. Zhang, Y. Li, Nano Lett. 2011, 11, 3505-3509.

[28] Y. Ling, G. Wang, D. A. Wheeler, J. Z. Zhang, Y. Li, Nano Lett. 2011, 11, 2119-2125.

[29] J. Y. Kim, G. Magesh, D. H. Youn, J. Jang, J. Kubota, K. Domen, J. S. Lee, Sci. Rep. 2013, 2681.

[30] Y. Zhang, S. Jiang, W. Song, P. Zhou, H. Ji, W. Ma, W. Hao, C. Chen, J. Zhao, Energy Environ. Sci. 2015, 8, 1231-1236.

[31] M. Zhang, W. Luo, Z. Li, T. Yu, Z. Zou, Appl. Phys. Lett. 2010, 97, 042105.

[32] Y. Ling, G. Wang, C. Wang, J. Z. Zhang, Y. Li, Angew. Chem. Int. Ed. 2012, 51, 4074-4079.

[33] A. Kudo, Y. Miseki, Chem. Soc. Rev. 2009, 38, 253-278.

[34] C. C. L. McCrory, S. Jung , J. C. Peters, T. F. Jaramillo, J. Am. Chem. Soc. 2013, 135, 16977 .

[35] R. Asai, H. Nemoto, Q. Jia, K. Saito, A. Iwase, A. Kudo, Chem. Commun. 2014, 50, 2543-2546.

[36] B. Klahr, S. Gimenez, F. Fabregat-Santiago, J. Bisquert, T. W. Hamann, J. Am. Chem. Soc. 2012, 134, 16693-16700.

[37] M. J. Kenney, M. Gong, Y. Li, J. Z. Wu, J. Feng, M. Lanza, H. Dai, Science 2013, 342, 836-840.

[38] D. Xu, Z. Fu, D. Wang, Y. Lin, Y. Sun, D. Meng, T. Xie, Phys. Chem. Chem. Phys. 2015, 17, 23924-23930.

[39] K. Ueda, T. Minegishi, J. Clune, M. Nakabayashi, T. Hisatomi, H. Nishiyama, M. Katayama, N. Shibata, J. Kubota, T. Yamada, K. Domen, J. Am. Chem. Soc. 2015, 137, 2227-2230.

[40] M. Yoshida, T. Yomogida, T. Mineo, K. Nitta, K. Kato, T. Masuda, H. Nitani, H. Abe, S. Takakusagi, T. Uruga, K. Asakura, K. Uosaki, H. Kondoh J. Phys. Chem. C 2014, 118, 24302-24309.

[41] Z. Li, S. Feng, S. Liu, X. Li, L. Wang, W. Lu, Nanoscale, 2015, 7, 45, 19178-19183.

[42] C. G. Morales-Guio, M. T. Mayer, A. Yella, S. D. Tilley, M. Grazel, X. Hu, J. Am. Chem. Soc. 2015, 137, 9927-9936.

[43] L. Wang, F. Doinigi, N. Nguyen, R. Kirchgeorg, M. Gliech, S. Grigorescu, P. Strasser, P. Schmuki, Chem. Mater. 2015, 27, 2360-2366.

[44] C. Du, X. Yang, M. T. Mayer, H. Hoyt, J. Xie, G. McMahon, G. Bischoping, D. Wang, Angew. Chem. Int. Ed. 2013, 52, 12692 –12695.

[45] Li, H. Zhou, Y. Tu, W. Ye, J. Zou, Z. Adv. Funct. Mater. 2015, 25, 998-1013.

[46] Y. Lin, Y. Xu, M. T. Mayer, Z. I. Simpson, G. McMahon, S. Zhou and D. Wang, J. Am. Chem. Soc., 2012, 134, 5508-5511.

[47] J. Li, F. Meng, S. Suri, W. Ding, F. Huang, N. Wu, Chem. Commun. 2012, 48, 8213- 8215.

[48] H. Wei, D. Ratchford, X. Q. Li, H. X. Xu, C. K. Shih, Nano Lett. 2009, 9, 4168.

[49] E. Thimsen, F. L. Formal, M. Gratzel, S. C. Warren, Nano Lett. 2011, 11, 35-43.

[50] H. Dotan, O. Kfir, E. Sharlin, O. Blank, M. Gross, I. Dumchin, G. Ankonina, A. Rothschild, Nat. Mater. 2013, 12, 158-164.

[51] B. V. Zeghbroeck, Principles of Electronic Devices, August 2007, http://ece-www.colorado.edu/~bart/book/

[52] J. Gu, Y. Yan, J. W. Krizan, Q. D. Gibson, Z. M. Detweiler, R. J. Cava, A. B. Bocarsly J. Am. Chem. Soc. 2014, 136, 830-833.

[53] J. Cao, Y. Zhang, L. Liu and J. Ye, Chem. Commun., 2013, 49, 3440.

[54] Z. Jiao, T. Chen, J. Xiong, T. Wang, G. Lu, J. Ye, Y. Bi Sci. Report 2013, 3, 2720

[55] K. Iwashina and A. Kudo, J. Am. Chem. Soc., 2011, 133, 13272.

[56] X. Qi, G. She, M. Wang, L. Mu and W. Shi, Chem. Commun., 2013, 49, 5742.

[57] C. Leygraf, M. Hendewerk, G. A. Somorjai J. Phys. Chem. 1982, 86, 4484.

[58] E. S. Kim, N. Nishimura, G. Magesh, J. Y. Kim, J. Jang, H. Jun, J. Kubota, K. Domen, J. S. Lee, J. Am. Chem. Soc. 2013, 135, 5375-5383.

[59] J. Brillet, J. Yum, M. Cornuz, T. Hisatomi, R. Solarska, J. Augustynski, M. Craetzel. K. Sivula, Nat. Photonics 6, 2012, 6, 824-828.

[60] F. F. Abdi, L. Han, A. H. M. Smets, M. Zeman, B. Dam, R. Krol. Nat. Commun. 2013, 4, 2195, doi:10.1038/ncomms3195.

[61] J. Jang, C. Du, Y. Ye, Y. Lin, X. Yao, J. Thorne, E. Liu, G. McMahon, J. Zhu, A. Javey, J. Guo, D. Wang, Nat. Commun. 6, 7447, DOI: 10.1038/ncomms8447.

# Chapter 2 Hematite Homojunctions without Foreign Element Doping

## 2.1 Introduction

As introduced previously, hematite ($\alpha$-$Fe_2O_3$) was studied extensively in recent years as one of the most attractive candidates for PEC water oxidation due to its excellent visible light responsibility with good stability, nontoxicity, and earth-abundance as discussed previously in Chapter 1.[1-2] However, as the life time of the excited state carriers is very short (~1 ps)[3,4], as well as the small hole diffusion length (~2 to 4 nm)[5], the efficiency of hematite in charge separation and collection as a PEC anode is limited. The improvement of hematite film is directly related to the photoelectric conversion efficiency of hematite-based PEC system. Since oxygen vacancies will be inevitably introduced into the material at a low concentration in general preparation process, hematite usually shows an n-type characteristic (Fermi level near the conduction band) and serves as photoanode for oxygen evolution. These unintentionally introduced oxygen vacancies also play an important role in photocatalytic applications by serving as reaction sites[6-8] or affecting the light absorption[9] of semiconductors.

Recently, there are a number of reports about improving the PEC water splitting performances by increasing the density of oxygen vacancies in semiconductors.[10-14] However, these oxygen vacancies are generally produced nearby the surface since they

are generated by a reductive post-treatment process after the formation of photoelectrodes.[10,12] As a result, they are very unstable and readily consumed during the anodic oxidation at the semiconductor/liquid interface.[10] These oxygen vacancies will be finally occupied by the oxygen species from the solution (such as water or oxygen). And fictive water splitting will be generally observed due to the vacancies consumption with the oxygen evolution rate less than half of hydrogen.[13]

Forming homojunctions offers an effective way to realize high charge separation efficiency via constructing a large magnitude of interfacial electric field within a semiconductor.[15-17] As is commonly known, the Fermi level of an n-type oxide semiconductors can be modulated nearer to conduction band by increasing the oxygen vacancies in it without intentional doping foreign elements.[9] This makes it possible to construct homojunction photoelectrodes within the same semiconductor possessing two different Fermi levels.

In this chapter, we realized the construction of n-n hematite homojunction photoelectrodes without foreign element doping using stabilized oxygen vacancies. Pulsed laser deposition (PLD) was used to prepare hematite homojunction photoelectrodes since it can effectively control the densities of oxygen vacancies by tuning the oxygen pressure during the deposition process,[18-21] and ultimately changed the Fermi level of the hematite films. Considering the charge flow in the homojunction as well as the water oxidation reaction occurred on the photoelectrodes, hematite with high oxygen vacancies (higher fermi level) was prepared as the inner

layer while that with low oxygen vacancy (lower fermi level) was prepared as the outer layer. The PEC performances of hematite would be remarkably enhanced due to the interfacial electric field formed in the homojunction. Besides, overall water splitting is expected to be realized by the hematite homojunction photoelectrode with $H_2$:$O_2$=2:1 without the consumption of oxygen vacancies. Both the photocurrent density and onset potential for the hematite homojunction is going to be improved compared with single type hematite photoanodes. And with this homojuction configuration, the hematite homojunctions showed several times higher stability compared with pure high-vacancy hematite phtoelectrodes for oxygen evolution.

## 2.2 Experiments

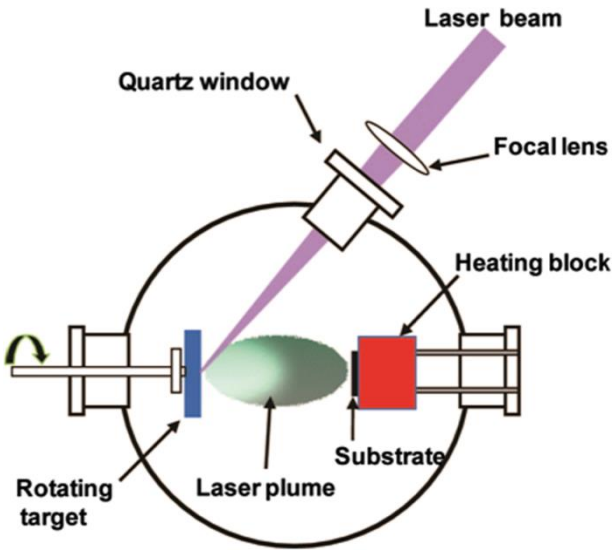
### 2.2.1 Pulsed laser deposition and preparation of photoelectrodes.

(1) General introduction of PLD.

Pulsed laser deposition (PLD) is one of the most promising physical vapor deposition methods, in which a high-power pulsed laser beam is placed inside the vacuum chamber and is used to strike a target of the unique material that going to be deposited. This material is vaporized from the target in form of a plasma plume by the laser and deposit as a thin film on a desired substrate. In addition, poly-component films can also be obtained by evaporating stoichiometric target through the pulsed laser and deposit on expected substrate. What's more, the deposition process can present in

different gas atmosphere, either in ultra-high vacuum or in the presence of a background gas, such as oxygen, nitrogen, or argon, according to the materials that going to be prepared with the pressure of the background gas can also be controlled.

The specific mechanisms of pulsed laser deposition for a film are very complicated which can be referred in Scheme 2.1, involving the ablation process of the prepositioned target material by the laser beam[32], the production of a plasma plume with high energetic ions, electrons or neutrals and the film growing into crystalline on the heated substrate in the chamber.




**Scheme 2.1** Schematic illustration of the pulsed laser deposition (PLD) setup.

The process of PLD can generally be divided into 5 steps: 1. the irradiation of the laser to the surface of the target. 2. Laser ablation of the target and the creation of plasma from the target material. 3. Dynamic of the plasma. 4. Deposition of the ablation material on the substrate. 5. Nucleation and growth of the film on the substrate surface.

As is commonly known, PLD is a conventional method to prepare films, and it is a repeatable method to obtain films with high quality and stability. Firstly, highly qualified films can be obtained by PLD. As is commonly known, the crystalline of materials plays a key role on the performance of photocatalysts especially photoelectrodes. Secondly, the contact between the films and conductive substrate will influence the efficiency and stability of electrodes. Similarly, as the particles irradiated by the laser during deposition have quite high energy, the contact of them with the substrate is tight. So films by PLD are likely to realize both high efficiency and durability. This is the most important advantage of PLD from other methods such as spin coating, electrodeposition, and hydrothermal methods and so on.

(2). Preparation of hematite films (HV-$Fe_2O_3$; LV-$Fe_2O_3$; HV/LV-$Fe_2O_3$ homojunction) by PLD.

Both the HV-$Fe_2O_3$ and LV-$Fe_2O_3$ were prepared by PLD (ST-PLD; Pascal Co. Ltd, Japan) method using a $Fe_2O_3$ pellet as the target and ITO as a substrate. The $Fe_2O_3$ target was purchased from the Hefei Kejing Materials Technology CO., LTD, China.

The temperature for deposition is 550°C. The film preparation chamber of the PLD machine was evacuated to 0.001 Pa firstly. Then for the preparation of HV-$Fe_2O_3$, no gas was introduced into the chamber with the laser directly irradiated on the target with different time. However, for the preparation of LV-$Fe_2O_3$, pure $O_2$ was introduced into the chamber until the pressure became 4 Pa, then the laser began to irradiate with

different time. After the laser irradiation, the film was kept at the same temperature in pure $O_2$ (160 Pa) for 30 min as a post-heat treatment.

For the preparation of HV/LV-$Fe_2O_3$ homojunction films: Firstly, the chamber of the PLD machine was evacuated to 0.001 Pa. Then the target was irradiated in pure vacuum to produce HV-$Fe_2O_3$. After that, pure $O_2$ was introduced into the chamber until the pressure became 4 Pa. Subsequently, the target was irradiated again to produce LV-$Fe_2O_3$. Finally, the film was kept at the same temperature in pure $O_2$ (160 Pa) for 30 min as a post-heat treatment. In all of these steps, the temperature of substrate is 550°C.

**2.2.2 Characterization.**

The phase of the samples was characterized by XRD (RIGAKU Rint-2000 X-ray diffractometer). Raman scattering spectra of samples were measured using the Raman spectroscope (NRS-1000, Jasco Corp. Japan). Field-emission scanning electron microscope JSM-6701 F, JEOL) and Atomic force microscopy (Nanocute H, Japan) were used to characterize the surface and cross morphology of the samples. Optical absorption properties of the $Fe_2O_3$ films were measured through an UV-vis spectrophotometer (UV-2500PC; Shimadzu Co., Japan). XPS experiments were performed in a Theta probe (Thermo Fisher) using monochromatic Al Kα x-rays at hν=1486.6 eV.

### 2.2.3 Photoelectrochemical properties

Photoelectrochemical measurements were processed by an electrochemical station (ALS/CH model 650A). Platinum were used as the counter electrode while SCE were used as the reference electrode. AM 1.5 solar simulation (WXS-80C-3 AM 1.5G) was utilized as the light sources. The solution is 1 M NaOH aqueous solution. All the measurements were carried out in a three-electrode system.

### 2.2.4 Water Splitting

Hydrogen and oxygen generation of HV/LV-$Fe_2O_3$ homojunction photoanodes were tested in a water splitting system. $1 \times 1$ $cm^2$ HV/LV-$Fe_2O_3$ film was deposited on $2 \times 1$ $cm^2$ ITO. 180 ml 1 M NaOH solution was put in a quartz glass cell as the source for water splitting. Then this glass cell was set on the water splitting system with a closed gas circulation system. The generated $H_2$ and $O_2$ were in situ analyzed with a TCD gas chromatograph (Shimadzu GC-8AIT, argon carrier). Air mass 1.5 G solar simulation (WXS-80C-3 AM 1.5G) was utilized as the light source, and the external bias is 1.23 V vs. RHE.

## 2.3 Results and discussion

### 2.3.1 Characterization of high-vacancy $Fe_2O_3$ (HV-$Fe_2O_3$) and low-vacancy $Fe_2O_3$ (LV-$Fe_2O_3$).

The high-vacancy $Fe_2O_3$ (HV-$Fe_2O_3$) and low-vacancy $Fe_2O_3$ (LV-$Fe_2O_3$) were prepared

by pulsed laser deposition (PLD) with controllable gas atmosphere. The HV-$Fe_2O_3$ was prepared in vacuum while the LV-$Fe_2O_3$ was prepared in 30 m torr pure oxygen. XRD was used to characterize the phase of the two iron oxide films. As the films obtained on ITO was very thin, XRD patterns for iron oxide films was suppressed by the ITO substrate. The only one peak can be detected for hematite and it confirmed that both of HV-$Fe_2O_3$ and LV-$Fe_2O_3$ had a pure phase of hematite (Figure 2.1).

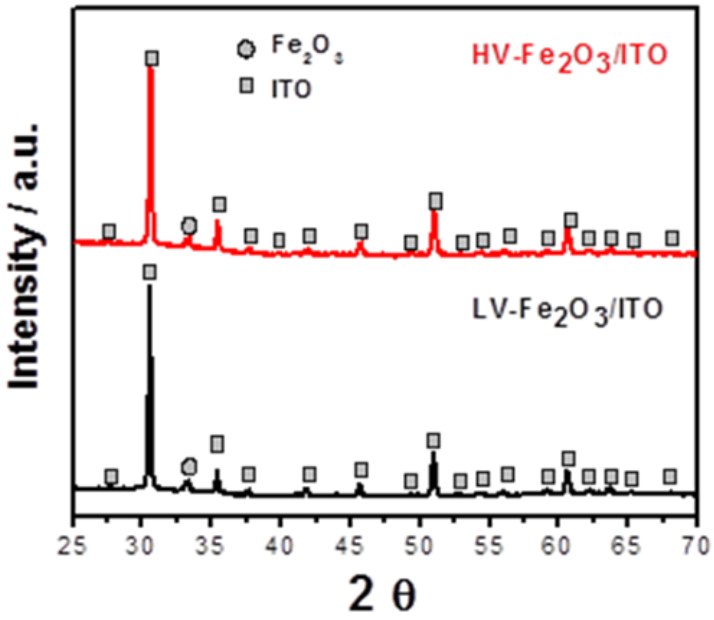



**Figure 2.1** XRD patterns for bare HV-$Fe_2O_3$ and bare LV-$Fe_2O_3$ respectively.

Raman spectra (Figure 2.2) of both HV-$Fe_2O_3$ and LV-$Fe_2O_3$ exhibited seven lines typical for hematite at about 226 (A1g), 245 (Eg), 293 (Eg), 298 (Eg), 412 (Eg), 500 (A1g) and 612 (Eg) $cm^{-1}$.[22] It should be noted that a mode (Eu) at 660 $cm^{-1}$ appeared in our results which is attributed to the existence of oxygen vacancies in the materials. The peak at 660 $cm^{-1}$ in HV-$Fe_2O_3$ was much more obvious than that in LV-$Fe_2O_3$, indicating there are more oxygen vacancies in HV-$Fe_2O_3$.[23-24]

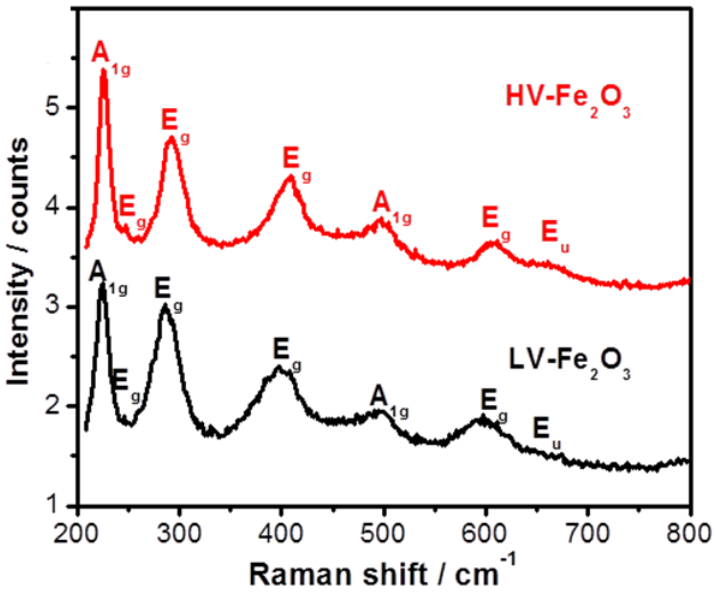



**Figure 2.2** Raman spectra of single HV-$Fe_2O_3$ and single LV-$Fe_2O_3$ films respectively.

XPS were also used to characterize the surface state of the hematite films (Figure 2.3). Both $Fe^{2+}$ ions $Fe^{3+}$ can be detected in the XPS spectra for Fe (2p) of HV-$Fe_2O_3$ and LV-$Fe_2O_3$ as shown in Figure 2.3 a. Plus, in the XPS spectra for O (1s), peaks at 530.1 eV 531.8 eV, 532.4 eV is commonly corresponded to the oxygen present in the lattice, adsorbed $OH^-$ (Fe-OH) and adsorbed water respectively.[25-28] From the O (1s) spectra for HV-$Fe_2O_3$ and LV-$Fe_2O_3$ (Figure 2.3 b), it is observed that the percentage of adsorbed OH on oxygen vacancies is 29.5% in LV-$Fe_2O_3$, while that in HV-$Fe_2O_3$ is 37.9%. The 8.4% higher adsorbed OH on the surface of HV-$Fe_2O_3$ indicating more oxygen vacancies existed in the samples of HV-$Fe_2O_3$.

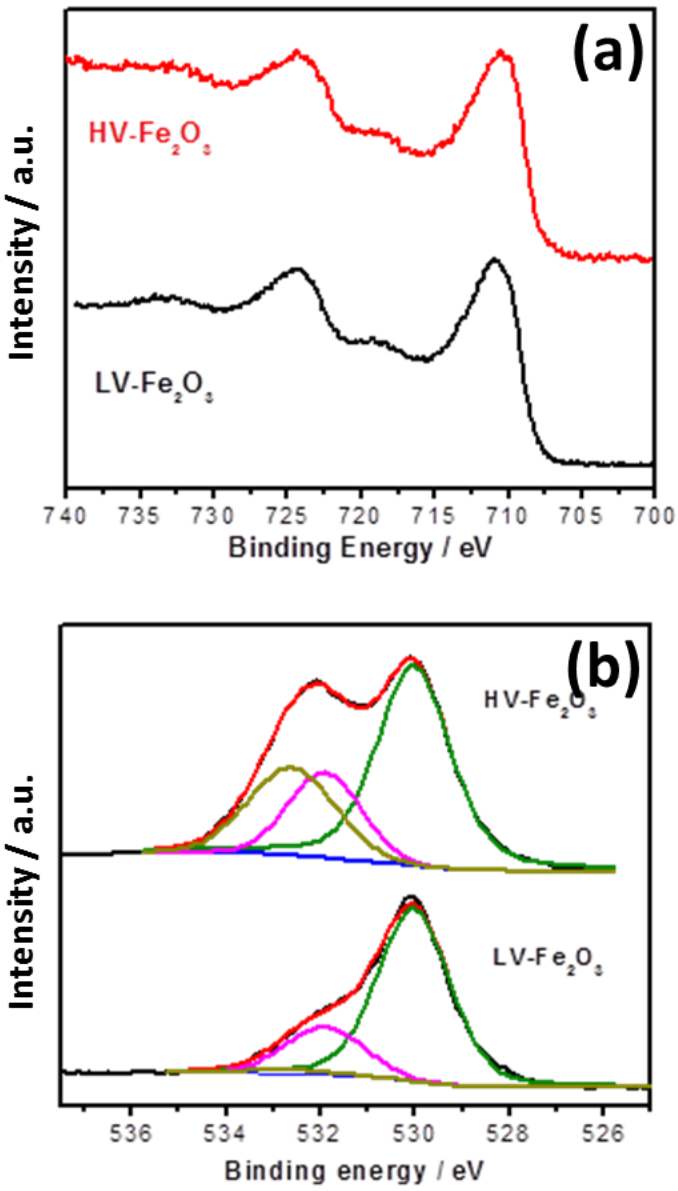



**Figure 2.3** XPS spectra of (a) Fe (2p) and (b) O (1s) of single HV-$Fe_2O_3$ and single LV-$Fe_2O_3$ films respectively.

Meanwhile, the absorption spectra for the samples were shown in Figure 2.4. The absorption edges for both HV-$Fe_2O_3$ and LV-$Fe_2O_3$ were the same, about 590 nm, means that the band gaps for the two types of hematite were the same. However, an obvious

absorption is observed after 600 nm in HV-$Fe_2O_3$ which also confirmed that there was oxygen vacancies existed in it.

To get further insight into the Fermi level positions of both types of hematite films, Mott-Schottky analysis was used.[29] The hematite film with high oxygen vacancies (HV-$Fe_2O_3$) showed 0.22 V negatively shifted Fermi level position compared with low-vacancy hematite (LV-$Fe_2O_3$) as shown in Figure 2.5. As the HV-$Fe_2O_3$ had higher amount of oxygen vacancies in it, its Fermi level is nearer to the conduction band and a negatively shifted Fermi level is observed in the Mott-Schottky plots. From the above results, two types of hematite with different Fermi levels were successfully obtained by controlling the amount of oxygen vacancies during the preparation process.

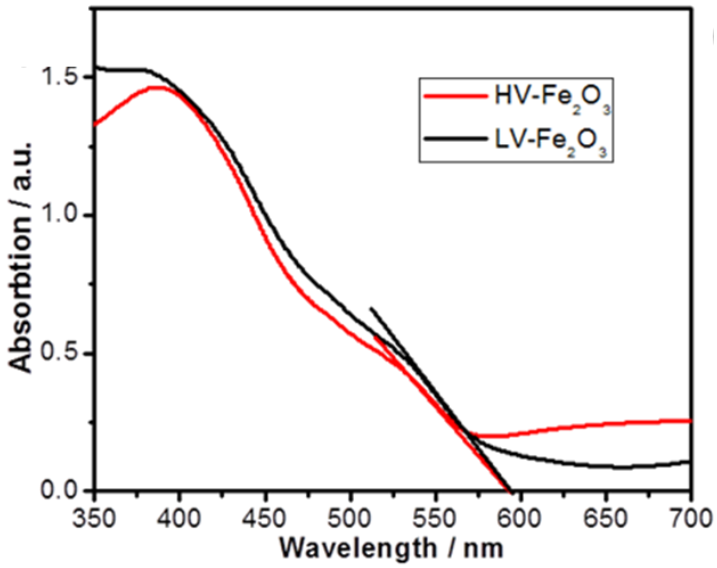



**Figure 2.4** UV-vis absorption spectra of single type of HV-$Fe_2O_3$ and single LV-$Fe_2O_3$ films respectively.

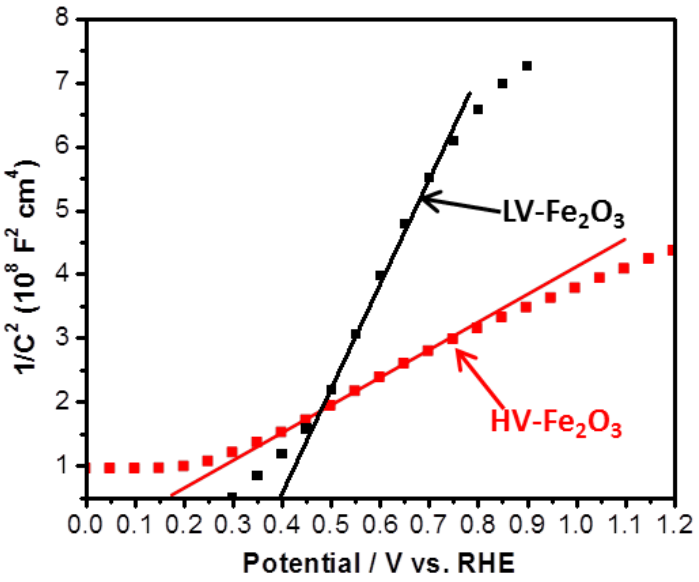



**Figure 2.5** Mott-schottky plots at 1 KHz of single type of HV-$Fe_2O_3$ and single LV-$Fe_2O_3$ films respectively

SEM images showed that the surfaces of HV-$Fe_2O_3$ and LV-$Fe_2O_3$ were similar, with a flat and smooth morphology (Figure 2.6). As reported in our previous reports, the deposition rates for Fe based oxide materials were almost the same (3.5 nm/min),[22] so the HV-$Fe_2O_3$ and LV-$Fe_2O_3$ films had nearly the same thickness with the same deposition time as shown in Figure 2.7.

Variation of photocurrent for hematite films with different thickness is tested and summarized. The photocurrent density for single HV-$Fe_2O_3$ increased gradually with the thickness increasing and it reached the highest at 70 nm. Then it decreased at a much lower rate when the thickness exceeded 70 nm (Figure 2.8). A similar relationship existed for LV-$Fe_2O_3$ between the photocurrent density and its thickness (Figure 2.9). As a result, both HV-$Fe_2O_3$ and LV-$Fe_2O_3$ would perform the highest photocurrent density

when the thickness was about 70 nm according to their linear sweep voltammetry curves.

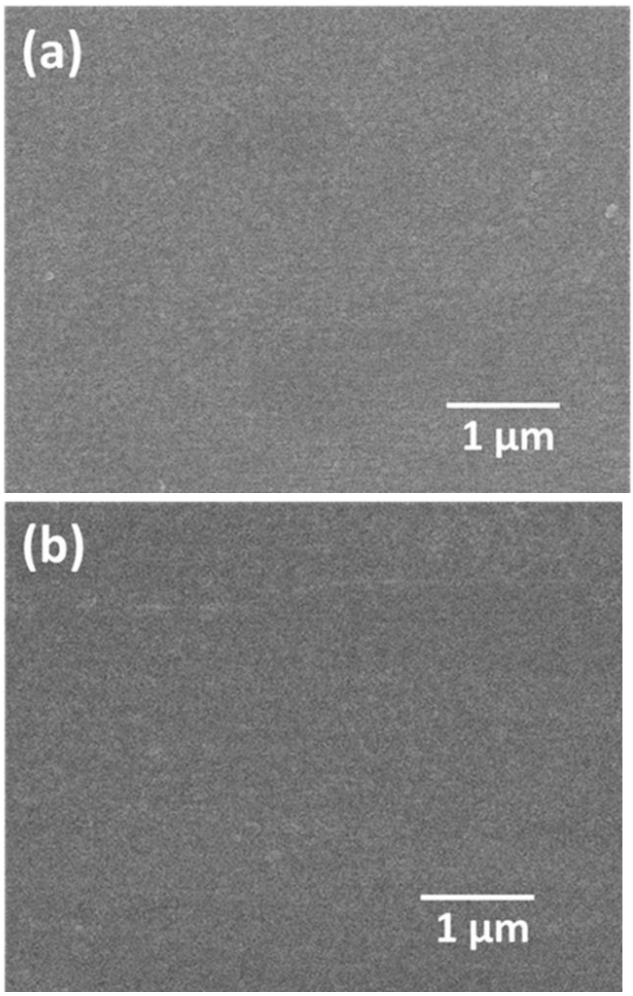



**Figure 2.6** SEM for the surface view of HV-$Fe_2O_3$ (a) and LV-$Fe_2O_3$ (b) irradiated by the laser for 20 minutes.

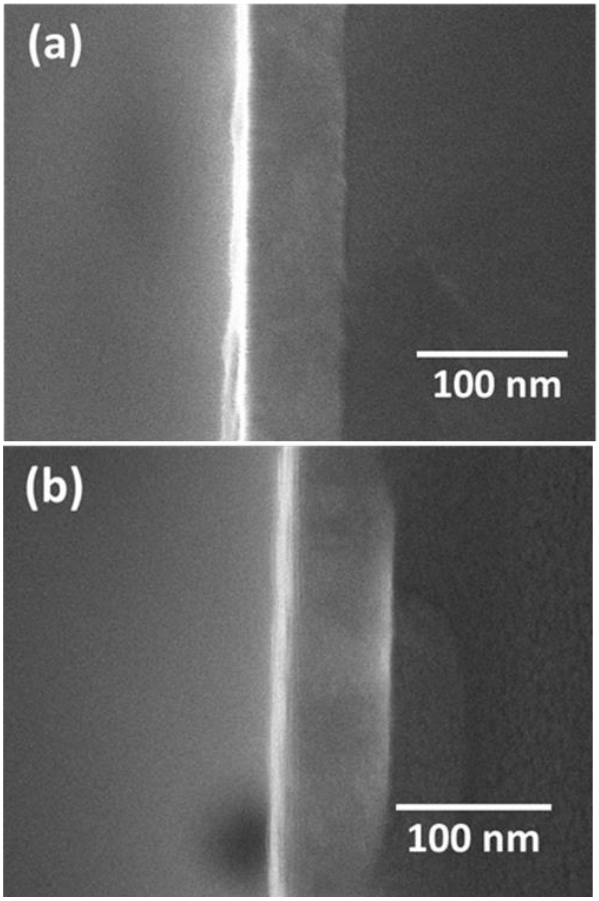



**Figure 2.7** SEM for the cross view of HV-$Fe_2O_3$ (a) and LV-$Fe_2O_3$ (b) irradiated by the laser for 20 minutes. The thicknesses of them are about 70 nm.

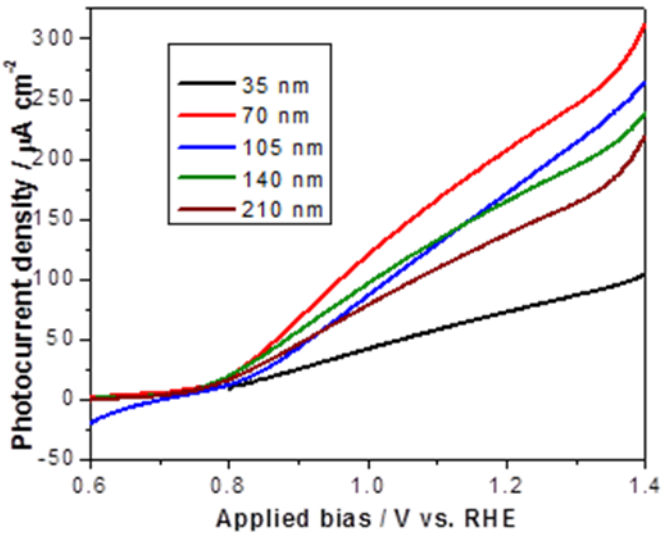



**Figure 2.8** LSV curves for HV-$Fe_2O_3$ films with different thicknesses.

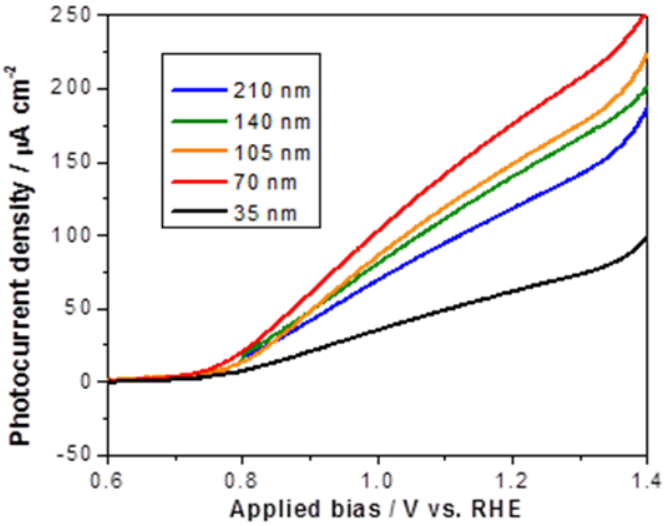



**Figure 2.9** LSV curves for LV-$Fe_2O_3$ films with different thicknesses.

### 2.3.2 Preparation and PEC perforance of hematite homojunction photoanodes (HV/LV-$Fe_2O_3$).

The photocurrent densities at 1.23 V vs. RHE for HV-$Fe_2O_3$ and LV-$Fe_2O_3$ were summarized in Figure 2.10 a. The HV-$Fe_2O_3$ had a little higher photocurrent density compared with LV-$Fe_2O_3$ due to its extra light absorption after 600 nm. The two types of hematite (HV-$Fe_2O_3$ and LV-$Fe_2O_3$) with different Fermi levels were combined into homojunctions to get an enhanced PEC performance for hematite.

HV-$Fe_2O_3$ was prepared on ITO firstly, and LV-$Fe_2O_3$ was deposited on the surface of HV-$Fe_2O_3$ subsequently. The thickness of the inner HV-$Fe_2O_3$ layer was fixed on 70 nm, as it showed the best PEC performance with this thickness. Linear sweep voltammetry curves (LSV) according to the thickness of the outer layer (LV-$Fe_2O_3$) were detected (Figure 2.10 b) to find the best match of HV-$Fe_2O_3$ and LV-$Fe_2O_3$. The onset potential was the lowest when the thickness of the LV-$Fe_2O_3$ reached about 70 nm. The

photocurrent densities with different thicknesses of hematite homojunction photoanodes (HV/LV-$Fe_2O_3$) were summarized in Figure 2.10 a (star points). It is clear that when the

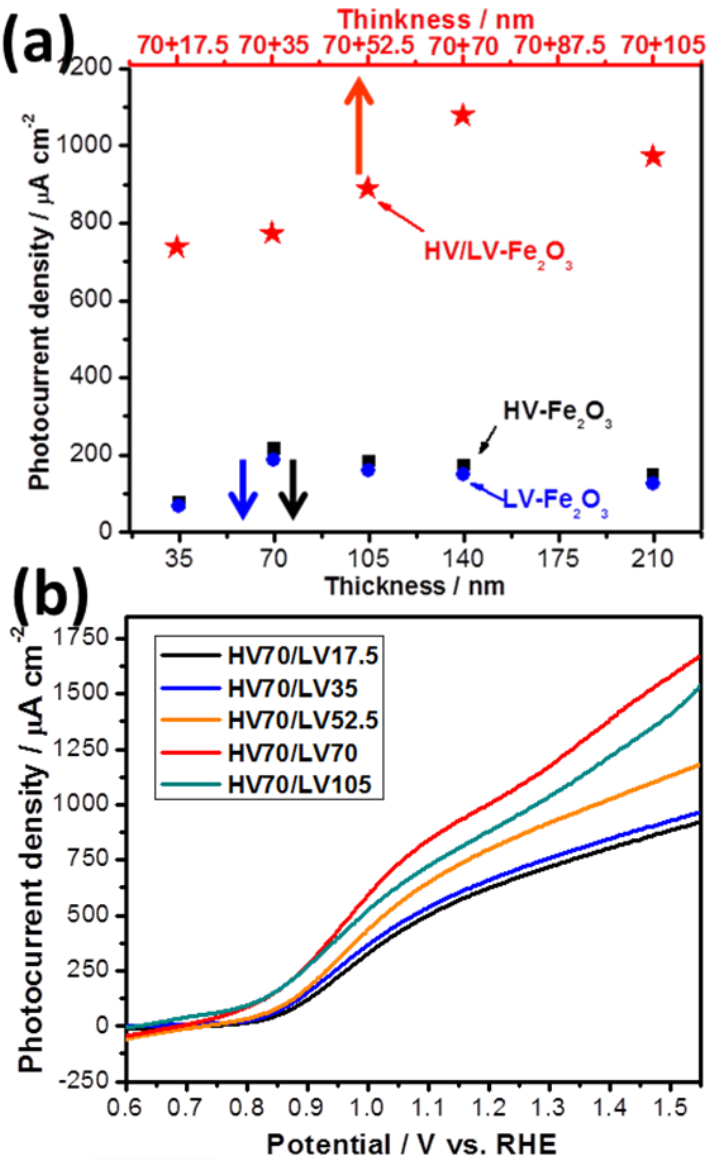



**Figure 2.10** (a) Comparison of photocurrent densities for single HV-$Fe_2O_3$ layer, single LV-$Fe_2O_3$ and HV/LV-$Fe_2O_3$ homojunctions at 1.23 V vs. RHE respectively. (b) Linear sweep voltammetry curves for HV/LV-$Fe_2O_3$ homojunctions with different thickness. The thickness of the inner HV-$Fe_2O_3$ layer was 70 nm. And the thicknesses of the outer LV-$Fe_2O_3$ layers were 17.5, 35, 52.5, 70 and 105 nm respectively. The light source is AM 1.5 G illumination.

thickness of the homojunction photoanodes reached 140 nm (70 nm for HV-$Fe_2O_3$ layer and 70 nm for LV-$Fe_2O_3$ layer), the photoanodes performed the highest photocurrent densities. As a result, the best design for hematite homojunctions was fixed as 70 nm for the inside HV-$Fe_2O_3$ layer and 70 nm for the outside LV-$Fe_2O_3$ layer.

The cross view for the best HV/LV-$Fe_2O_3$ homojunction photoanode is shown in Figure 2.11 while the inset in it is the picture illustrated for the structure of HV/LV-$Fe_2O_3$ homojunction photoanodes. The surface morphology by Atomic Force Microscopy (AFM) is shown in Figure 2.12. The roughness was about 4.6 nm, indicating the obtained photoanodes had a quite flat and smooth morphology similar with single HV-$Fe_2O_3$ and single LV-$Fe_2O_3$ films (Figure 2.6).

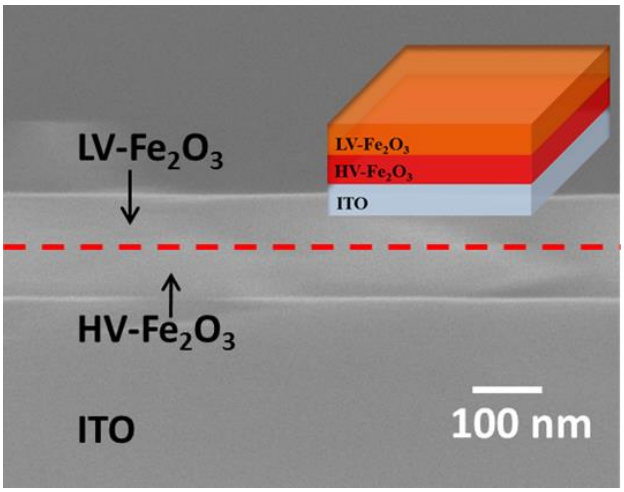



**Figure 2.11** SEM for the cross view of HV/LV-$Fe_2O_3$ homojunction photoanodes.

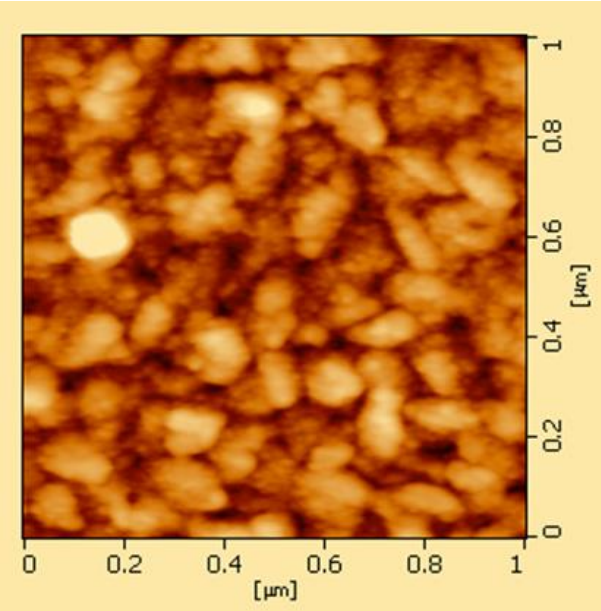



**Figure 2.12** AFM for HV/LV-$Fe_2O_3$ homojunction photoanodes.

The comparison of PEC performances for single HV-$Fe_2O_3$, single LV-$Fe_2O_3$ and HV/LV-$Fe_2O_3$ homojunction photoanodes are shown in Figure 2.13 and 2.14. The onset potential for single HV-$Fe_2O_3$ and LV-$Fe_2O_3$ was relatively high, about 1.08 V vs. RHE, while that of HV/LV-$Fe_2O_3$ was only 0.86 V vs. RHE (Figure 2.13). The detailed photocurrent density at 1.23 V vs. RHE is illustrated in Figure 2.14. The photocurrent densities for single HV-$Fe_2O_3$ and LV-$Fe_2O_3$ were 217 µA/$cm^2$ and 189 µA/$cm^2$ respectively. Interestingly, the photocurrent density for HV/LV-$Fe_2O_3$ was ~1070 µA/$cm^2$, which was about 5 times of single HV-$Fe_2O_3$ and LV-$Fe_2O_3$. The improvement of photocurrent density is much more obvious for the as-preapred HV/LV-$Fe_2O_3$ homojunction (~5 times imprvement) than the previous reported Mg-$Fe_2O_3$/$Fe_2O_3$ p-n junction (1.3 times improvement).[31] Besides, the photocurrent density at 1.23 V vs. RHE for HV/LV-$Fe_2O_3$ homojunction is ~2 times of Mg-$Fe_2O_3$/$Fe_2O_3$ homojunction,

indicating hematite homojunction formed by oxygen vacancy controlling is more effective than that doped with Mg element.

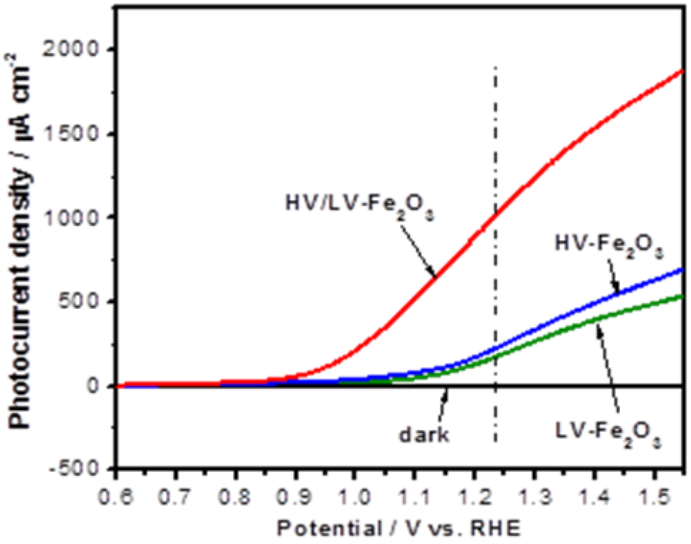



**Figure 2.13** Linear sweep voltammetry curves for single HV-$Fe_2O_3$ layer, single LV-$Fe_2O_3$ and HV/LV-$Fe_2O_3$ homojunction photoanodes respectively.

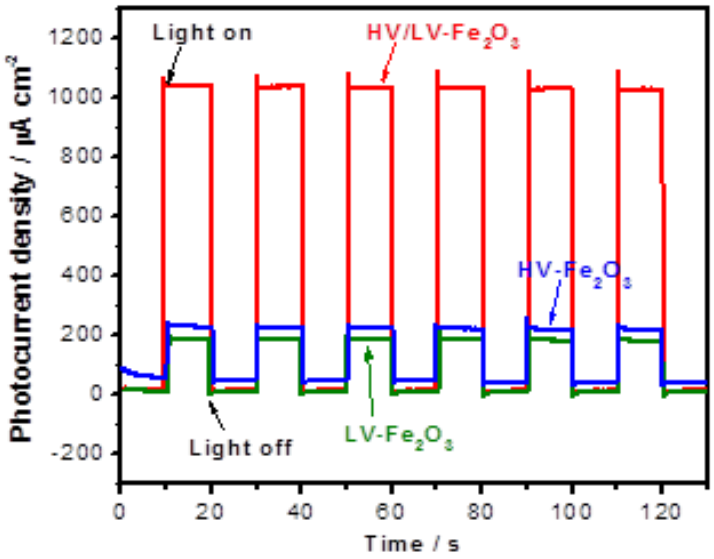



**Figure 2.14** Current-time curves for single HV-$Fe_2O_3$ layer, single LV-$Fe_2O_3$ and HV/LV-$Fe_2O_3$ homojunction photoanodes respectively.

### 2.3.3 Mechanism discussion.

The greatly improved photocurrent density in Figure 2.13 and 2.14 indicated that a homojunction was really existed in the HV/LV-$Fe_2O_3$ photoanodes. To gain further insight into the charge-transfer process, electrochemical impedance spectra (EIS) plots (Figure 2.15) and open circuit photovoltage (OCP) curves (Figure 2.16) were collected under light illumination. The radius of the arcs of Nyquist plots for HV/LV-$Fe_2O_3$ homojunctions was much smaller than both single HV-$Fe_2O_3$ and LV-$Fe_2O_3$, indicating the HV/LV-$Fe_2O_3$ homojunctions had higher charge transfer efficiency under light illumination. Besides, a nearly two-times larger OCP is observed for the sample of HV/LV-$Fe_2O_3$ homojunction than single type of hematie, indicating an enlarged band bending at the photoanode/electrolyte interface existed in it which represents the enhanced electron-hole separation.[30] From these two figures, both the charge transportation efficiency and the charge separation efficiency were improved after the formation of homojunctions.

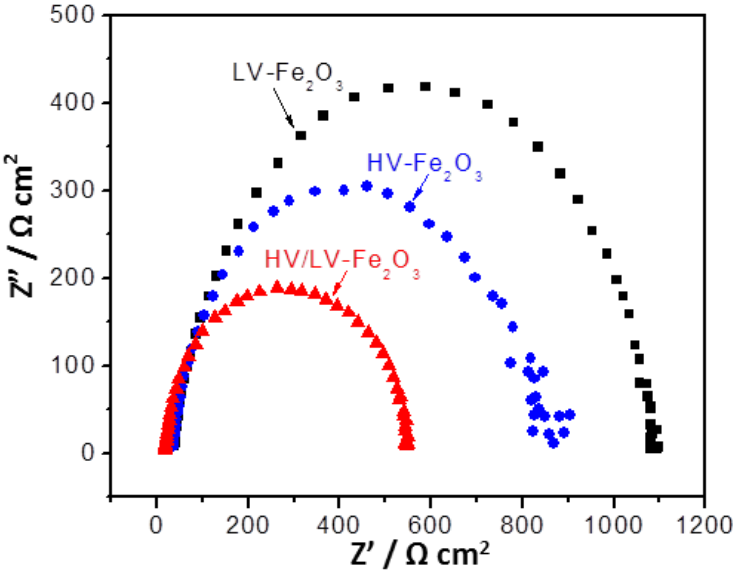



**Figure 2.15** Electrochemical impedance spectra curves and for single HV-$Fe_2O_3$ layer, single LV-$Fe_2O_3$ and HV/LV-$Fe_2O_3$ homojunction photoanodes respectively.

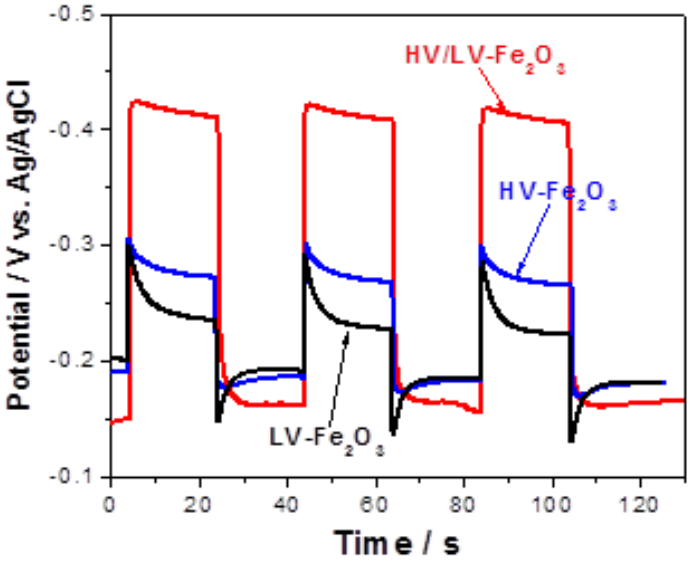



**Figure 2.16** Open circuit potentials for single HV-$Fe_2O_3$ layer, single LV-$Fe_2O_3$ and HV/LV-$Fe_2O_3$ homojunction photoanodes respectively.

The energy diagrams of single HV-$Fe_2O_3$, single LV-$Fe_2O_3$ and HV/LV-$Fe_2O_3$ homojunction are shown in Figure 2.17 as well as the expected charge flow of

homojunction photoanode. Since the HV-$Fe_2O_3$ and LV-$Fe_2O_3$ had the same phases (Figure 2.1, Figure 2.3) and band gaps (Figure 2.4), it is considered that the positions of their conduction band and valence band are the same before contact. The difference between them in the energy diagram was that the Fermi level in HV-$Fe_2O_3$ is 0.22 V negatively shifted than LV-$Fe_2O_3$ as discussed previously. After these two types of hematite contacted with each other, a homojunction formed at the interface between them. The holes in HV-$Fe_2O_3$ transferred to the valance band of LV-$Fe_2O_3$, while the electrons in LV-$Fe_2O_3$ transferred to the conduction band of HV-$Fe_2O_3$. Therefore, more holes would accumulate on the surface of LV-$Fe_2O_3$ and involved in the water oxidation reaction due to the electronic field formed in the homojunction. The homojunction made the charge transfer efficiency (Figure 2.15) and charge separation efficiency (Figure 2.16) in the photoanodes much higher than single type of hematite therefore a dramatically enhanced photocurrent density occurred as shown in the current-time curves (Figure 2.14). Besides, as the holes were mainly accumulated on the surface of the LV-$Fe_2O_3$, the inner layer with high oxygen vacancy can be stabilized and protected by the outer layer with low oxygen vacancy during the anodic oxidation for oxygen evolution at semiconductor/liquid interface.

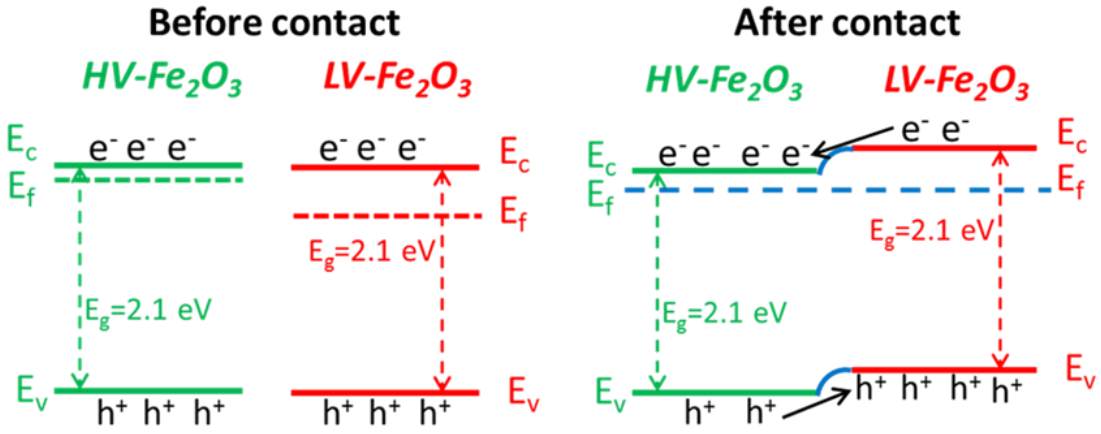



**Figure 2.17** Energy diagrams of single HV-$Fe_2O_3$ layer, single LV-$Fe_2O_3$ and HV/LV-$Fe_2O_3$ homojunction photoanodes respectively and the expected charge flow of homojunction photoanode.

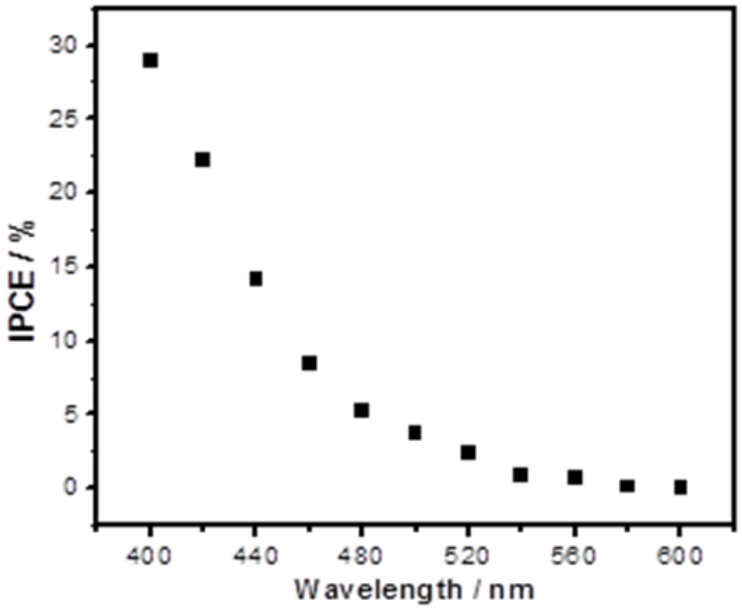



**Figure 2.18** Incident photo-to-current conversion efficiency (IPCE) of the HV/LV-$Fe_2O_3$ homojunction.

Incident photo-to-current efficiency (IPCE) curves (Figure 2.18) was used to determine the light usage efficiency of the HV/LV-$Fe_2O_3$ homojunction photoanodes. It is observed that light with wavelength below 600 nm can make some contribution to the

photocurrent density according to the IPCE curve. The IPCE increased gradually with light wavelength decreased and it reached the highest at 400 nm for about 29.0%.

### 2.3.4 Long-time water splitting perforances of hematite homojunction photoanodes (HV/LV-$Fe_2O_3$).

Long-time water splitting experiments were further monitored using air mass 1.5 G (AM 1.5 G) as the light source with a 1.23 V vs. RHE (Figure 2.19) external bias in 1 M NaOH solution. Its corresponding current-time curves are shown in Figure 2.10. The dashed line in Figure 8a is the theory amount of oxygen gas calculated from the current-time curves. It is observed that the dashed line was almost the same with the oxygen evolution dots, indicating the anodic photocurrent generated by the HV/LV-$Fe_2O_3$ homojunction photoanode is the exclusive result of $O_2$ evolution from water splitting. The ratio of $H_2$ and $O_2$ evolution rates was nearly 2:1, implying the oxygen vacancies were not involved in the water oxidation reaction and overall water splitting occurred in this HV/LV-$Fe_2O_3$-Pt PEC system. The water splitting rates in this system were high, which were about 22.9 μmol/h for $H_2$ evolution and 12.6 μmol/h for $O_2$ evolution respevtively. A Faradaic efficiency of nearly 100% was achieved by comparing the ideal oxygen evolution curve (dashed line) and the actual oxygen evolution curve. Moreover, the HV/LV-$Fe_2O_3$ homojunction photoanode (Figure 2.20) showed 15 times higher stability compared with single HV-$Fe_2O_3$ (Figure 2.21). This also confirmed that the inner HV-$Fe_2O_3$ is successfully protected by the outer LV-$Fe_2O_3$.

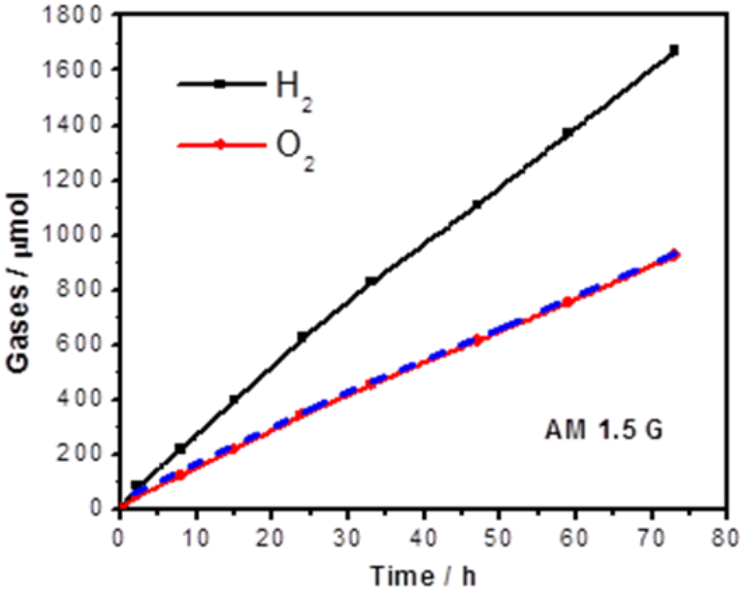



**Figure 2.19** Time courses of gases evolution for HV/LV-$Fe_2O_3$ homojunction photoanodes. The dashed line is the oxygen gases calculated from the corresponding current-time curves (Figure 2.20).

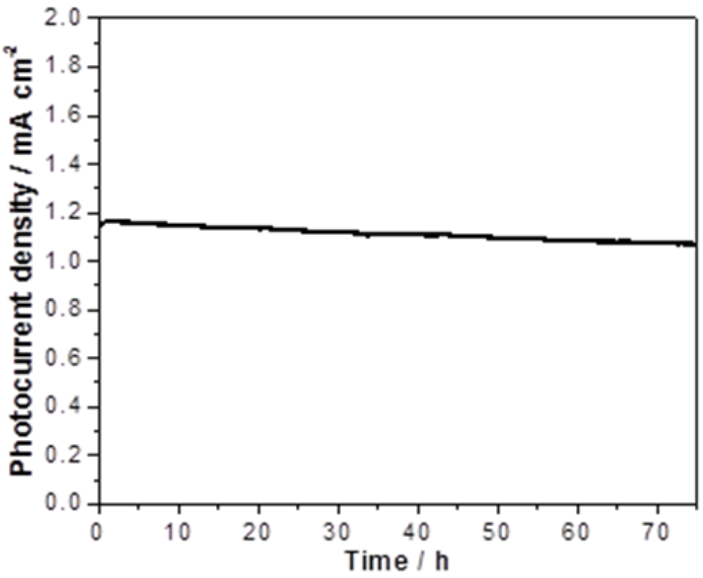



**Figure 2.20** The current-time curve for HV/LV-$Fe_2O_3$ homojunction photoanodes.

The gases evolution amounts for HV/LV-$Fe_2O_3$ increased almost linearly with time accumulating for 73 hours. And the photocurrent still held 92.2% even after 73 hours

water splitting.

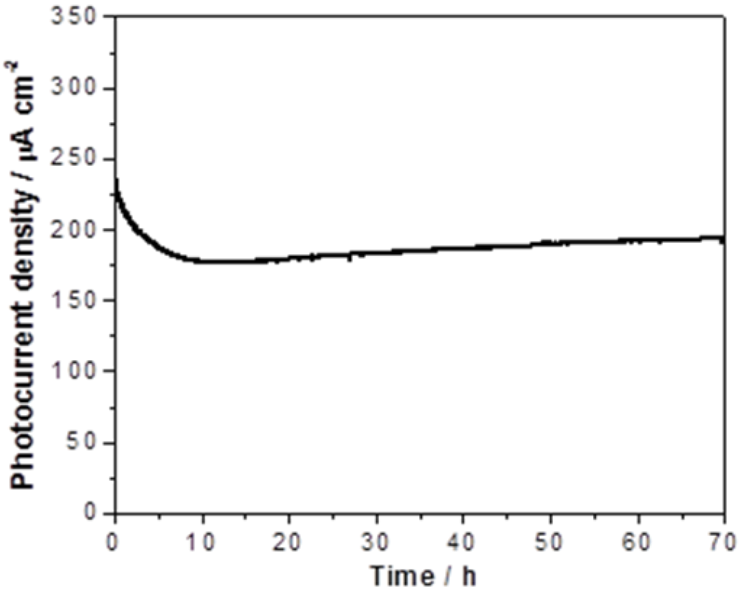



**Figure 2.21** Long-time I-T curves of single HV-$Fe_2O_3$.

## 2.4 Conclusions

In this chapter, hematite homojunction photoanodes were prepared by controlling the density of oxygen vacancies in hematite. With the homojunction configuration, the photoelectrochemical performances of hematite have been greatly improved due to the high charge separation efficiency in the electrode.

As is commonly known, the Fermi level of an n-type oxide semiconductor can be modulated nearer to conduction band by increasing the majority carrier concentration in it. This makes it possible to construct homojunction photoelectrodes within hematite by combining two layers with different carrier concentrations. As a result, two types of hematite layers with different carrier concentration can be easily obtained by

introducing artificial oxygen vacancies in them. After combining two hematite layers with different Fermi levels, a homojunction formed between them which made the hole-electron separation more efficient in photoanodes. The PEC performances of hematite is greatly improved after homojunction formation with the onset potential decreased more than 100 mV while the photocurrent density increased to nearly 5 times (1.1 $mA/cm^2$) at 1.23 V vs. RHE under AM 1.5 G illumination. And with this homojuction configuration, the hematite homojunctions showed 15 times higher stability compared with the high-vacancy (high-donor-concentration) $Fe_2O_3$ phtoelectrodes for oxygen evolution. Open-circuit-potential study proved that the photovoltage generated by hematite homojunction is more than two times of single layer hematite films and indicated the charge separation efficiency is successfully increased due to the formation of homojunction.

Overall, hematite homojunction photoelectrode was firstly obtained by tuning the vacancy densities in different layers, and showed high efficiency and durability for PEC water oxidation. We believe that the method to tune the Fermi level of semiconductor films by controlling the oxygen vacancies can be extended to other metal oxide semiconductors such as $TiO_2$ and ZnO *et al*. And the formation of homojunction photoelectrodes within these metal oxide semiconductors will offer new opportunities to improve the PEC water splitting efficiency.

## References

[1] S. C. Warren, K. Voitchovsky, H. Dotan, C. M. Leroy, M. Cornuz, F. Stellacci, C. Hebert, A. Rothschild, M. Gratzel, *Nat. Mater.* 2013, **12**, 842.

[2] B. Klahr, S. Gimenez, F. Fabregat-santiago, T. Hamann, J. Bisquert, *J. Am. Chem. Soc.* 2012, **134**, 4294.

[3] N. J. Cherepy, D. B. Liston, J. A. Lovejoy, H. Deng and J. Z. Zhang, *J. Phys. Chem. B*, 1998, **102**, 770–776.

[4] A. G. Joly, J. R. Williams, S. A. Chambers, G. Xiong, W. P. Hess and D. M. Laman, *J. Appl. Phys.*, 2006, **99**, 053521.

[5] J. H. Kennedy and J. K. W. Frese, *J. Electrochem. Soc.*, 1978, **125**, 709.

[6] I. Justicia, P. Ordej´on, G. Canto, J. L. Mozos, J. Fraxedas, G. A. Battiston, R. Gerbasi and A. Figueras, *Adv. Mater.* 2002, **14**, 1399.

[7] S. Polarz, J. Strunk, V. Ischenko, M. W. E. van den Berg, O. Hinrichsen, M. Muhler, M. Driess, *Angew. Chem., Int. Ed.* 2006, **45**, 2965.

[8] R. Schaub, P. Thostrup, N. Lopez, E. Lægsgaard, I. Stensgaard, J. K. Nørskov, F. Besenbacher, *Phys. Rev. Lett.* 2001, **87**, 266104.

[9] I. S. Cho, M. Logar, C. H. Lee, L. Cai, F. B. Prinz, X. Zheng, *Nano Lett.* 2014, **14**, 24.

[10] C. Mao, F. Zuo, Y. Hou, X. Bu, P. Feng, *Angew. Chem. Int. Ed.* 2014, **53**, 10485.

[11] X. Chen, L. Liu, P. Y. Yu and S. S. Mao, *Science* 2011, **331**, 746.

[12] G. Wang, H. Wang, Y. Ling, Y. Tang, X. Yang, R. C. Fitzmorris, C. Wang, J. Z. Zhang, Y. Li, *Nano Lett.* 2011, **11**, 3026.

[13] Q. Kang, J. Cao, Y. Zhang, L. Liu, H. Xu, J. Ye, *J. Mater. Chem. A* 2013, **1**, 5766.

[14] F. Zuo, L. Wang, T. Wu, Z. Zhang, D. Borchardt and P. Feng, *J. Am. Chem. Soc.* 2010, **132**, 11856.

[15] H. Li, Y. Zhou, W. Tu, J. Ye, Z. Zou, *Adv. Funct. Mater.* 2015, **25**, 998.

[16] S. W. Boettcher, E. L. Warren, M. C. Putnam, E. A. Santori, D. Turner-Evans, M. D. Kelzenberg, M. G. Walter, J. R. McKone, B. S. Brunschwig, H. A. Atwater, N. S. Lewis, *J. Am. Chem. Soc.* 2011, **133**, 1216.

[17] F. F. Abdi , L. H. Han , A. H. M. Smets , M. Zeman , B. Dam , R. vande Krol , *Nat. Commun.*2013, **4**, 2195.

[18] J. Cao, J. Xing, Y. Zhang, H. Tong, Y. Bi, T. Kako, M. Takeguchi, J. Ye, *Langmuir* 2013, **29**, 3116.

[19] J. Cao, Y. Zhang, H. Tong, P. Li, T. Kako, J. Ye, *Chem. Commun.*, 2012, **48**, 8649.

[20] Y. W. Li, Z. G. Hu, F. Y. Yue, P. X. Yang, Y. N. Qian, W. J. cheng, X. M. Ma, J. H. Chu, *J. Phys. D: Appl. Phys.* 2008, **41**, 215403.

[21] H. Lin, A. K. rumaiz, M. Schulz, D. Wang, R. Rock, C. P. Huang, S. I. Shah, *Mater. Sci. Eng. B* 2008, **151**, 133.

[22] J. Cao, T. Kako , N. Kikugawa , J. Ye , *J. Phys. D: Appl. Phys.* 2010, **43**, 325101.

[23] I. V. Chernyshova, M. F. Hochella Jr, A. S. Madden, *Phys. Chem. Chem. Phys.* 2007, **9**, 1736.

[24] N. D. Phu, D. T. Ngo, L. H. Hoang, N. H. Luong, N. Chau, N. H. Hai, *J. Phys. D: Appl. Phys.* 2011, **44**, 345002.

[25] J. Gan, X. Lu, J. Wu, S. Xie, T. Zhai, M. Yu, Z. Zhang, Y. Mao, S. Wang, Y. Shen, Y. Tong, *Sci. Rep.* 2013, **3**, 1021.

[26] X. Lu, Y. Zeng, M. Yu, T. Zhai, C. Liang, S. Xie, M. Balogun, Y. Tong, *Adv. Mater.* 2014, **26**, 3148.

[27] A. Tamilselvan, S. Balakumar, M. Sakar, C. Nayek, P. Murugavel, K. S. Kumar, *Dalton Trans.* 2014, **43**, 5731.

[28] S. Park, J. Lee, J. S. Jang, H. Rhu, H. Yu, B. Y. You, C. S. Kim, K. J. Kim, Y. J. Cho, S. Baik, W. Lee, *Nanotechnology* 2013, **24**, 295202.

[29] M. Grätzel, *Nature* 2001, **414**, 338.

[30] M. Zhong, T. Hisatomi, Y. Kuang, J. Zhao, M. Liu, , A. Iwase Q. Jia, H. Nishiyama, T. Minegishi, M. Nakabayashi, N. Shibata, R. Niishiro, C. Katayama, H. Shibano, M. Katayama, A. Kudo, T. Yamada, K. Domen, *J. Am. Chem. Soc.*, 2015, **137**, 5053.

[31] Y. Lin, Y. Xu, M. T. Mayer, Z. I. Simpson, G. McMahon, S. Zhou, D. Wang, *J. Am. Chem. Soc.*, 2012, **134**, 5508.

[32] Pulsed Laser Deposition of Thin Films, edited by Douglas B. Chrisey and Graham K. Hubler, John Wiley & Sons, 1994 ISBN 0-471-59218-8

# Chapter 3 Hematite Films Decorated with Nanostructured Ferric Oxyhydroxide

## 3.1 Introduction

Hematite ($\alpha$-$Fe_2O_3$) photoanodes is one of the most promising candidates for water splitting due to its suitable band gap (2.0-2.1 eV) in the visible-light range, high durability in aqueous and under water oxidation potentials, nontoxicity, and earth-abundance.[1-3] However, the low conductivity, limited carrier life time, short hole diffusion length (2-4 nm) and high electron-hole recombination rate have prevented the performance of hematite for future applications in photo-to-electricity conversion.[4-6] Consequently, it is preferable to prepare hematite films within hundreds of nanometers so that the photo-generated holes can be transferred to the electrode/electrolyte interface to react with water before recombining with electrons at the defects area in the material. Hematite homojunction has been successfully obtained with superior activity as introduced in Chapter 2 due to the improved charge separation efficiency. However, the photocurrent density is still far from required and the onset potential is too large due to the high charge transfer kinetic bariers at the hematite/electrolyte surface. The charge trasfer resistance need to be further reduced to improve the PEC performance of hematite. In addition, providing high specific surface area for efficient light harvesting towards these thin absorber films ($Fe_2O_3$, $BiFe_2O_4$ and other iron based films) is an effective pathway to overcome the above-mentioned

disadvantages.[7-14]

Generally, loading oxygen evolution catalysts on the surface of hematite as cocatalysts is one of the most popular means to lower oxygen evolution reaction barrier, which has obtained considerable developments due to rich choices in such kind of materials for matching.[15] Up-to-date, various materials have been tried to deposited on the surface of hematite, including $IrO_2$ nanoparticles,[16] cobalt phosphate (Co-pi) nanoparticles,[17] nickel(II) hydroxide layers,[18] and $NiFeO_x$ layers[19]. Although these cocatalysts have already realized reduction of onset potential to pure hematite for oxygen evolution, some of them are still faced with limitations such as instability and light absorbance competition in the visible-light range. In addition, considering the possibility for future application, the full-scale photoanodes should not contain any expensive elements such as Au, Pd, Rh *et al.*, so oxygen evolution reaction catalysts like $RuO_x$ and $IrO_x$ were out of researchers' considerations. Ferric oxyhydroxide (FeO(OH)) is considered as a new choice of cocatalyst for water oxidation just in this decades. The applications for FeO(OH) have been studied by several groups in recent years since Fe element is very abundant in the earth just after Si, Al, and O. Plus, it is a stable material in neuter and alkaline conditions under water oxidation potentials. As a result, it has been loaded on the surface of some promising photoanodes including Si[20-22], $BiVO_4$[5], and have shown developed photoelectrochemical performances for both onset potentials and photocurrent densities.

In this chapter, FeO(OH) were expected to decorate on the surface of hematite to

improve the photoelectrochemical performance of it. As the hematite films we obtained previously were prepared by pulsed laser deposition (PLD) on Indium Tin oxide (ITO) substrate, it usually has a smooth and flat morphology. The photoelectrochemical perforamnces of hematite were limited due to its low specific surface area. To overcome such drawbacks, nanostructured materials is preferred to load on the surface to increase its reaction area. Although FeO(OH) prepared in the previous report are usually have a flat morphology,[5,20] it is likely to form nanostructured morphology on the surface of hematite due to the similar Fe-O bands between them. Overall, nanostructured FeO(OH) is expected to firstly decorate on the surface of $Fe_2O_3$ photoanode (simplified as $Fe_2O_3$/FeO(OH)) to realize higher water oxidation rate and durability. And the FeO(OH) decorated hematite may show potentials as an all-Fe-based photoanode for photoelectrochemical water oxidation.

## 3.2 Experiments

### 3.2.1 Preparation of FeO(OH) decorated hematite photoanodes

Firstly, $Fe_2O_3$ thin films were prepared by PLD method using a $Fe_2O_3$ pellet as the target and In doped tin oxide (ITO) as a substrate according to previous articles.[23] The temperature for hematite deposition was 550°C, and the target was irradiated by laser for 20 min. After the laser irradiation, the film was kept at the same temperature in pure oxygen for 20 min. Such prepared hematite film had a thickness about 70 nm.

Secondly, nanostructured FeO(OH) were deposit on the $Fe_2O_3$ by

photoelectrochemical deposition at 0.2 V vs. Ag/AgCl in 0.1 M $FeSO_4$ solution. The light source for PEC deposition was AM 1.5 G.

Finally, the obtained photoanodes were put into the finance at 300 $^{o}$C for 2 hours.

### 3.2.2 **Characterization.**

Raman scattering spectra were measured using the Raman spectroscope (NRS-1000; Jasco Corp. Japan) equipped with an Nd: YAG laser (532 nm). The laser power is 1 mW. Field-emission scanning electron microscope (JSM-6701 F, JEOL) were used to characterize the morphology of the samples. Energy dispersive spectroscopy (SU8000, Hitachi Co., Japan) were used for element characterization. X-ray Photoelectron Spectroscopy (XPS) experiments were performed in a Theta probe (Thermo Fisher) using monochromatic Al Kα X-rays at hν=1486.6 eV. Optical absorption properties of the $Fe_2O_3$ and FeO(OH) were measured through an UV-vis spectrophotometer (UV-2500PC; Shimadzu Co., Japan).

### 3.2.3 Photoelectrochemical Properties

Photoelectrochemical measurements were obtained with an electrochemical station (ALS/CH model 650A) in a three-electrode mode. Platinum and SCE were used as the counter electrode and reference electrode, respectively. AM 1.5 G solar simulation (WXS-80C-3 AM 1.5 G) was utilized as the light sources directly without adding any light filter. The solution for PEC measurements was 1 M NaOH aqueous.

### 3.2.4 Water Splitting

Hydrogen and oxygen generation of the prepared $Fe_2O_3$/FeO(OH) photoanodes were measured using a water splitting system. FeO(OH)/$Fe_2O_3$ film with an area of 1 $cm^2$ on ITO (2 × 1 $cm^2$) was used. 180 ml 1 M NaOH solution was put in a quartz glass cell (~1.0L). Then this glass cell was fixed on the water splitting system which was connected with a closed gas circulation system. There are three parts in the water splitting system including a vacuum line, a reaction cell and a gas sampling port which were shown in Figure S9. The generated $H_2$ and $O_2$ were in situ analyzed with a TCD gas chromatograph (Shimadzu GC-8AIT, argon carrier). Similarly, AM 1.5 G solar simulation (WXS-80C-3 AM 1.5 G) with a light intensity of 100 mW $cm^{-2}$ was utilized as the light sources directly without adding any light filter.

## 3.3 Results and discussion

### 3.3.1 Characterization of FeO(OH) cocatalyst

The details for preparing hematie films by PLD have been illustrated in our previous articles.[23] The freshly prepared $Fe_2O_3$ photoanode showed relatively lower photocurrent compared with other reports. This is because that the films fabricated by PLD are generally smooth with low reaction area. In order to improve the efficiency of

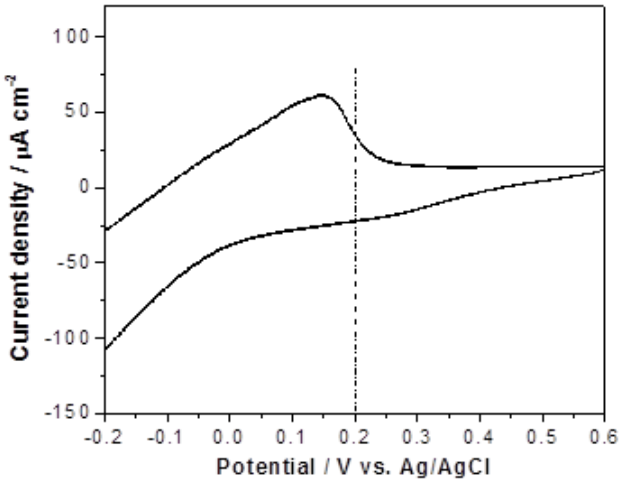



**Figure 3.1** Representative CV scans of $Fe_2O_3$ in Fe deposition bath. The solution is 0.5 M $FeSO_4$.

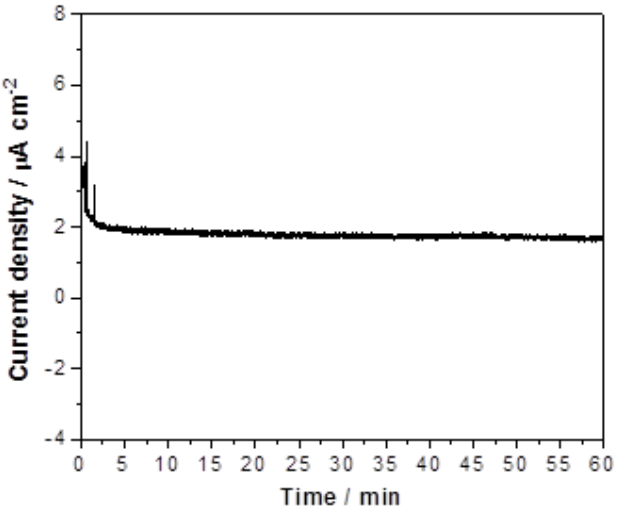



**Figure 3.2** Representative current-time trace at 0.2 V vs. Ag/AgCl of $Fe_2O_3$ in Fe deposition bath. The solution is 0.5 M $FeSO_4$.

the photo generated holes to oxygen and lower the over-potential of $Fe_2O_3$ photoanode, FeO(OH) were deposited by photoelectrodepositon from $FeSO_4$ solution as previous reports.[5] The cyclic-voltammetry (CV) curves of $FeSO_4$ solution baths on $Fe_2O_3$ are shown in Figure 3.1 . Based on the CV curves, the oxidation peak of $Fe^{2+}$ to $Fe^{3+}$ occurred at about 0.14 V vs. Ag/AgCl. As a result, the voltage for FeO(OH) deposition

from $FeSO_4$ was fixed on 0.2 V vs. Ag/AgCl under AM 1.5 G illumination. Representative current-time trace for FeO(OH) deposition is shown in Figure 3.2.

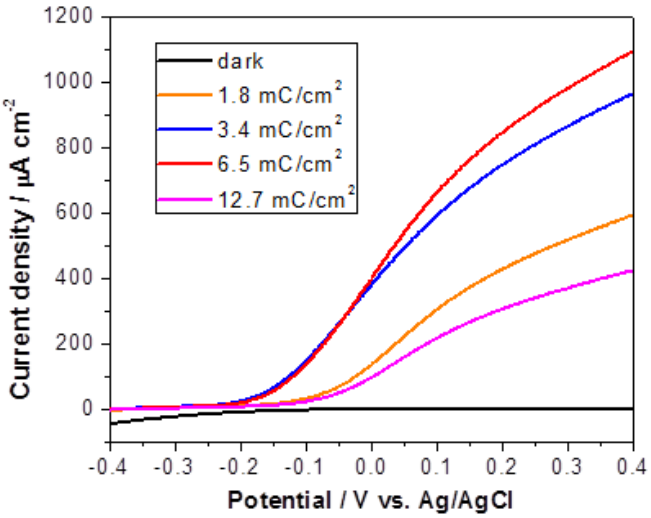



**Figure 3.3** Current-potential curves of $Fe_2O_3$ decorated with different amount of FeO(OH).

FeO(OH) with different amount were fabricated by controlling the deposition time to optimize the maximum photocurrent. The photoelectrochemical performances increase gradually when the amount of FeO(OH) increase until 6.5 $mC \cdot cm^{-2}$. And then decrease dramatically if the amount of FeO(OH) goes on increasing (Figure 3.3). The onset potentials of different samples were shown in (Figure 3.4). The dots were collected from the liner-sweep-voltage curves (Figure 3.3) of them. By comparing all the samples, it is demonstrated that hematite photoanode with about 6.5 $mC \cdot cm^{-2}$ amount of nanostructured FeO(OH) showed the best improvement both in photocurrent density (Figure 3.3) and onset potential (Figure 3.4). As a result, in the following experiments, the FeO(OH) cocatalyst were obtained by photoelectrodeposition on hematite in $FeSO_4$ solution under 0.2 V vs. Ag/AgCl applied bias for 1 hour. And the FeO(OH) amount is

fixed on 6.5 mC·cm$^{-2}$.

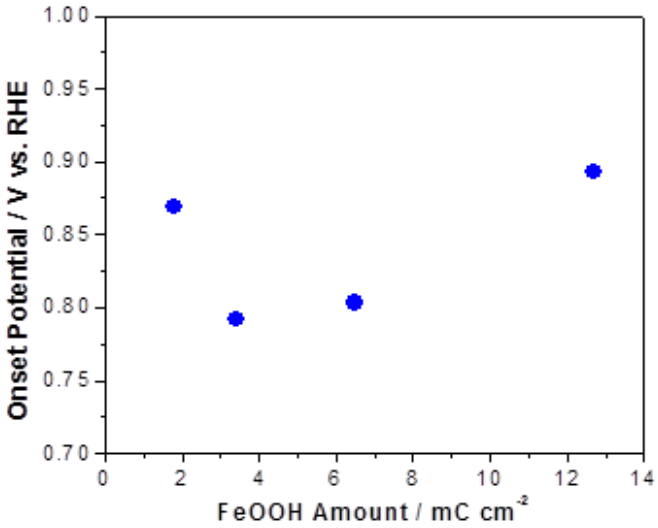



**Figure 3.4** Onset potential of $Fe_2O_3$ decorated with different amount of FeO(OH).

The surface morphology of bare $Fe_2O_3$ and $Fe_2O_3$ loaded with different amount of FeO(OH) cocatalysts are shown in Figure 3.5. The amount of FeO(OH) for samples in Figure 1 b-d were 3.4 mC • cm$^{-2}$, 6.5 mC • cm$^{-2}$, 12.7 mC • cm$^{-2}$ respectively. So the sample showed in Figure 3.5 c had the maxmium photocurrent density among the three samples. It is observed that the surface morphology of $Fe_2O_3$ and FeO(OH) were quite different. The surface of $Fe_2O_3$ by PLD showed a relatively smooth morphology (Figure 3.5 a). And the average roughness was only ~4.5 nm (Figure 3.6). While FeO(OH) by PEC deposition have nanostructured morphologies which slightly varied from the deposition time (Figure 3.5 b-d). It can be observed that in the initial stage of deposition, the FeO(OH) was in form of nanosheet (Figure 3.5 b and c) with thickness only ~15 nm (insert in Figure 3.5 c). The thicknesses of FeO(OH) layer were ~70 nm and ~100 nm respectively as shown in Figure 3.7. As a result, with deposition time increased, not

only the thickness but also the density of FeO(OH) layer was increased. Since the FeO(OH) nanosheets were grown cross the surface of $Fe_2O_3$, the rugged surface formed would

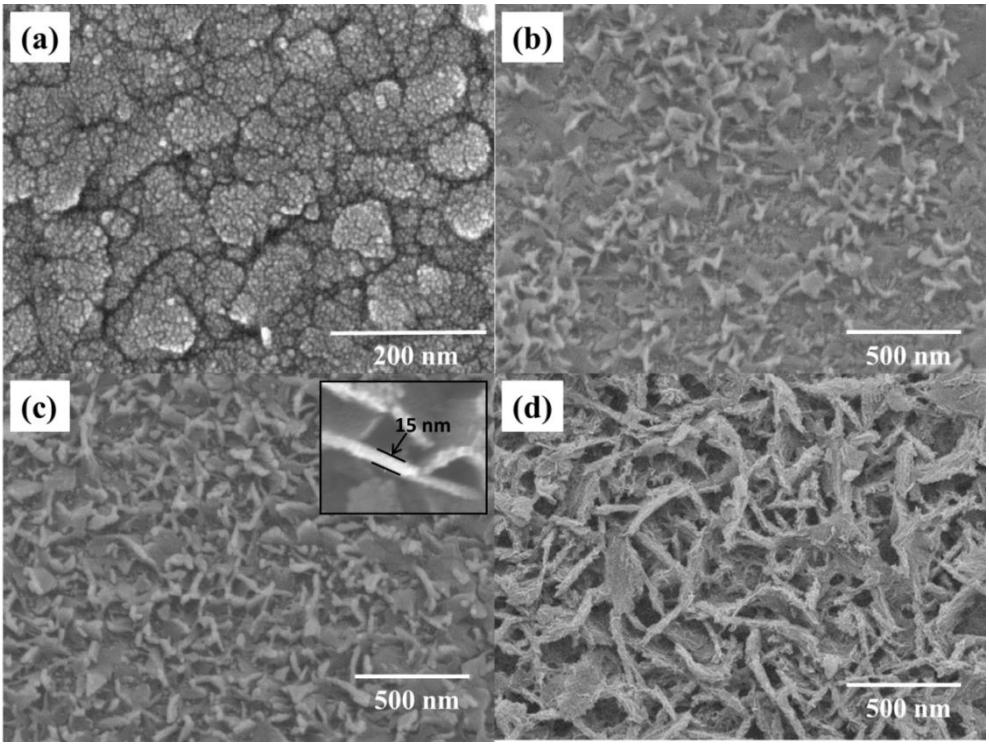



**Figure 3.5** SEM images of (a) bare $Fe_2O_3$, (b)-(d) $Fe_2O_3$ with different amount of FeO(OH). The amount of FeO(OH) for (b)-(d) are 3.4 mC • $cm^{-2}$, 6.5 mC • $cm^{-2}$, 12.7 mC • $cm^{-2}$ respectively.

increase the reaction area of the photoanodes. Besides, after uniformly covered by FeO(OH), the reaction area increased with the deposition time extending. However, when FeO(OH) reached a certain amount, the particles of FeO(OH) grew bigger as shown in Figure 3.5 d. The FeO(OH) were no longer in form of nanosheets, but like ribbons which covered almost the whole surface of $Fe_2O_3$. The FeO(OH) cocatalysts layer is too thick, which prevented the holes from hematite transporting to the surface of

photoanodes. And a decreased photoelectrochemical performance is observed for this sample.

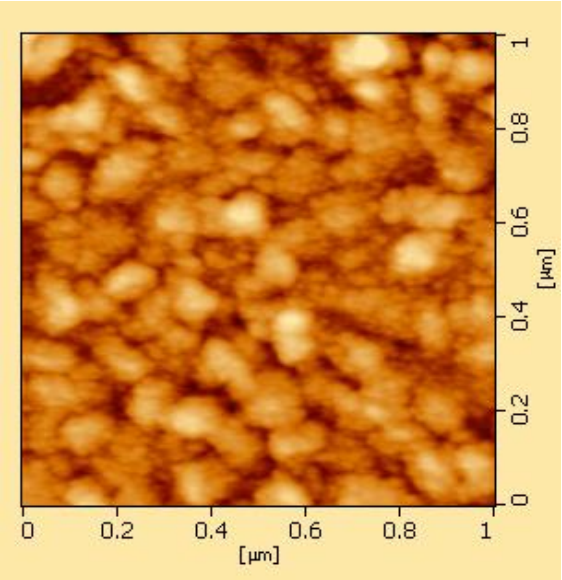



**Figure 3.6** AFM of $Fe_2O_3$ photoanodes.

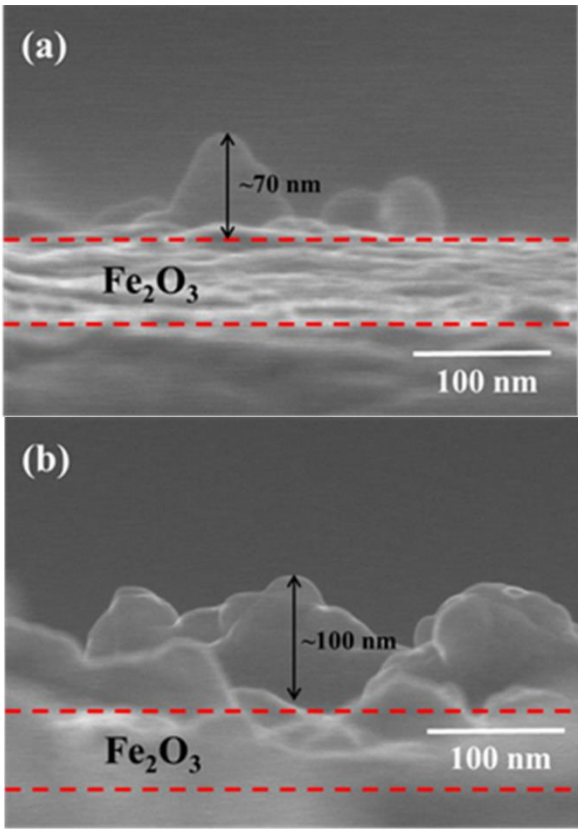



**Figure 3.7** Cross view of $Fe_2O_3$ with 3.4 mC • $cm^{-2}$, 6.5 mC • $cm^{-2}$ FeO(OH) respectively.

As the FeO(OH) was prepared by PEC deposition, it is likely to be amorphous according to previous reports.[4] And the XRD pattern of bare FeO(OH) is shown in the following picture (Figure 3.8). Since the FeO(OH) were prepared by PEC deposition, ITO was used as the conductive substrate. From the XRD, only peaks of ITO were found. This is because of the amorphous FeO(OH) or the limited amount of FeO(OH). However, the wide shape around 30 degree indicates the FeO(OH) were likely to be amorphous in our cases.

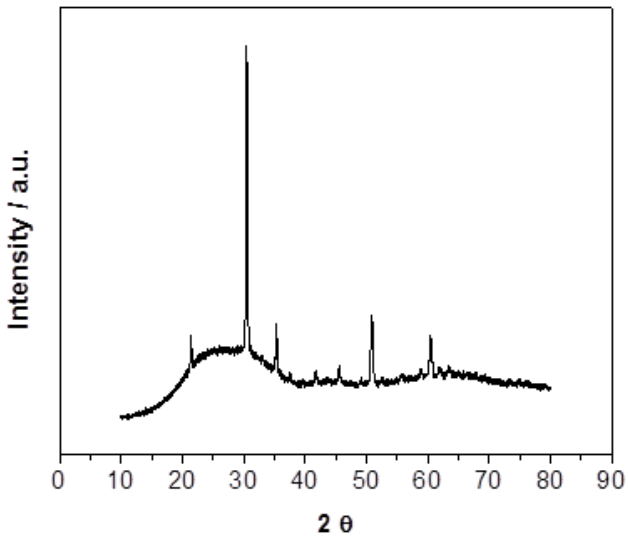



**Figure 3.8** XRD pattern of FeO(OH) deposit on ITO substrate.

As no peaks of FeO(OH) can be found from the XRD, the FeO(OH) was further characterized by XPS (Figure 3.9) and Raman (Figure 3.10). From the XPS spectra of Fe (2p), $Fe^{3+}$ is obviously found. The large area of $Fe^{3+}$ indicates that almost all the $Fe^{2+}$ in $FeSO_4$ was oxidized to $Fe^{3+}$ during the deposition process. In the region of O (1s) in XPS spectra, there are three strong peaks. The lower peak (529.3 eV) is attributed to $O^{2-}$ species while the higher peak (531.0 eV) is attributed to $OH^-$. The peak at 532 eV is attributed to adsorbed water.[20-22] In order to get more insight into the as prepared

FeO(OH) cocatalyst, Raman spectroscopy was also used. The sample for Raman characterization was deposited for 12 hours to get a relatively strong signal. The combination of clear peaks at 475 $cm^{-1}$ and 1000 $cm^{-1}$ are easily distinguished from other iron (oxy)hydroxide spectrums indicating goethite (α-FeO(OH)) was obtained in our experiments (Figure 3.8).[20] The peaks were broad. This is because the goethite prepared by photoelectrodeposition was amorphous in which only a short range order exists.[21,22] Besides, no sulphur peak is found in the EDS spectra as shown in Figure 3.11. From all the results discussed above, the $FeSO_4$ was totally transformed into FeO(OH) on the surface of $Fe_2O_3$ after deposition and post annealing.

Normally, a good cocatalyst should have two aspects. On one hand, the absorption of cocatalysts should not compete with the electrodes. On the other hand, the cocatalysts are usually has no photo-response under illumination since they are usually amorphous. The absorption spectra of $Fe_2O_3$ photoelectrodes with or without nanostructured FeO(OH) are shown in Figure 3.12. The absorption region of FeO(OH) is below 350 nm, indicating the FeO(OH) are not able to compete with $Fe_2O_3$ for the light absorption in the visible light region. Current-potential curves of pure FeO(OH) were further used to make sure whether it made any contribution to the photocurrent density (Figure 3.13).

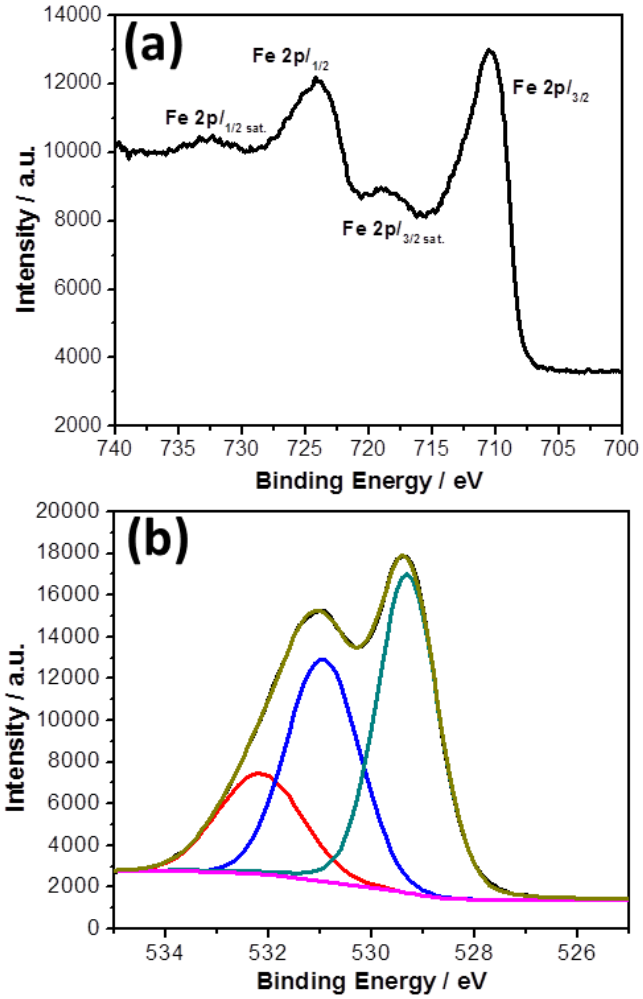



**Figure 3.9** XPS spectrums of Fe (2p) (a) and O (1s) (b) for FeO(OH).

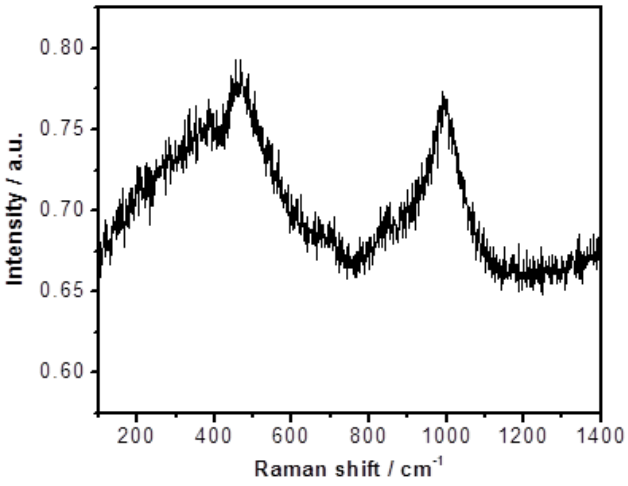



**Figure 3.10** Raman shift of FeO(OH) deposited for 12 hours.

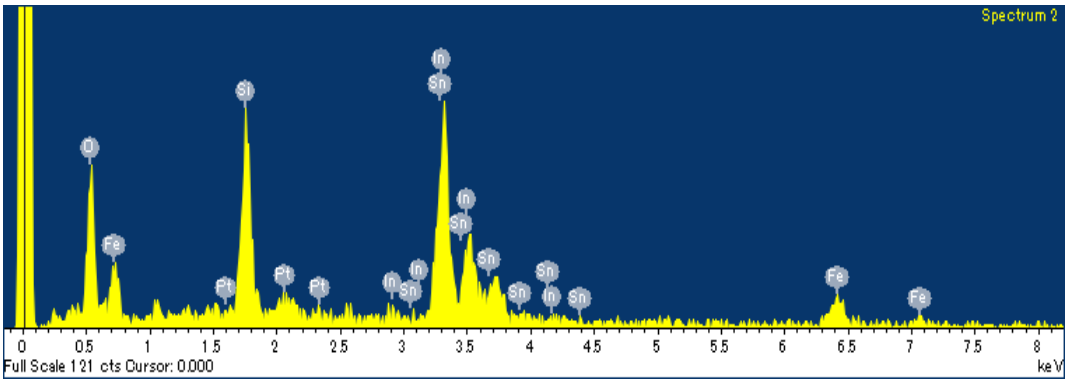



**Figure 3.11** EDS spectrum of $Fe_2O_3$/FeO(OH).

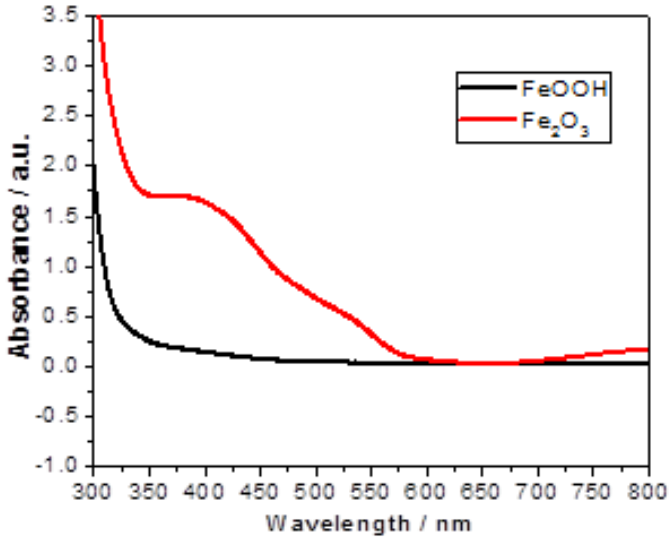



**Figure 3.12** Absorption spectra of bare $Fe_2O_3$ and bare FeO(OH) respectively.

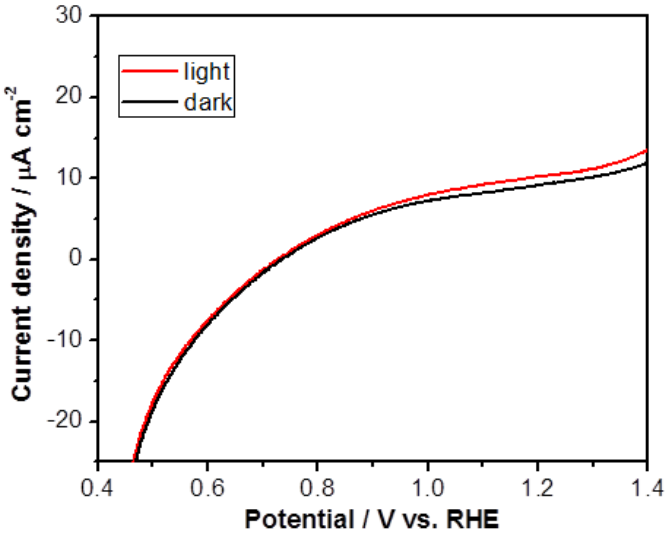



**Figure 3.13** Current-potential curves of bare FeO(OH) deposited for 1 hour.

The current density in dark and light for FeO(OH) were almost the same, meaning the nanostructured FeO(OH) have very limited light response under irradiation. As a result, the photo-generated holes in $Fe_2O_3$/FeO(OH) photoanodes are mainly come from the $Fe_2O_3$ layer prepared by PLD, while the nanostructured FeO(OH) are only functioned as cocatalyst to increase the amount of holes involved in the water oxidation reaction.

### 3.3.2 Photoelectrochemical performances of $Fe_2O_3$/FeO(OH) photoanode

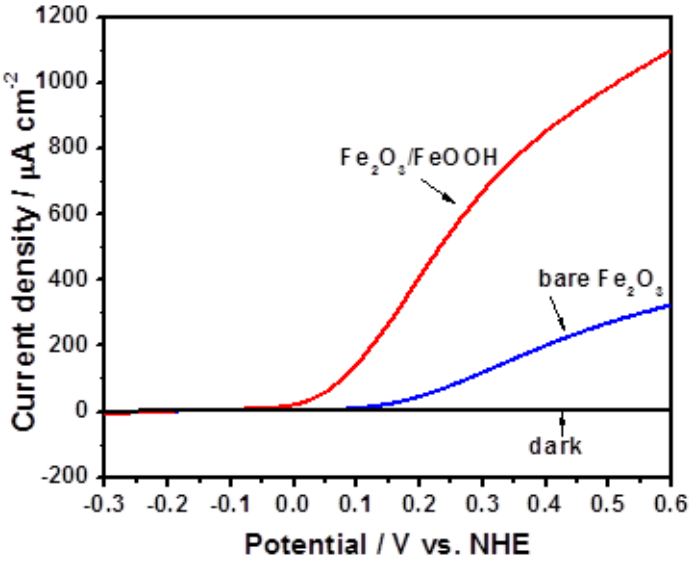



**Figure 3.14** Comparison of the current-potential curves of $Fe_2O_3$ with or without FeO(OH) under AM 1.5 G illumination in 1 M NaOH solution.

Linear-sweep-voltammetry (LSV) curves for $Fe_2O_3$/FeO(OH) and bare $Fe_2O_3$ photoanode were performed in 1 M NaOH solution both in dark and light under AM 1.5 G illumination (Figure 3.14). Both the onset potential and photocurrent density is enhanced for hematite after FeO(OH) decoration.

Details about comparison of the PEC performance between $Fe_2O_3$ with or without

FeO(OH) present are shown in Figure 3.15 and Figure 3.16.

To quantitatively value the amount of cathodic shift on onset potential from the FeO(OH) decorated $Fe_2O_3$ photoanode, we further analysed the LSV curve according to the report by Formal[24] and Wang[19]. Firstly, the differential curve between potential and current density were made. And then the onset potential is defined as the value at which $dJ/dV>0.2\ mA{\cdot}cm^{-2}{\cdot}V^{1}$ (Figure 3.15). The onset potential for bare $Fe_2O_3$ was 0.08 while for FeO(OH) decorated $Fe_2O_3$ was -0.06. The 140 mV potential shifts are almost consistent with the current-potential curves as shown in Figure 3.14.

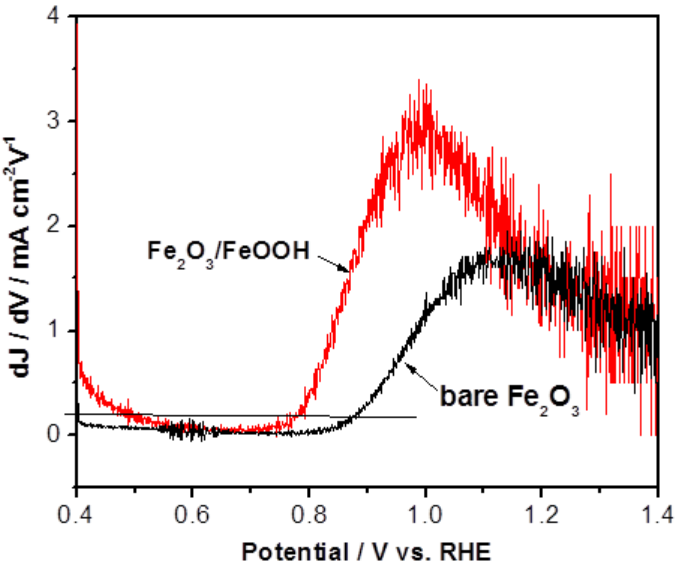



**Figure 3.15** First-order derivative of the photocurrent density as a function of voltage base on Figure 3.12. $V_{on}$ is defined as the value at which $dJ/dV>0.2\ mA{\cdot}cm^{-2}{\cdot}V^{-1}$.

The photo-response of the nanostructured FeO(OH) decorated $Fe_2O_3$ over time were examined by I-T curve of $Fe_2O_3$/FeO(OH) at 1.23 V vs. RHE (Figure 3.16). Once the light was turned on, a spike in the photoresponse can be observed for all the samples because of the rapid effect upon power excitation, but the photocurrent quickly turned

back to a steady state within 1 second. It can be observed that the photocurrent density of hematite at 1.23 V vs. RHE increased nearly 4 times after FeO(OH) decoration, from 220μA $cm^{-2}$ to 835 μA $cm^{-2}$. From the above two curves, we can draw the conclusion that both the onset potential and current density of hematite had been improved after loading nanostructured FeO(OH).

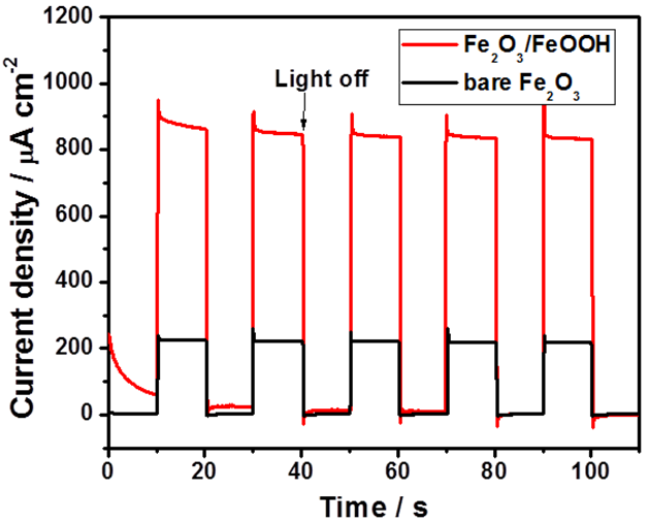



**Figure 3.16** Current-potential curves of $Fe_2O_3$ with or without FeO(OH) under AM 1.5 G illumination in 1 M NaOH solution.

The nanostructured FeO(OH) decorated $Fe_2O_3$ exhibited superior PEC performance, increased photocurrent density and decreased onset potential. The highly improved photocurrent density was partly owed to the nanostructured FeO(OH). Besides, the contact between FeO(OH) cocatalyst and $Fe_2O_3$ were so good that make the recombination rate at the $Fe_2O_3$/FeO(OH) interface maintained at a low range. The decreased recombination rate could certainly make the current density increased significantly.

Moreover, it is proposed that the existence of FeO(OH) decreased the reaction

barriers for water oxidation and facilitated the holes transfer to the electrode/electrolyte interface, accounting for the greatly improved PEC performance. It is commonly known that the electrochemical impedance spectroscopy (EIS) analysis provides information about the interfacial properties of electrodes.[25,26] The diameter of the semicircle in EIS equals the electron transfer resistance, which subjects the electron transfer kinetics of the redox probe at the electrode interface.[25,26] Figure 3.17 shows the typical EIS curves for bare $Fe_2O_3$ photoanode and $Fe_2O_3$/FeO(OH) photoanodes in 1 M NaOH solution under illumination respectively. A smaller diameter in the semicircle is observed in the curve of $Fe_2O_3$/FeO(OH) photoanode under illumination relative to bare $Fe_2O_3$, which means the resistance between FeO(OH)/electrolyte interfaces was much smaller than the $Fe_2O_3$/electrolyte interface. This indicates a conducting effect of the FeO(OH) on the charge-transfer process which would decrease the charge transfer barrier at the electrode interface. As a result, the oxygen evolution reaction barrier was reduced by decreasing the charge transfer barrier as reported in previous reports.[27-29] Water oxidation was easier to realize due to the decreased reaction barrier, so a negatively shift appeared in the onset potential curves.

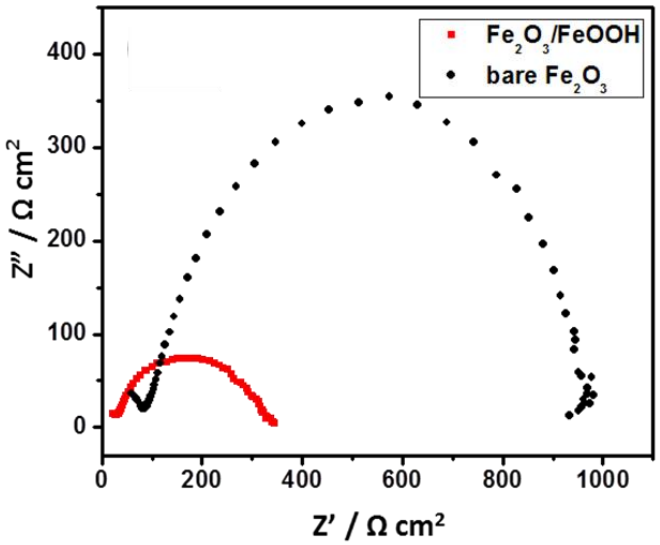



**Figure 3.17** Nyquist plots measured of $Fe_2O_3$ with or without FeO(OH) under the same illumination at1.23 V vs. RHE.

The effect of FeO(OH) on enhancing PEC performance of $Fe_2O_3$ was further confirmed by comparing the potential providing the same current density (0.5 $mA \cdot cm^{-2}$) as well as the current density at the same applied voltage (1.23 V vs. RHE) as shown in Figure 3.18. The potentials to generate current density about 0.5 $mA \cdot cm^{-2}$ for $Fe_2O_3$ and $Fe_2O_3$/FeO(OH) photoanodes were 0.43 V vs. Ag/AgCl and 0.03 V vs. Ag/AgCl respectively (Figure 3.18 a). The potential to generate 0.5 $mA \cdot cm^{-2}$ photocurrent density was reduced to 72% after loading FeO(OH) on $Fe_2O_3$. Besides, the photocurrent density at 1.23 V vs. RHE for bare $Fe_2O_3$ was only 217 $\mu A \cdot cm^{-2}$. However, when nanostructured FeO(OH) was decorated on the surface of $Fe_2O_3$ with appropriate amount (6.5 $mC \cdot cm^{-2}$), the photocurrent reached about 850 $\mu A \cdot cm^{-2}$, which is nearly 4 times of the $Fe_2O_3$ without FeO(OH) loading (Figure 3.18 b).

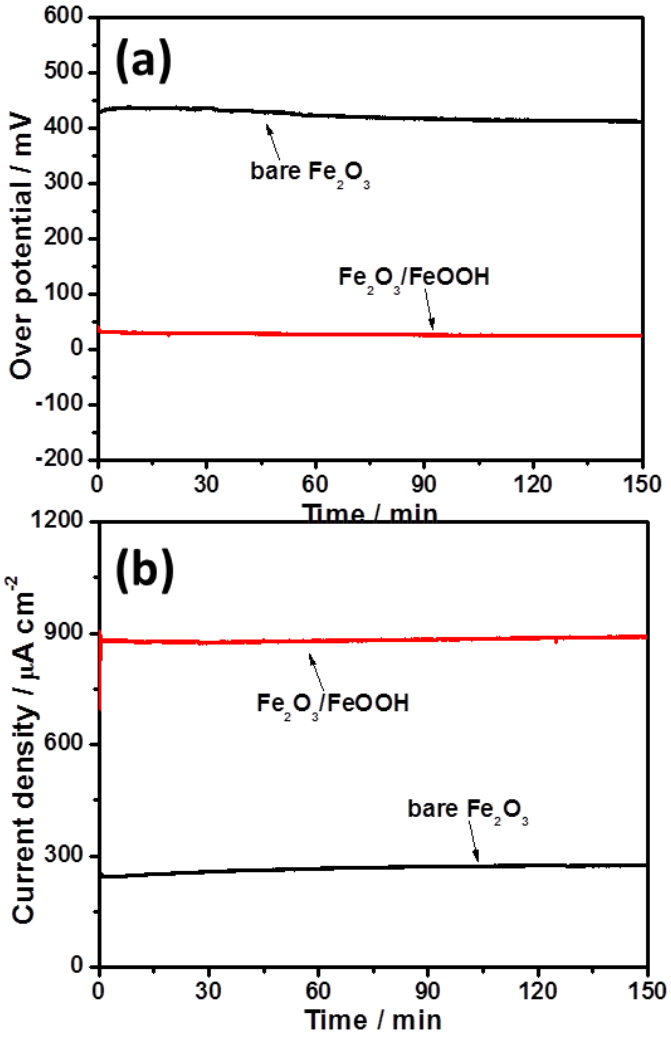



**Figure 3.18** (a) Potential (V vs. Ag/AgCl) versus time for $Fe_2O_3$ and $Fe_2O_3$/FeO(OH) respectively at 0.5 mA·cm$^{-2}$. (b) Photocurrent obtained at 1.23 V vs. RHE of $Fe_2O_3$ and $Fe_2O_3$/FeO(OH) respectively. The solution is 1 M NaOH while the light is AM 1.5 G.

Conclusively, the existences of FeO(OH) cocatalysts help lower the overpotential of $Fe_2O_3$ photoanode and increase the photocurrent density significantly. Besides, both the $Fe_2O_3$ photoanode and $Fe_2O_3$/FeO(OH) photoanode showed stable current density after illuminated for 150 minutes. This also confirmed that the contact between FeO(OH) and $Fe_2O_3$ was well qualified even an external bias is applied.

Water splitting experiments at 1.23 V vs. RHE were monitored using AM 1.5 G illumination to certificate whether the anodic photocurrent generated by the $Fe_2O_3$/FeO(OH) photoanode is the exclusive result of $O_2$ evolution (Figure 3.19). The PEC water splitting experiments were carried out for more than 70 hours to make sure its long-term stability. The rate for $O_2$ evolution at the surface of $Fe_2O_3$/FeO(OH) photoanode was 10.1 $\mu mol \cdot h^{-1} \cdot cm^{-2}$ (Figure 3.20), while there was no obvious decay in this performance even after 70 hours. This performance is comparable with $Co_3O_4/La_2Ti_2O_7$ (~3 $\mu mol\ h^{-1}$, 2.5 hours)[30] and $BaWO_xN_y$-$BaTaO_2N$ (~11 $\mu mol\ h^{-1}$, 10 hours)[31] photocells. Moreover, the stability of the devices was much better compared with the above mentioned samples.

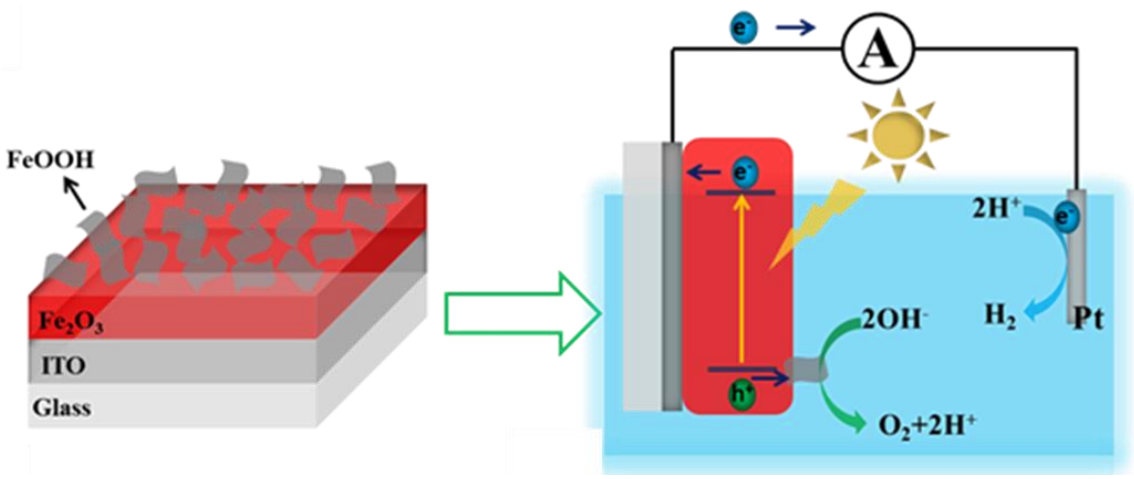



**Figure 3.19** Schematic view of $Fe_2O_3$/FeO(OH) photoanodes and their energy diagram for PEC water splitting.

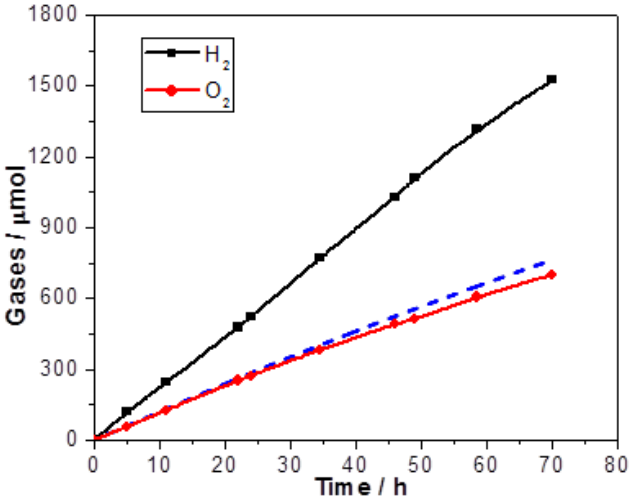



**Figure 3.20** Long-time gas evolution curves for FeO(OH) decorated $Fe_2O_3$ photoelectrode under AM 1.5 G illumination at 1.23 V vs. RHE. Broken line is the amount of $O_2$ calculated from photocurrent assuming 100% faradaic efficiency.

The high durability can be easily observed from the I-T curve for water splitting as shown in Figure 3.21. The current density went steadily with time increasing, and only showed 4.4% decay even after 70 hours reaction. This can be attributed to the high quality of $Fe_2O_3$ prepared by PLD and the good contact between the nanostructured FeO(OH) and $Fe_2O_3$. The gas generation rates of $H_2$ and $O_2$ for the $Fe_2O_3$/FeO(OH)-Pt PEC device was nearly 2:1, indicating the photocurrent density truly come from pure water splitting in this system. The dark current of this PEC device was quite low and no gases were detected without light turned on. Plus, the amount of $O_2$ generated was in good agreement with half amount of the holes passing through the outer circuit ($e^-/4$, indicated by the broken line), indicating that the obtained photocurrent was derived from water splitting. A 97.3% Faradaic efficiency was calculated based on the amount of generated $O_2$ and the holes. This means nearly all the holes in the circuit were used

for water oxidation.

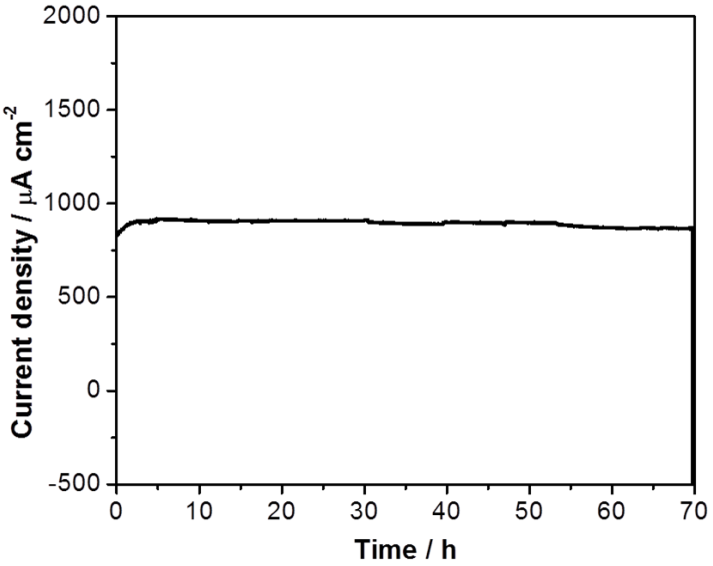



**Figure 3.21** Current-time curve of FeO(OH) decorated $Fe_2O_3$ photoelectrode under AM 1.5 G illumination at 1.23 V vs. RHE.

Incident photo conversion efficiency (IPCE) analysis of $Fe_2O_3$/FeO(OH) photoanode was processed in 1 M NaOH at 1.23 V vs. RHE under AM 1.5 G illumination, and the curve is shown in Figure 3.22. The IPCE decreased gradually with the wavelength increases. It can be observed that solar light with wavelength below 600 nm make contribution to the photocurrent density of $Fe_2O_3$/FeO(OH) photoanodes, and the IPCE reached a maximum of 20.2% at 400 nm. Since the nanostructured FeO(OH) cannot change the absorption performance of $Fe_2O_3$ in the visible light region as discussed in the previous part, the trend of IPCE for $Fe_2O_3$/FeO(OH) photoanode was in good accordance with the absorption spectrum for bare $Fe_2O_3$ (Figure 3.12).

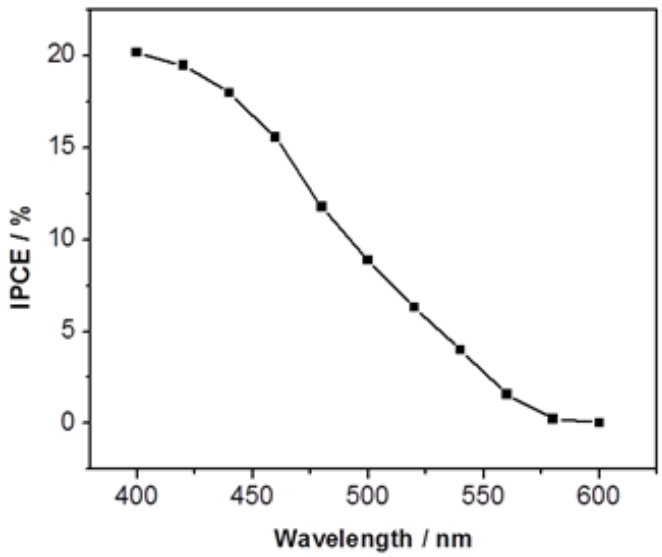



**Figure 3.22** IPCE curve of $Fe_2O_3$/FeO(OH) photoelectrode at1.23 V vs. RHE.

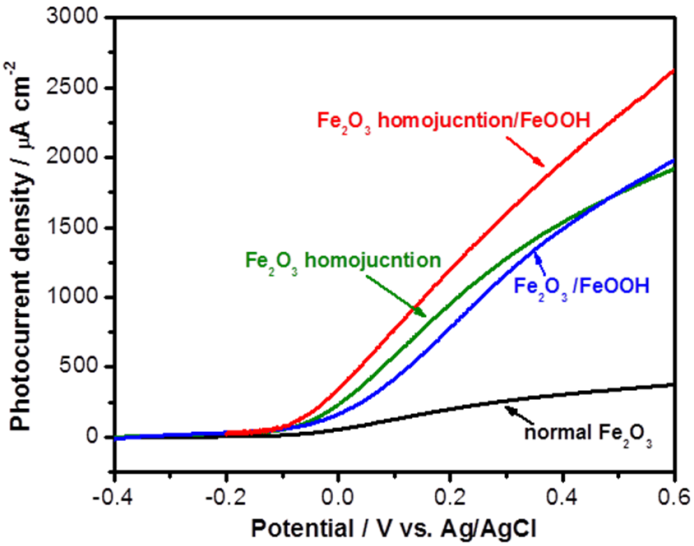



**Figure 3.22** LSV curves for normal $Fe_2O_3$, hematite homojunction, FeO(OH)/$Fe_2O_3$, hematite homojunction with FeO(OH) respectively.

Finally, hematite homojunction obtained in Chapter 2 were decorated by nanostructured FeO(OH) on the surface. The LSV curves for normal $Fe_2O_3$, hematite homojunction, FeO(OH)/$Fe_2O_3$, hematite homojunction with FeO(OH) under AM 1.5 G illumination are shown in Figure 3.23. Hematite homojunction with FeO(OH) showed

the highest photocurrent and lowest onset potential. And the photocurrent density at 1.23 V vs. RHE was about 1.3 $mA/cm^2$.

## 3.4 Conclusions

In this chapter, nanostructured FeO(OH) were deposit on the surface of hematite and superior photoelectrochemical performances were realized due to the higher charge transfer kinetics between the electrode/electrolyte interfaces.

Although FeO(OH) are proved to be a good cocatalyst for water oxidation on some photoanodes such as $BiVO_4$ and Si, they were usually grown parallel to the surface of the photoanodes which decreased reaction area of electrodes. However, this situation changed when we load FeO(OH) on the surface of hematite and nanostructured FeO(OH) were obtained on hematite due to the similar Fe-O bond between them. FeO(OH) nanosheet with thickness only ~15 nm was loaded on the surface of hematite successfully by electrodepostion.

The photocurrent onset potential shifted negatively by 140 mV, and the photocurrent density increased to nearly 4 times at 1.23 V vs. RHE compared to pure hematite photoanodes. Water splitting activity showed that gases generation rates of $H_2$ and $O_2$ for the $Fe_2O_3$/FeO(OH)-Pt PEC device was nearly 2:1, indicating pure water splitting was really occurred in this system. Moreover, the oxygen evolution rate for such prepared $Fe_2O_3$/FeO(OH) photoanode was as high as 10.1 $\mu mol \cdot h^{-1} \cdot cm^{-2}$ showed higher stability (>70 hours) compared with previous photoanodes.

EIS study proved that the existence of FeO(OH) made the charge transfer kinetics significantly reduced on the FeO(OH)/electrolyte interface and serving as cocatalyst to lower the overpotential of photoanode. Furthermore, due to the nanosheet morphology of FeO(OH), the reaction area is dramatically increased compared with the previously flat surface of hematite.

Overall, the nanostructured FeO(OH) decorated $Fe_2O_3$ photoanode was firstly obtained with visible light responsibility, high photocurrent density, and long-term stability, and showed great potential as an all-Fe-based photoanode for photoelectrochemical water oxidation.

## References

[1] Y. Lin, G. Yuan, S. Sheehan, S. Zhou and D. Wang, *Energy Environ. Sci.* 2011, **4**, 4862.

[2] L. A. Marusak, R. Messier and W. B. White, *J. Phys. Chem. Solids* 1980, **41**, 981.

[3] Y. Lin, Y. Xu, M. T. Mayer, Z. I. Simpson, G. McMahon, S. Zhou and D. Wang, *J. Am. Chem. Soc.* 2012, **134**, 5508.

[4] A. Kay, I. Cesar and M. Grätzel, *J. Am. Chem. Soc.* 2006, **128**, 15714.

[5] M. G. Walter, E. L. Warren, J. R. McKone, S. W. Boettcher, Q. Mi, E. A. Santori and N. S. Levis, *Chem. Rev.* 2010, **110**, 6446.

[6] Y. Hu, S. Kleriman, G. D. Stucky and E. W. McFarland, *Chem. Commun.* 2009, **19**, 2652.

[7] A. A. Tahir,V. Mckee, *Chem. Mater.* 2009, **21** 3763.

[8] J. Y. Kim, G. Magesh, D. H. Youn, J. Jang, J. Kubota, K. Domen, J. S. Lee, *Sci, Rep.* 2013, **3**, 2681.

[9] G. Wang, Y. Ling, D. A. Wheeler, K. E. N. George, K. Horsley, C. Heske, J. Z. Zhang, Y. Li, *Nano Lett.* 2011, **11**, 3503.

[10] L. Vayssieres, N. Beermann, S. E. Lindquist and A. Hagfeldt, *Chem. Mater.*, 2001, **13**, 2331.

[11] L. S. Zhong, J. S. Hu, H. P. Liang, A. M. Cao, W. G. Song and L. J. Wan, *Adv. Mater.*, 2006, **18**, 2426.

[12] Y. Liang, C. C. Wang, C. C. Kei, Y. C. Hsueh, W. H. Cho and T. P. Perng, *J. Phys. Chem. C*, 2011, **115**, 9498.

[13] .J. Wu, Y. L. Lee, H. H. Chiang and D. K. P. Wong, *J. Phys. Chem. B*, 2006, **110**, 18108.

[14] A. Kay, I. Cesar and M. Gratzel, *J. Am. Chem. Soc.*, 2006, **128**, 15714.

[15] C. C. L. McCrory, S. Jung ,J. C. Peters and T. F. Jaramillo, *J. Am. Chem. Soc.* 2013, **135**, 16977.

[16] S. Tilley, D. M. Cornuz, K. Sivula and M. Grätzel, *Angew. Chem.*, **2010**, **122,** 6549.

[17] B. Klahr, S. Gimenez, F. Fabregat-santiago, J. Bisquert and T. W. Hamann, *J. Am. Chem. Soc.*, 2012, **134**, 16693.

[18] K. M. H. Young and T. W. Hamann, *Chem. Commun.* 2014, **50**, 8727.

[19] C. Du, X. Yang, M. T. Mayer, H. Hoyt, J. Xie, G. McMahon, G. Bischoping and D. Wang, *Angew. Chem., Int. Ed.*, 2013, **52**, 12692.

[20] W. D. Chemelewski, H. Lee, J. Lin, A. J. Bard and C. B. Mullins, *J. Am. Chem. Soc.* 2014, **136**, 2843;

[21] R. Alben, D. Weaire, J. E. Smith, M. H. Brodsky, *Phys. Rev. B* 1975, **11**, 2271;

[22] B. Ludovic, N. Delphine, R. Solenn, M. Judith, S. Mandana, *J. Nano Res.* 2009, **8**, 147.

[23] J. Cao, T. Kako, N. Kikugawa and J. Ye, *J. Phys. D: Appl. Phys.* 2010, **43**, 325101.

[24] F. L. Formal, M. Grätzel and K. Sivula, *Adv. Funct. Mater.* 2010, **20**, 1099.

[25] J. F. Zang, S. J. Bao, C. M. Li, Bian, H. J.; X. Q. Cui, Q. L. Bao, C. Q. Sun, J. Guo and K. R. Lian, *J. Phys. Chem. C* 2008, **112**, 14843 ;

[26] A. D. Fabio, A. Giorgi, M. Mastragostino and F. Soavi, *J. Electrochem. Soc.* 2001, **148**, A845.

[27] S. C. Riha, B. M. Klahr, E. C. Tyo, S. Seifert, S. Vajda, M. J. Pellin, T. W. Hamann and A. B. F. Martinson, *ACS Nano*, 2013, **7**, 2396.

[28] L. Steier, I. H. Cardona, S. Gimenez, F. F. Santiago, J. Bisquert, S. D. Tilley and M. Grätzel, *Adv. Funct. Mater.* 2014, **24**, 7681.

[29] M. Shao, F. Ning, M. Wei, D. G. Evans and X. Duan, *Adv. Funct. Mater.* 2014, **24**, 580.

[30] J. Feng, W. Luo, T. Fang, H. Lv, Z. Wang, J. Gao, W. Liu, T. Yu, Z. Li, Z. Zou, *Adv. Funct. Mater.* 2014, **24**, 3535.

[31] K. Maeda, D. Lu, K. Domen, *Angew. Chem. Int. Ed.* 2013, **52**, 6488.

# Chapter 4 p-Type $LaFeO_3$ photocathodes and construction of p-$LaFeO_3$/n-$Fe_2O_3$ photocell

## 4.1 Introduction

In the past years, a series of n-type semiconductors have been researched as photoanodes for oxygen evolution, such as titanium dioxide[1-3], iron oxide[4,5], bismuth vanadate[6] and (oxy)nitrides[7] due to their enough high valence band position.[8] To further improve the photoelectrochemical performance, present research of photoelectrodes are usually sorted into two categories: one is loading proper hole storage layers as cocatalysts to improve the activity and stability of temporary available photoanode materials, which has made great effects due to rich choices for matching;[9] the other is focusing on looking for new p-type semiconductors as photocathodes for water reduction.[10-17] P-type photocathodes have many superiorities compared with traditional Pt electrodes. On one hand, p-type photocathodes can effectively reduce the back reaction of water formation which is easily occurring over Pt.[18] On the other hand, p-type photocathodes can also make some contribution to photo-response while the high-cost Pt can only serve as conductors to transfer carriers without any photo-response. Although the research of some p-type semiconductors (ex., $CaFe_2O_4$[10,11], $Cu_2O$[12], Rh doped $SrTiO_3$[13], Cr doped $TiO_2$[14], Zn doped $Fe_2O_3$[15] and $CuRhO_2$[16]) in photoelectrochemical photocells have been reported, they still meet with challenges such as low hydrogen generation rate, high onset

potential, poor stability in long-term photo-response and high cost, *et al.*, which seriously limited their application in photoelectrochemical water splitting systems. As a result, new alternative of p-type semiconductors as photocathode materials as well as low cost designing of highly stable photoelectrochemical photocells still need to be further developed.

Perovskite semiconductors have a general formula of $ABO_3$, and have found wide applications in photocatalysis, solar cells and photoelectrochemical water splitting. Due to their unique crystal and electronic structure, the photo-response and carrier motilities of perovskite semiconductors are attractive.[19-21] The nearly 180º B-O-B atom chains inside the $ABO_3$ structure offers an ideal three-dimensional transportation channel for photo-excited carriers. Perovskite oxides such as $SrTiO_3$ ($A^{2+}B^{4+}O$), $NaNbO_3$, and $NaTaO_3$ ($A^{+}B^{5+}O$) are classic photocatalytic semiconductors with excellent photocatlaytic performances. However, these semiconductors with n-type properties usually have poor photon harvesting performances because of their wide band gap and only express promising potential as photoanodes under UV-vis light unless other strategies can be employed (ex., noble metal Rh doped $SrTiO_3$[13]). Historically, the Fe based perovskite oxides (with general formula $A^{3+}Fe^{3+}O$) as photoelectrode materials,[22] especially for p-type photocathode materials which are relatively undeveloped although they show good potentials in the construction of visible light responsive electrode materials. Lanthanum orthoferrite ($LaFeO_3$) is one of the most familiar perovskite oxides. Previous research works for $LaFeO_3$ involve a few reports

on its photocatlaytic property using powder samples.[23-29] And to the best of our knowledge, the study on $LaFeO_3$ photocathodes as well as their effort in improving the photoresponse have met with failure due to the lack of sophisticated preparative technique for $LaFeO_3$ film with high quality. [30]

In Chapter 2 and 3, hematite photoanodes are well studied by forming homojunction and loading nanostructured FeOOH on the surface to improve the PEC performances. As an important part in photosystems, p-type photocathodes should also be studied to further improve the light harvesting property of the whole PEC system. In this chapter, $LaFeO_3$ films were prepared and explored as a new choice of photocathodes for water reduction. Pulsed laser deposition (PLD) is used to prepare $LaFeO_3$ films. As reported by previous studies, $LaFeO_3$ will exhibit p-type conductivity at high oxygen partial pressures ($P_{O2}>10^{-4}$ atm) with high temperatures (>1000 ºC)[31]. The temperature is so high that the traditional conductive substrates such as F doped tin oxide (FTO) and In doped tin oxide (ITO) cannot endure. However, PLD can prepare films at a relatively low temperature (<650 ºC). Besides, in order to realize the p-type property, high amount of oxygen in the atmosphere are needed. By introducing pure oxygen into the PLD chamber, p-type property of $LaFeO_3$ is likely to be achieved. Finally, according to the previous report[30], $LaFeO_3$ nanoparticle films with higher specific area were obtained with current density only around 10 μA $cm^{-2}$ at 0 V vs. RHE. The $LaFeO_3$ photocathodes they prepared has a higher specific surface area, but they still show poor activity. This is due to the poor quality (too much defects) of the films which greatly

increase the electro-hole recombination rates. Base on their work, PLD is a good choice to prepare $LaFeO_3$ films with p-type property and high quality.

## 4.2 Experiments

### 4.2.1 Preparation of p-$LaFeO_3$ photocathodes

The preparation process of $LaFeO_3$ films by PLD has three steps. And the details were shown as follows.

Firstly, $LaFeO_3$ powders were prepared by annealing the mixture of $La_2O_3$ and $Fe_2O_3$ 1300 °C for 24 hours.

Then, the $LaFeO_3$ powders were pressed and annealed at 1300 ºC to form the PLD target. The quality of film is largely depended on the quality of the target. To make the higher quality of films, the target must result in a dense structure with low specific surface area.

Finally, $LaFeO_3$ films were prepared by PLD at 650 ºC using the obtained target. The conductive substrate is In doped tin oxide. The details to prepare $LaFeO_3$ films are as fellows. The target and ITO substrate are set on the PLD machine (ST-PLD; Pascal co., Japan). The distance between the target and the ITO was set to be 5 cm. Before the laser start to irradiate, pure $O_2$ was introduced into the chamber until the pressure was researched 4 Pa. When the temperature of ITO substrate researched 650 °C, the target was irradiated by laser (Nd:YAG) with wavelength of 355 nm. The frequency and energy of the laser pulse length were fixed on 10 Hz and 62 mJ per pulse, respectively.

After the laser irradiation, the film was kept at the same temperature for 30 min in presence of $O_2$ (160 Pa) as a post-heat treatment.

### 4.2.2 Characterization

The phase characterizations of the samples were carried out by X-ray diffraction (XRD) (RIGAKU Rint-2000 X-ray diffractometer). Field-emission scanning electron microscope (JSM-6701 F, JEOL) were used to characterize the morphology of the samples. Optical absorption properties of the $LaFeO_3$ films were measured through an UV–vis spectrophotometer (UV-2500PC; Shimadzu Co., Japan).

### 4.2.3 PEC Properties

Liner-sweep voltage curves, current-time curves and Mott-Schottky plots are obtained with an electrochemical station (ALS/CH model 650A) in a three-electrode mode. Platinum and SCE were used as the counter electrode and reference electrode, respectively. AM 1.5 solar simulation (WXS-80C-3 AM 1.5G) with a light intensity of was utilized as the light sources.

### 4.2.4 Water Splitting

Hydrogen and oxygen generation of the prepared $LaFeO_3$-Pt and $LaFeO_3$-$Fe_2O_3$ photocell were measured using a water splitting system in a two-electrode system. In the $LaFeO_3$-Pt, $LaFeO_3$ film with an area of $1 \times 1$ $cm^2$ on ITO ($1 \times 3$ $cm^2$) was set as the

photocathode, while Pt (1 × 3 $cm^2$) was set as the photoanode. In the $LaFeO_3$-$Fe_2O_3$, $LaFeO_3$ film with an area of 2 × 2 $cm^2$ on ITO (2 × 3 $cm^2$) was set as the photocathode, while $Fe_2O_3$ film with an area of 1 × 1 $cm^2$ on ITO (1 × 3 $cm^2$) was set as the photoanode. 180 ml 1 M NaOH solution was put in a quartz glass cell. Then this glass cell was fixed on the water splitting system which was connected with a closed gas circulation system. The generated $H_2$ and $O_2$ were in situ analyzed with a TCD gas chromatograph (Shimadzu GC-8AIT, argon carrier). A 300 W Xe arc lamp (ILC Technology, CERMAX LX-300) was used as the light source. Visible light was realized by using a 300 W Xe lamp with a L42 wavelength cut-off filter. Besides, a water filter is needed between the 300 W Xe lamp and the photocell.

## 4.3 PEC performances for the $LaFeO_3$ photocathodes

$LaFeO_3$ samples of both powders and films were characterized by XRD to show the phase of them (Figure 4.1 a and b), with that of ITO as reference (Figure 4.1 c). The $LaFeO_3$ powders are in a single phase with perovskite structure (Figure 4.1 a, orthorhombic phase, JCPDS 00-037-1493). As the $LaFeO_3$ film is too thin on ITO, the XRD patterns of $LaFeO_3$ on ITO are not so obvious which is shown in Figure 4.1 b. It is observed that XRD patterns of $LaFeO_3$ films are the same with the powders, which is in a single phase with perovskite structure.

$LaFeO_3$ films with different deposition time 15 min, 30 min, 60 min and 100 min were prepared by PLD on ITO substrate. The thicknesses of films depositing 15 min, 30

min, 60 min and 100 min were 55 nm, 100 nm, 198 nm and 352 nm respectively by SEM as shown in Figure 4.2 a. And the detailed relationship between deposition time and thickness were shown in Figure 4.2 b. It can be concluded that there is a liner relationship between the laser irradiation time and the thickness of $LaFeO_3$ film. Besides, the deposition rate for $LaFeO_3$ films at the current deposition condition is about 3.5 nm/min.

The photocurrent densities of films with different thickness were tested and summarized in Figure 4.3. It is observed that the photocurrent density increased gradually with the thickness increasing and reached the highest at about 100 nm. When the thickness exceeded 100 nm, the current density will decrease gradually in virtue of the high recombination rate and the short diffuse length of carriers as other Fe based oxides.[32]

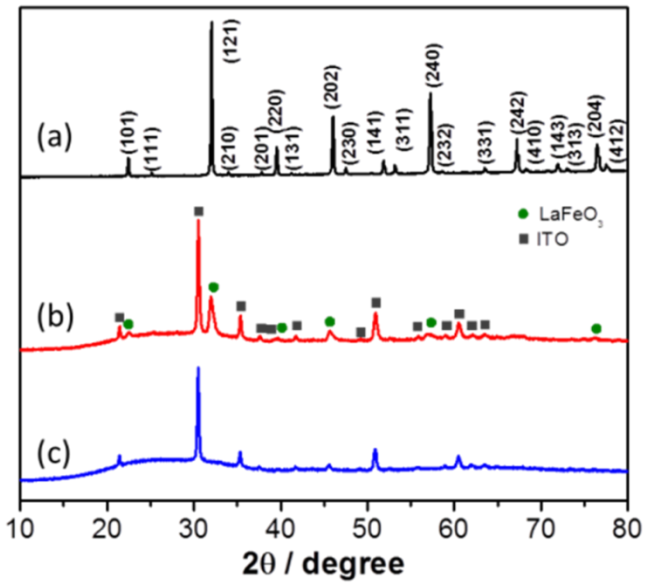



**Figure 4.1** XRD patterns of (a) $LaFeO_3$ powders, (b) $LaFeO_3$ film deposit on ITO substrate, and (c) naked ITO substrate respectively.

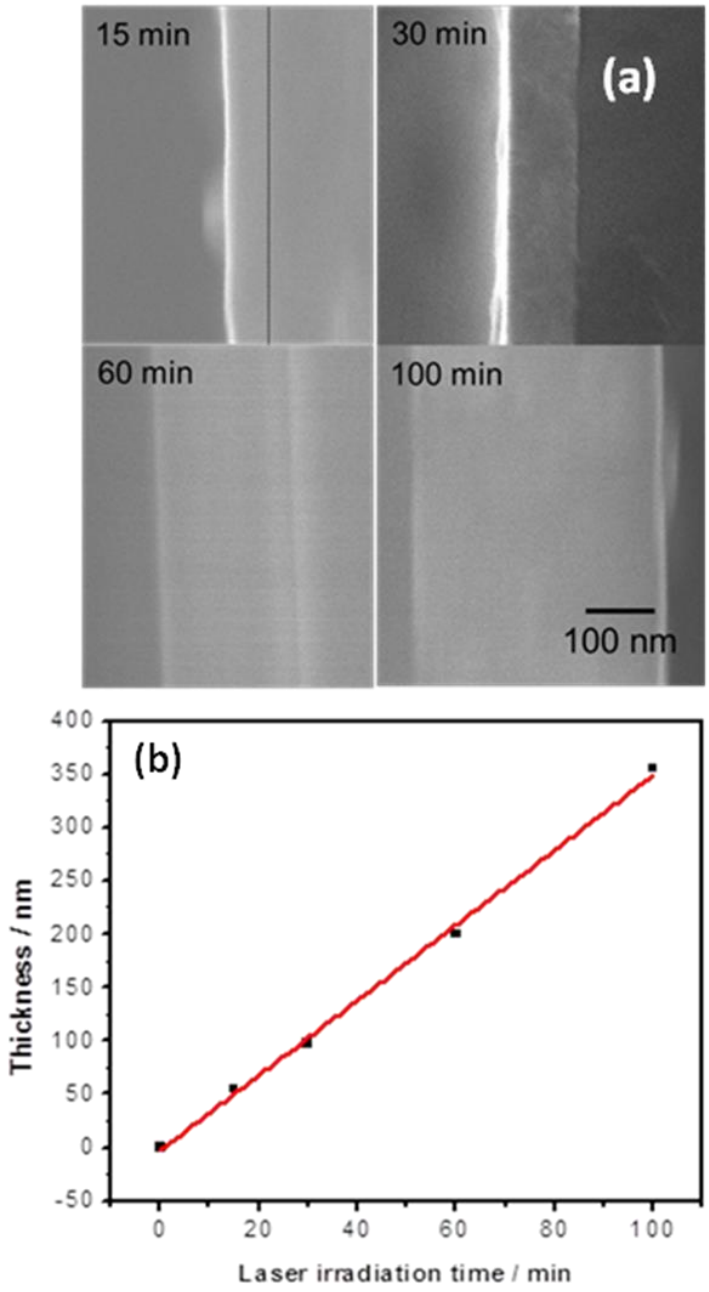



**Figure 4.2** (a) SEM images of films deposing with different time. (b) Liner relationship between thickness of $LaFeO_3$ films and laser irradiation time.

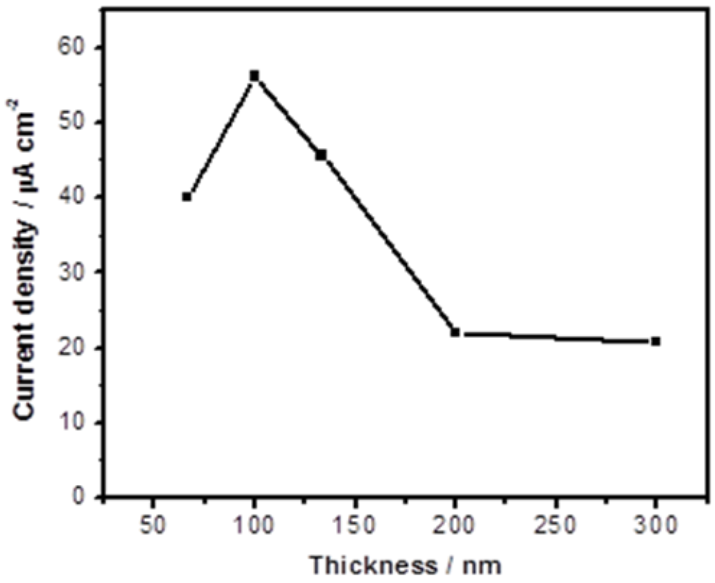



**Figure 4.3** Relationship between current density and thickness of $LaFeO_3$ films in 0.1 M $Na_2SO_4$ solution at -0.4 V vs. RHE external bias under AM 1.5 solar simulation.

The photoelectrochemical performances of the 100 nm $LaFeO_3$ film were detected in 1 M NaOH solution under AM 1.5 G illumination by liner-sweep-voltage curves (LSV) curves and current-time (I-T) curves respectively as shown in Figure 4.4. The $LaFeO_3$ photocathodes exhibited a cathodic photo-respnse, indicating a p-type property in the obtained $LaFeO_3$ (Figure 4.4 a). The dark current before 0 V vs. RHE is very low, implying that the material is stable under water reduction potential. The onset potential is about 0.8 V vs. RHE, and the photocurrent density icreased gradually if external biased increased. The photocurrent density at 0 V vs. RHE is about 54.5 μA $cm^{-2}$ as shown in the current-time curves (Figure 4.4 b). This performance is compareable the reported Rh-doped $SrTiO_3$[13], Cr doped $TiO_2$[14], Mg or Zn doped $Fe_2O_3$[15,16] and $CaFe_2O_4$[11] photocathodes.

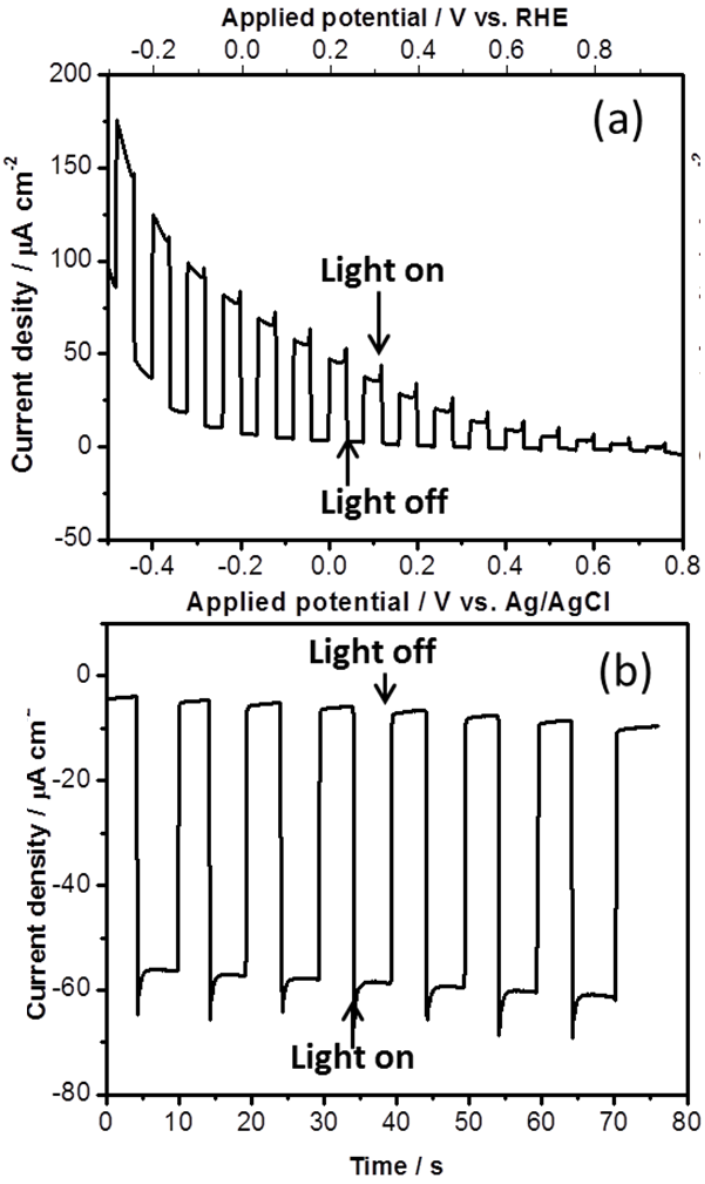



**Figure 4.4** (a) Current-potential curve and (b) the current-time curve at 0 V vs. RHE under for $LaFeO_3$ photocathodes under AM 1.5G illumination in 1 M NaOH solution.

As mentioned in previous manuscript, $LaFeO_3$ exhibits p-type conductivity at high oxygen partial pressures ($P_{O2}>10^{-4}$ atm).[24] There are cation-vacations exist in $LaFeO_3$. When the $P_{O2}$ increases, the population of cation (Fe) vacancies will become significant, and the conductivity will correspond to a material with cation (Fe) vacancies. Under this

condition, the $LaFeO_3$ will show p-type properties. In the case of our materials, the $LaFeO_3$ films were prepared in pure $O_2$ (4 Pa) atmosphere by PLD. As a result, cation vacancies also exist in the samples and p-type $LaFeO_3$ films may be obtained. Mott-Schottky plots were used to determine whether the obtained $LaFeO_3$ is a p-type semiconductor (Figure 4.5). Negative slopes of plots is observed in the Mott-Schottky plots. And it can be further confirmed that the prepared $LaFeO_3$ show a p-type property. As a result, the obtained $LaFeO_3$ films can be used as photocathodes for water reduction. [17]

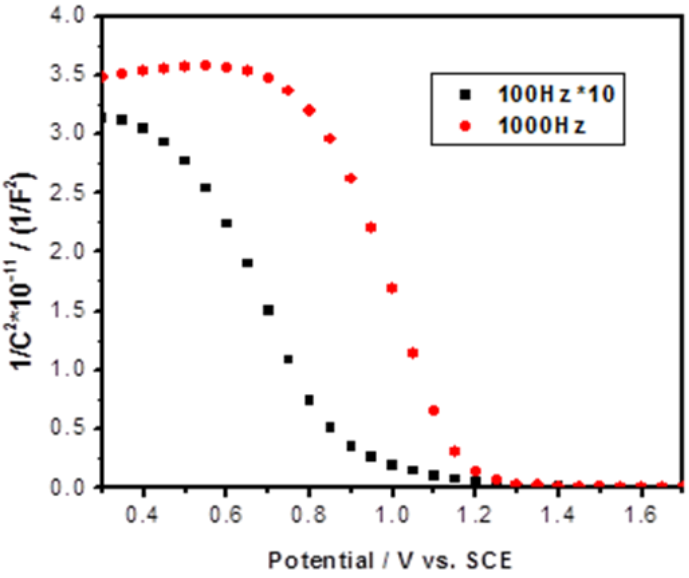



**Figure 4.5** Mott-Schottky plots at 100 Hz and 1000 Hz measured under dark conditions in 0.1M $Na_2SO_4$ solution.

Furthermore, photoaction spectra of the 100 nm $LaFeO_3$ electrodes were investigated by determining the incident photon-to-current conversion efficiency (IPCE) as shown in Figure 4.6. The IPCE spectra were tested at 0.2 V, 0 V, -0.2 V and -0.4 V vs. RHE

respectively to show the light usage of the materials. The UV-vis absorption spectra of the 100 nm $LaFeO_3$ film is shown as well. It can be clearly observed that the 100 nm $LaFeO_3$ film are capable of absorbing solar light with wavelength shorter than 400 nm more efficiently, while solar light longer than 500 nm is slightly be absorbed. It's the same case as in the IPCE curve. The IPCE in UV region is much higher while less than 1% in visible light region. The IPCE at visible light region is weak because the absorption of the $LaFeO_3$ films in the visible light region is limited. The absorption of $LaFeO_3$ may in the similar situation like other iron oxide such as $Fe_2O_3$[34] and $CaFe_2O_4$[11]. In general, the absorption of UV light (<400 nm) is connected with a direct transition ($O^{2-}$ 2p→$Fe^{3+}$ 3d charge transfer). While the absorption of visible light (>400 nm) is connected with an indirect transition (spin-forbidden $Fe^{3+}$ d→d excitation), which is a little difficult to realize in perovskite-type iron-based oxides such as $LaFeO_3$. In a word, the IPCE curve exhibits a good dependency relationship with the UV-vis absorption spectra (dashed lines in Figure 4.6) and is comparable with other p-type oxide photocathodes.[11]

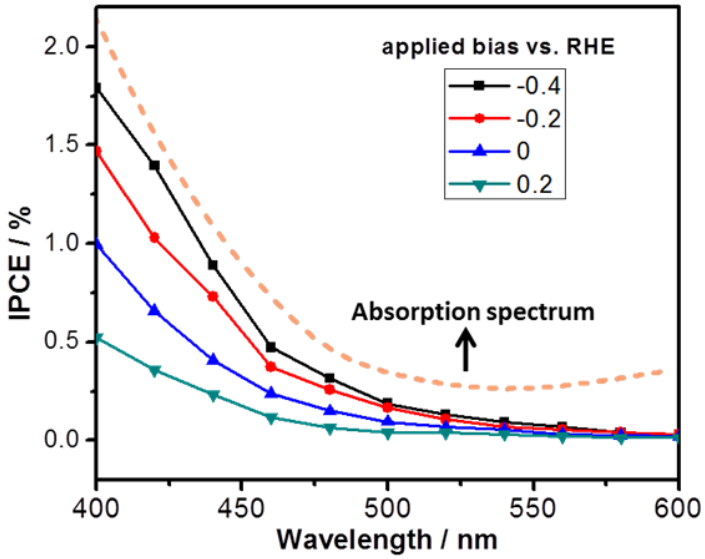



**Figure 4.6** IPCE spectra of $LaFeO_3$ photocathodes at 0.2 V, 0 V, -0.2 V and -0.4 V vs. RHE applied potential in 1 M NaOH solution. The dashed line is the absorption spectra of $LaFeO_3$ photocathodes.

Finally, to value the gas evolution efficiency of the obtained $LaFeO_3$ photocathode, hydrogen evolution experiments were carried out under AM 1.5 illumination as is shown in Figure 4.7. The gases evolution rates were ~1.8 μmol $h^{-1}$ for hydrogen and ~1.0 μmol $h^{-1}$ for oxygen respectively. $H_2$ and $O_2$ were evolved in a nearly stoichiometric manner, indicating the $LaFeO_3$ photocathode can be used for pure water splitting without any loss of generated $H_2$ and $O_2$. This also guarantees the long durability of the electrodes. In fact, limited p-type photocathodes have been found for pure water splitting. Most of the reported p-type photocathodes cannot be used for pure water splitting, such as $CaFe_2O_4$[11], $CuRhO_2$[17] et al., with some obvious self-decomposition in the performance after several hours.

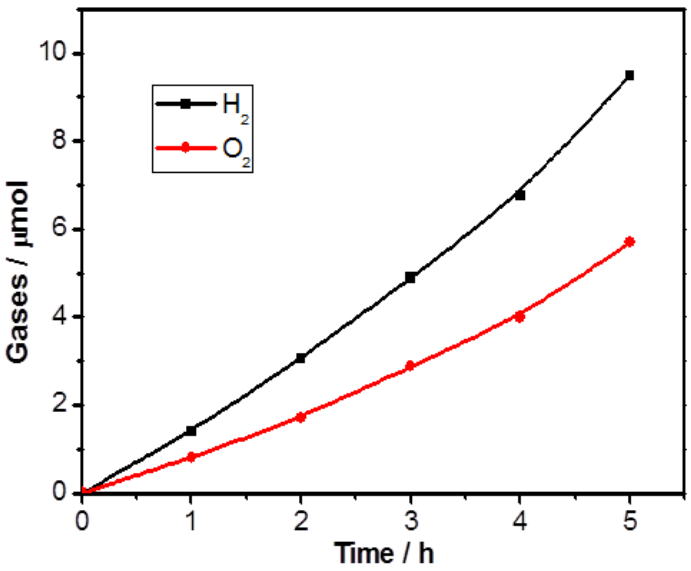



**Figure 4.7** Gases evolution of $LaFeO_3$ (~1 $cm^2$) at a 0 V vs. RHE external bias in three-electrode system.

## 4.4 p-$LaFeO_3$/n-$Fe_2O_3$ photocell for water spiltting

PEC photocell for water splitting was designed by combination of p-type $LaFeO_3$ photocathodes (4 $cm^2$， work electrode) and n-type $Fe_2O_3$ photoanodes (1 $cm^2$， counter and reference electrode) in 1 M NaOH solutions in a two-electrode system. Both of the two electrodes were faced with window to make sure they can absorb enough light as shown in the insert picture in Figure 4.8. The current-potential curves of this photocell in two-electrode system were shown in Figure 4.8 under AM 1.5G illumination. Photo current density can be noticeably observed when external bias is more negative than -0.3 V. And within the investigation range, the photocurrent density increased gradually when a more negatively external bias is applied.

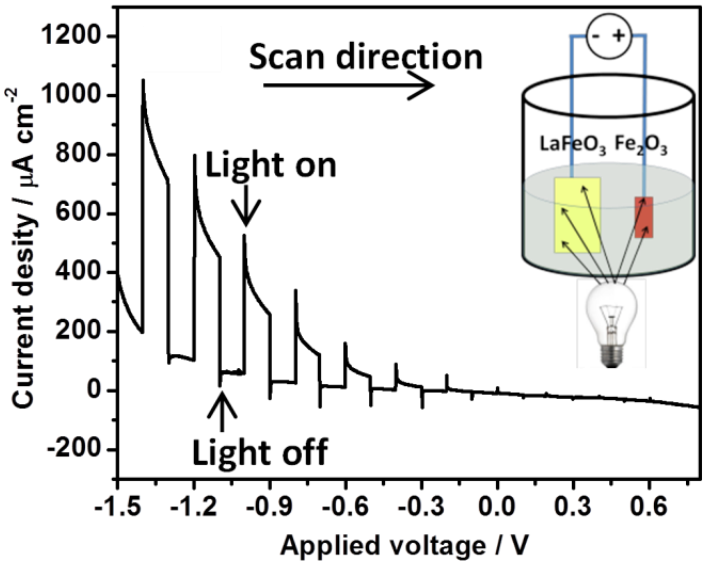



**Figure 4.8** Current-potential curves of $LaFeO_3/Fe_2O_3$ photocell under AM 1.5G illumination.

Based on the current-potential curve of the p-$LaFeO_3$/n-$Fe_2O_3$ photocell, water splitting was carried out at a -1.5 V external biases under visible light irradiation ($\lambda$>420 nm) (Figure 4.9). The volume ratio of the photo generated hydrogen and oxygen is nearly 2:1, as is expected from pure water splitting. The rate for gases evolution is very high, which is about 28.3 μmol $h^{-1}$ for $H_2$ and 14.0 μmol $h^{-1}$ for $O_2$. What's more, to value the light influence on the water splitting activity, UV-vis light is also used. The rate for gases evolution is higher than that under visible light, which is about 80.1 μmol $h^{-1}$ for $H_2$ and 41.0 μmol $h^{-1}$ for $O_2$. The activity under visible light is only 37.4% of that under UV-vis light. The relatively poor activity under visible-light is mainly limited by the p-$LaFeO_3$ photocathode, which cannot absorb visible light efficiently. This is a limitation for the current p-$LaFeO_3$ photocathode that should be solved in the future.

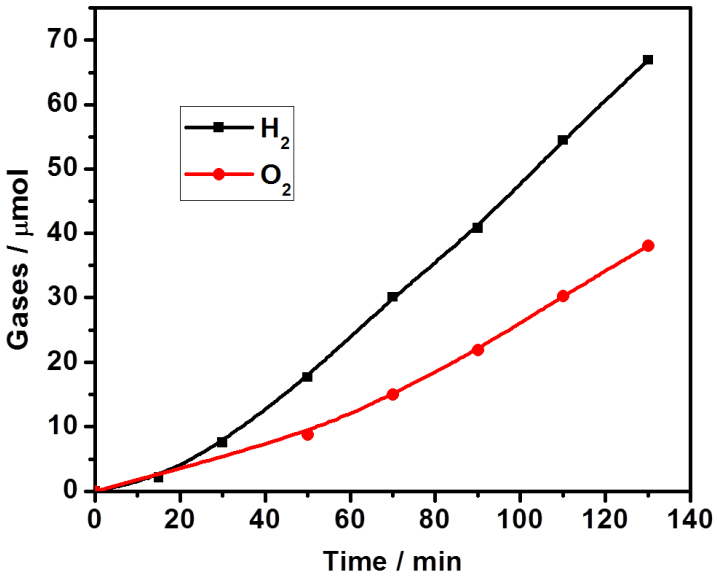



**Figure 4.9** Time course of gases evolution of $LaFeO_3/Fe_2O_3$ photocell with a -1.5 V external bias under visible light (λ>420 nm) irradiation by 300 W Xe lamp.

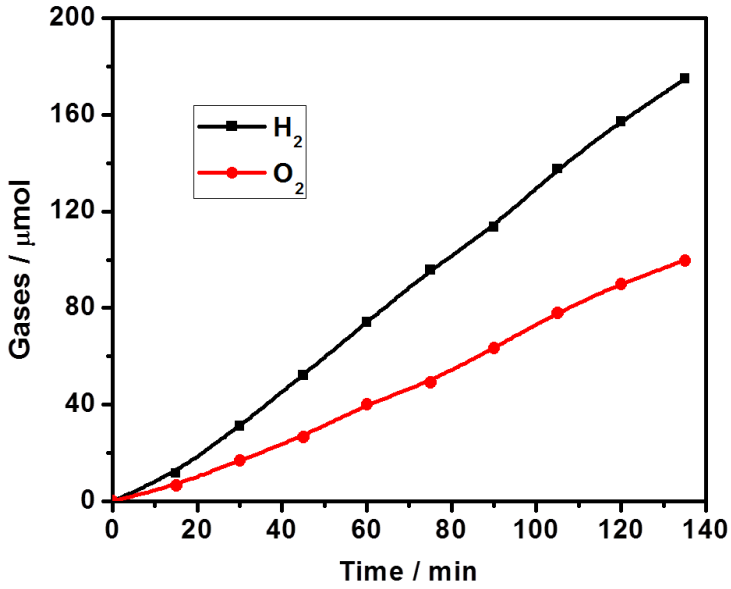



**Figure 4.10** Time course of gases evolution of $LaFeO_3/Fe_2O_3$ photocell with a -1.5 V external bias under UV-vis light irradiation by 300 W Xe lamp.

Besides, water splitting had also been carried out under a -1.5 V external bias without light (Figure 4.11, light off). The current density in the dark is quite low, which is only

about one percent against the current density in the UV-vis light. And no hydrogen and oxygen were detected without light irradiation. The low current density in the dark indicates all the photocurrent in the light could be attributed to photoinduced water splitting by p-$LaFeO_3$/n-$Fe_2O_3$ photocell.

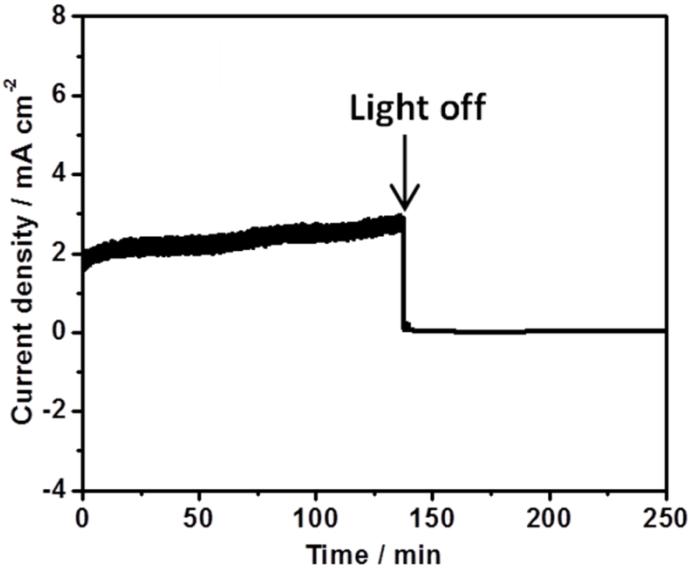



**Figure 4.11** Current-time curves of $LaFeO_3$/$Fe_2O_3$ photocell with a -1.5 V external bias under visible light (λ>420 nm) irradiation by 300 W Xe lamp.

Moreover, a very interesting phenomenon is that both the photocurrent density (Figure 4.11) and gases evolution rate (Figure 4.9 and 4.10) increased gradually in the first two hours after light turned on. This should be caused by the slightly reassemble on the surface of the $LaFeO_3$ films during the initial stage of PEC water splitting, which can be clearly observed from the morphology change before and after reaction (Figure 4.12 and Figure 4.13). The slightly reassemble increased the specific surface area of $LaFeO_3$ films and therefore favored the interfacial reaction. Such structure adjustment

adopted by $LaFeO_3$ seems to be adapting the big difference in photo-response between $LaFeO_3$ photocathode and $Fe_2O_3$ photoanode when they are used for dual PEC electrodes for water splitting.

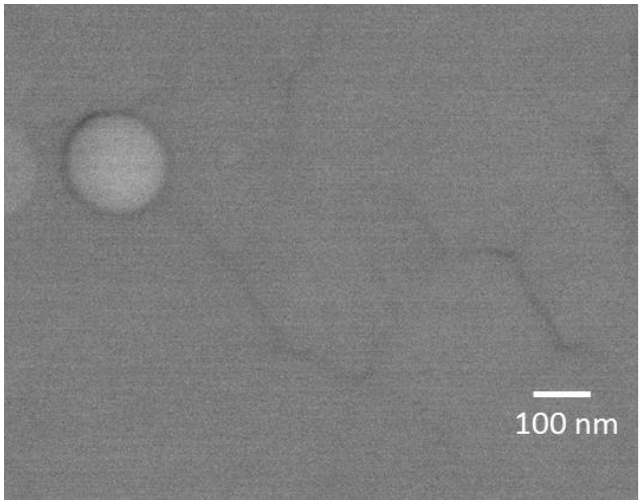



**Figure 4.12** SEM images of $LaFeO_3$ films before reaction.

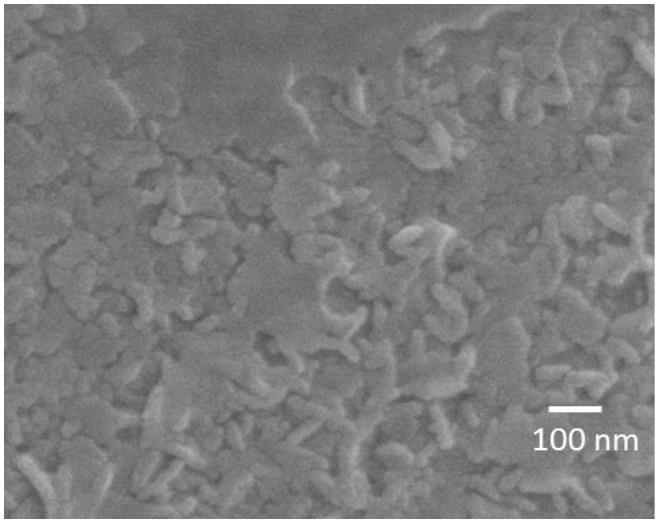



**Figure 4.13** SEM images of $LaFeO_3$ films after (b) 30 hours under visible light irradiation. The external bias is -1.5 V.

What's more, in order to demonstrate that $LaFeO_3$ photocathode is more effective than Pt, the comparison of $Fe_2O_3/LaFeO_3$ system and $Fe_2O_3$/Pt system were made. The

LSV curves for both systems are shown in Figure 4.14. Although the onset potential of the $Fe_2O_3/LaFeO_3$ system had not been lowered obviously, the current density had been improved gradually with the external potential increased as shown in the current-potential curves of these two systems (Figure 4.14). Plus, it can be observed that the dark current of $Fe_2O_3/Pt$ is much higher than $Fe_2O_3/LaFeO_3$ system. This proved that the $Fe_2O_3/Pt$ is easiliy reduced under reduction potential. In addition, the dark current density for $Fe_2O_3/Pt$ is as high as 0.3 $mA/cm^2$ under -1.0 V external bias, while that of $Fe_2O_3/LaFeO_3$ is only 40 $\mu A/cm^2$, indicating that $Fe_2O_3/LaFeO_3$ is more stable especially the external bias is larger than -1.0 V.

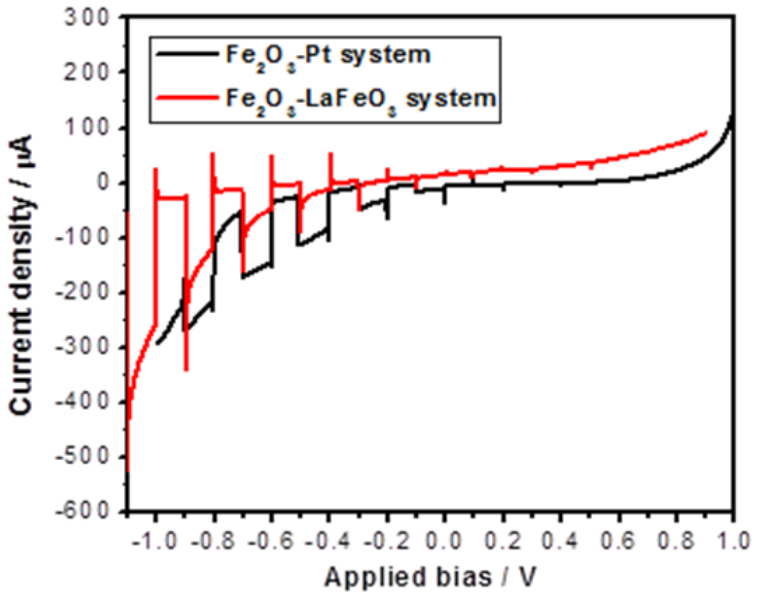



**Figure 4.14** Current-potential curves of $Fe_2O_3/Pt$ (black line) and $Fe_2O_3/LaFeO_3$ (red line) respectively in 1 M NaOH solution under AM 1.5 illumination in two electrode system.

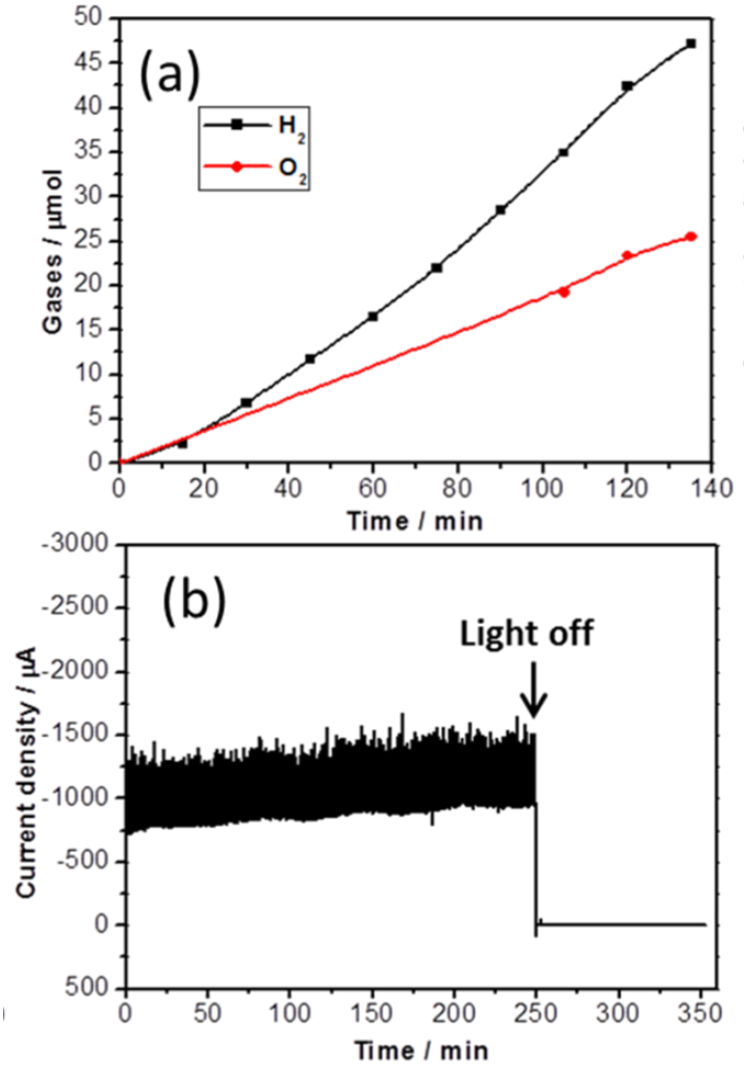



**Figure 4.15** (a) time courses of gas evolution for the $LaFeO_3/Fe_2O_3$ photocell under UV-vis light irradiation. (b) is the corresponding current-time curves. The external bias is -1.0 V.

The detailed comparison of activity between the $Fe_2O_3$/Pt and $Fe_2O_3/LaFeO_3$ photocells was firstly carried out at external bias -1.0 V (Figure 4.15 and 4.16). When the external bias is fixed on -1.0 V, the hydrogen generation rate of $Fe_2O_3/LaFeO_3$ system is nearly 42.0 μmol $h^{-1}$, while that for the $Fe_2O_3$/Pt system is 25.2 μmol $h^{-1}$. The hydrogen evolution efficiency of $Fe_2O_3/LaFeO_3$ system is about 70% higher than the

$Fe_2O_3$/Pt system. Moreover, it seems the stability when using $LaFeO_3$ as the photocathodes is higher than Pt by comparing the current-time curves. This indicates that the $Fe_2O_3$ can endure a longer time especially under larger external potentials.

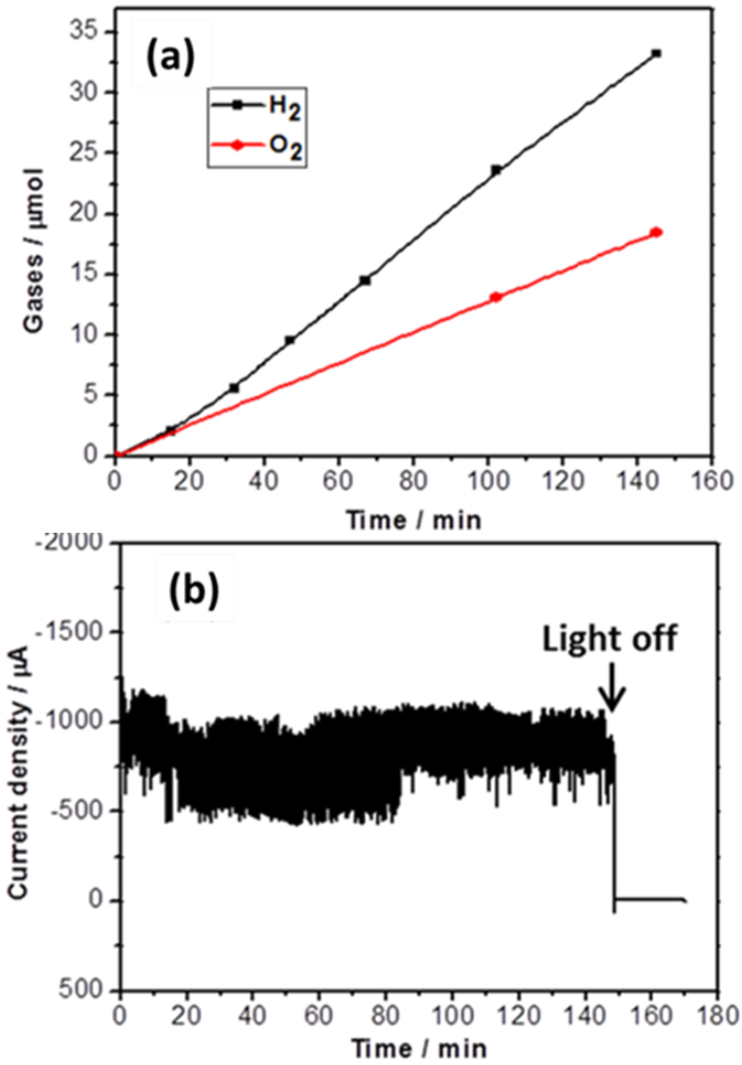



**Figure 4.16** (a) time courses of gas evolution for the $Fe_2O_3$/Pt photocell under UV-vis light irradiation. (b) is the corresponding current-time curves. The external bias is -1.0 V. The solution is 1 M NaOH.

And when the external bias is fixed on -1.5 V, the current density of $Fe_2O_3$/Pt system reaches its highest at about 17 hours, and then decreased obviously to 58.8% after 45

hours (Figure 4.17 a). However, the $Fe_2O_3/LaFeO_3$ system still holds a very large current density and keeps increasing after 45 hours (Figure 4.17 b). In conclusion, the introduction of p-type $LaFeO_3$ photocathodes (instead of Pt) have greatly improved the gas evolution rates especially the stability of the whole PEC water splitting system.

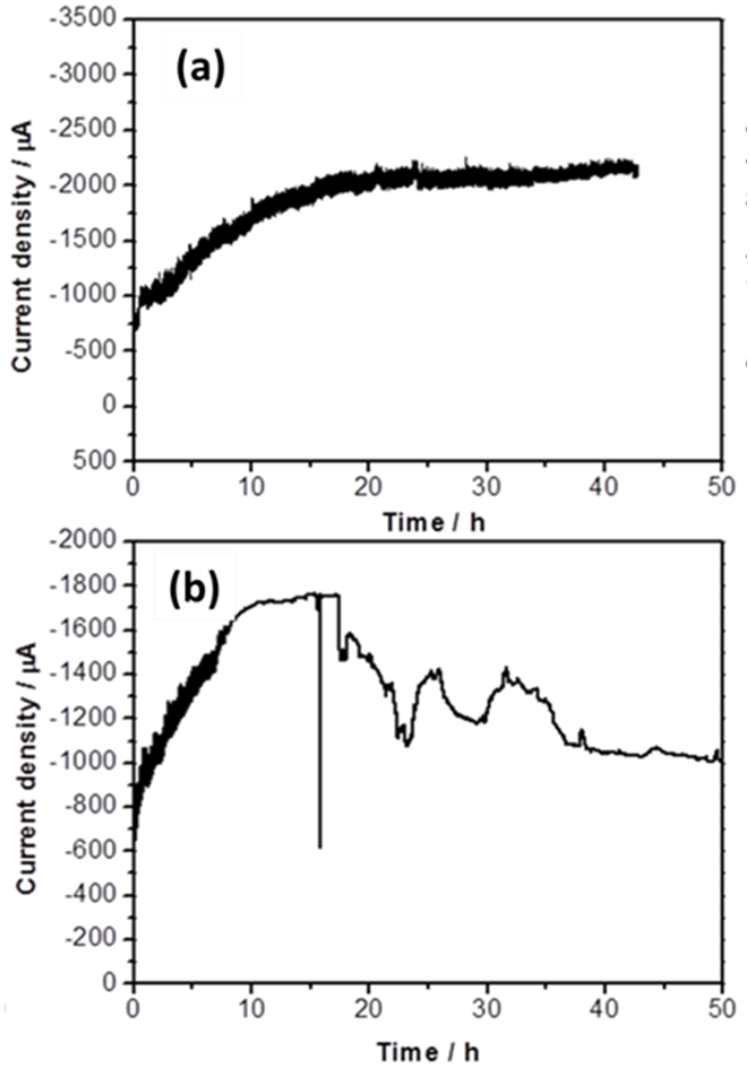



**Figure 4.17** Current-time curves at -1.5V external bias for $LaFeO_3/Fe_2O_3$ (a) and $Fe_2O_3$/Pt (b) respectively.

Generally, stability is one of the most important factors to value whether a water

splitting system is suitable for practical use. In order to test the stability of $LaFeO_3/Fe_2O_3$ photocell, water splitting experiment was carried out under a -1.2 V external bias for about 120 hours under visible light (λ>420 nm) (Figure 4.18). The corresponding current-time curve is shown in Figure 4.19. The current density is about 0.2 mA $cm^{-2}$ at the very beginning. The current density increased gradually after 80 hours. And the photocurrent density increased to 1 mA $cm^{-2}$, which is nearly 5 times as that in the beginning. This indicates the reassemble still occurred even after 80 hours. Plus, after 130 hours, the current density is still about 750 μA $cm^{-2}$, which is 3 times more than that at the very beginning.

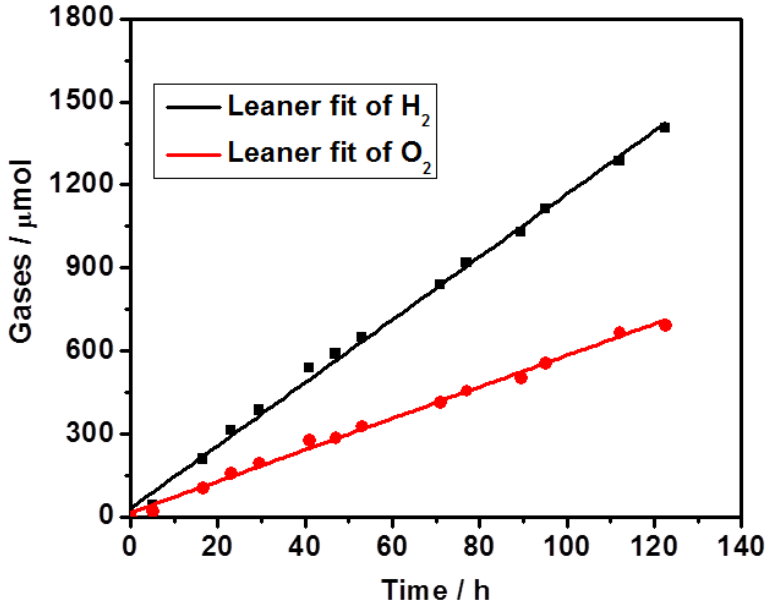



**Figure 4.18** Time course of gases evolution from $LaFeO_3$ (cathode, 4 $cm^2$)/$Fe_2O_3$ (anode, 1 $cm^2$) photocell in 1 M NaOH solution under visible light (300W Xe lamp, λ>420 nm) illumination. The external bias is -1.2 V in two-electrode system.

Overall, the average gases evolution rates of such obtained PEC device under visible-light irradiation are 11.5 μmol $h^{-1}$ for $H_2$ and 5.7 μmol $h^{-1}$ for $O_2$ respectively.

This performance is better than $CuRhO_2$-Pt[17], $BiVO_4$-Pt[6], $SrNbO_2N$-Pt[35] and less than $BaTaO_2N$-Pt[36] photocells which were also processed in two-electrode systems. By comparing the activity with its current density, a faradaic effciency of 80.2% is obtained for the photocell.

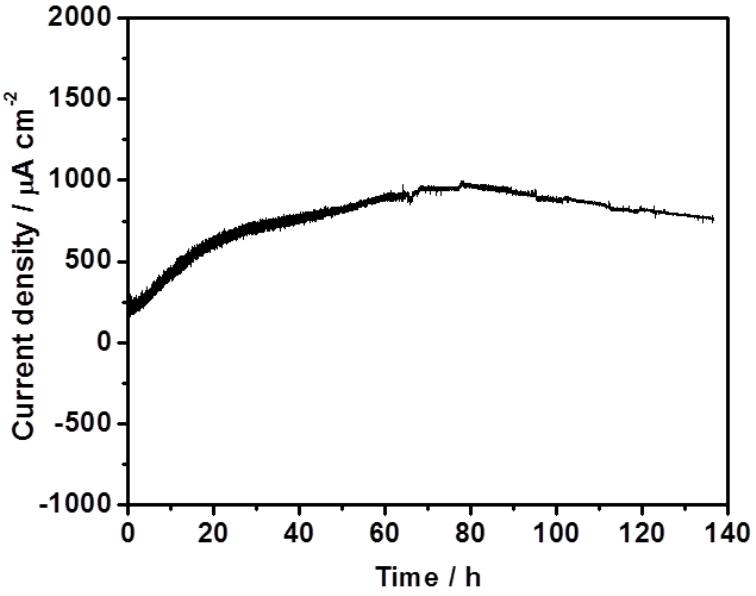



**Figure 4.19** Current-time curve from $LaFeO_3$ (cathode, 4 $cm^2$)/$Fe_2O_3$ (anode, 1 $cm^2$) photocell in 1 M NaOH solution under visible light (300W Xe lamp, λ>420 nm) illumination. The external bias is -1.2 V in two-electrode system.

Most importantly, the high gas evolution rate can be maintained for 120 hours without any obvious sigh of decay (Figure 4.18) and showed a much better stability compared with the above mentioned samples. To the best of our knowledge, the $LaFeO_3$/$Fe_2O_3$ photocell shows the longest working life among all the reported PEC water splitting devices. We believe that the long durability of such prepared photoelectrodes is mainly contributed to the high quality of the films and the good contact between $LaFeO_3$ and ITO substrate by using PLD method.

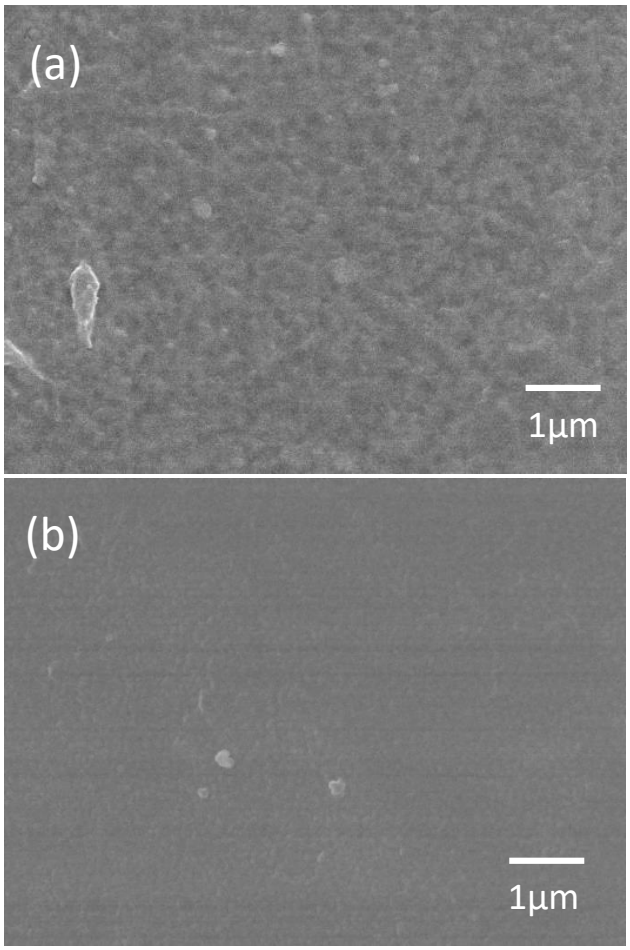



**Figure 4.20** SEM images of $LaFeO_3$ photocathode (a) and $Fe_2O_3$ photoanode (b) after 120 hours under visible light irradiation. The external bias is -1.2V.

As discussed by the previous part, the $LaFeO_3/Fe_2O_3$ photocell show a high activity for 120 hours. To further proved the higher stability of $LaFeO_3$ photocathodes, SEM images (Figure 4.20) and XRD patterns (Figure 4.21) of the samples were characerized after 120 hours reaction. From the SEM images, it is clearly observed that no cracks and peeling off occurred in both the $LaFeO_3$ and $Fe_2O_3$ photoelectrodes. In addition, the XRD patterns of $LaFeO_3$ did not change at all even after 120 hours, indicating the phase did not change after long time reaction.

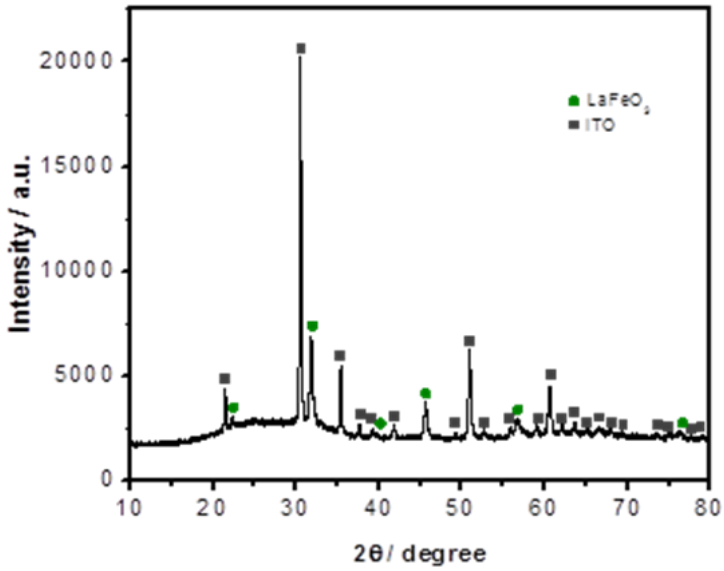



**Figure 4.21** XRD patterns of $LaFeO_3$ photocathodes after water splitting under visible light irradiation for 120 hours. The external bias is -1.2V.

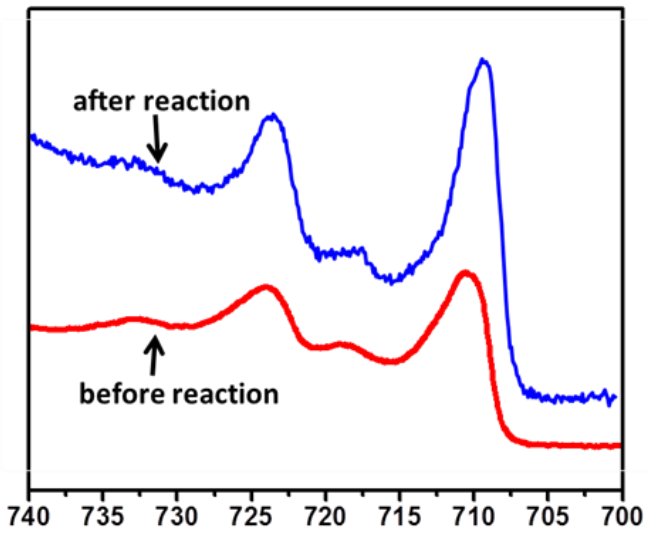



**Figure 4.22** XPS spectra of Fe (2p) in $LaFeO_3$ photocathodes before and after water splitting under visible light irradiation for 120 hours. The external bias is -1.2V.

Except the body characterization by XRD, binding energy of Fe 2p in the XPS analysis (Figure 4.22) were used to detect the surface state change for $LaFeO_3$

photocathodes. It can be observed that only $Fe^{3+}$ can be identified after reaction, indicating that the valence state is unchanged after the water reduction.[37] Therefore, from all the result above, the $LaFeO_3$ showed high stability for water reduction even after 120 hours.

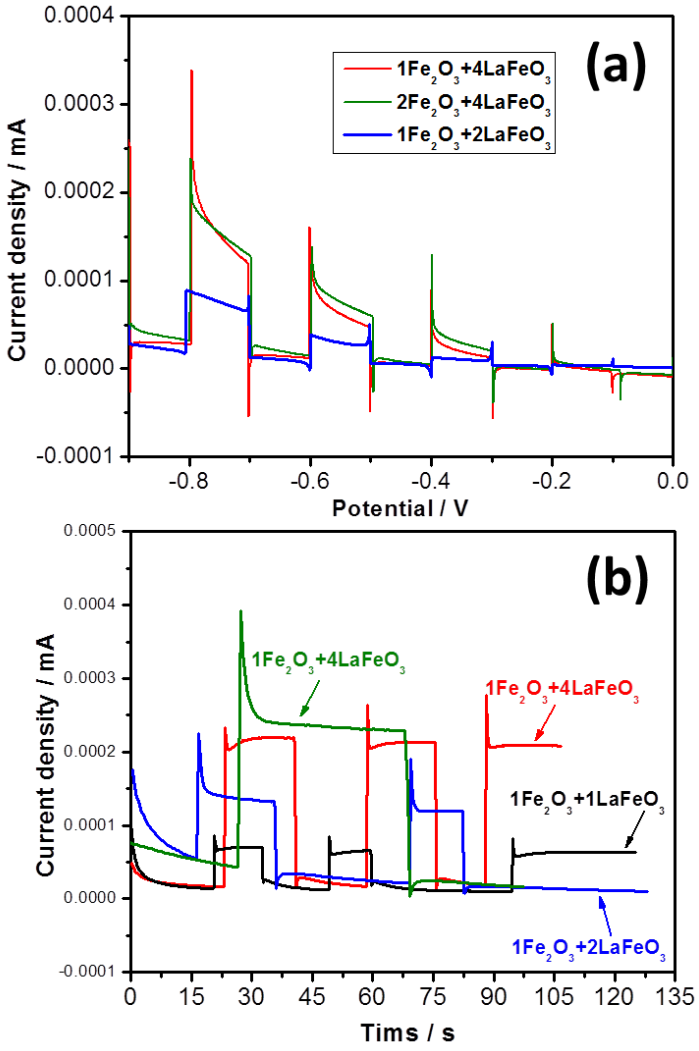



**Figure 4.23** Comparison of $Fe_2O_3/LaFeO_3$ tandem cell with different areas. (a) is the LSV curves and (b) is the I-T curves at -1 V in two electrode system.

In order to find the relation between electrode area and photocurrent density for the $Fe_2O_3/LaFeO_3$ tandem cell, both the area of $Fe_2O_3$ and $LaFeO_3$ is changed and

illustrated in Figure 4.23. It can be observed that when the area of hematite is fixed on 1 $cm^2$, the photocurrent density increased almost linearly with the area of $LaFeO_3$ film. As the maximum area of film by temporary PLD machine is 4 $cm^2$, the largest $LaFeO_3$ film is 4 $cm^2$. When the area of $LaFeO_3$ film is fixed on 4 $cm^2$, the photocurrent density changed slightly when enlarge the area of hematite films. This result revealed that the photocurrent density for the obtained $Fe_2O_3/LaFeO_3$ tandem cell is mainly depended on the cathode side.

## 4.5 Conclusions

In this chapter, the main idea is to propose a new choice of p-type photocathodes ($LaFeO_3$) and an all-iron-based photocell, p-$LaFeO_3$/n-$Fe_2O_3$ tandem cell, were obtained for the first time.

In order to improve the light absorption efficiency of the whole hematite-based photocell, a new p-type $LaFeO_3$ thin film was prepared as photocathodes for PEC water reduction. As choices for initial p-type semiconductors are limited, studies of photocathodes are much fewer than n-type photoanodes. And they are still faced with problems such as low efficiency and stability. As $LaFeO_3$ has a perovskite structure, the nearly 180º B-O-B atom chains inside the $ABO_3$ structure could offer an ideal three-dimensional transportation channel for photo-excited carriers. Base on this theory, $LaFeO_3$ thin films were prepared by pulsed laser deposition and used as photocathodes for the first time for water reduction.

The p-type $LaFeO_3$ photocathodes have been prepared by PLD on conductive substrate. The photo current density of 100 nm $LaFeO_3$ photocathodes is about 54.5 μA $cm^{-2}$ at 0 V vs. RHE under AM 1.5G irradiation. The gases evolution rates for this photocathode were ~7.0 μmol $h^{-1}$ for hydrogen and ~3.8 μmol $h^{-1}$ for oxygen respectively. This performance is comparable with other p-type semiconductors.

Meanwhile, p-$LaFeO_3$/n-$Fe_2O_3$ photocell has been designed for the first time and used for water splitting under visible light irradiation without loading any cocatalysts. The introduction of p-type $LaFeO_3$ have improved the gas evolution rates especially the stability of $Fe_2O_3$. Firstly, by introducing $LaFeO_3$ as photocathode instead of Pt, the photocurrent density is increased by 0.4 mA $cm^{-2}$, while the gases evolution rate increased 70% as well. Secondly, by introducing $LaFeO_3$ as cathode instead of Pt, the stability has been greatly improved.

In a word, By combining p-type $LaFeO_3$ photocathodes with hematite photoanodes, p-$LaFeO_3$/n-$Fe_2O_3$ tandem cell were obtained. And we offered the first example of an all-iron-based tandem cell for solar hydrogen conversion.

## References

[1] C. Mao, F. Zuo, Y. Hou, X. Bu, P. Feng, *Angew. Chem. Int. Ed.* 2014, **53**, 10485.

[2] C. Du, X. Yang, M. T. Mayer, H. Hoyt, J. Xie, G. McMahon, G. Bischoping, D. Wang, *Angew. Chem. Int. Ed.* 2013, **52**, 12692.

[3] I. S. Cho, M. Logar, C. H. Lee, L. Cai, F. B. Prinz, X. Zheng, *Nano. Lett.* 2014, **14**, 24.

[4] Y, Hou, F. Zuo, A. Dagg, P. Feng, *Angew. Chem. Int. Ed*. 2013, **52**, 1248.

[5] S. C. Warren, K. Voïtchovsky, H. Dotan, C. M. Leroy, M. Cornuz, F. Stellacci, C. Hébert, A. Rothschild, M. Grätzel, *Nat. Mater.* 2013, **12**, 842.

[6] T. W. Kim, K. Choi, *Science* 2014, **343**, 990.

[7] K. Maeda, D. Lu, K. Domen, *Angew. Chem. Int. Ed*. 2013, **52**, 6488.

[8] M. Grätzel, *Nature* 2001, **414**, 338.

[9] C. C. L. McCrory, S. Jung, J. C. Peters, T. F. Jaramillo, *J. Am. Chem. Soc.* 2013, **135**, 16977.

[10] S. Ida, K. Yamada, T. Matsunaga, H. Hagiwara, Y. Matsumoto, T. Ishihara, *J. Am. Chem. Soc.* 2010, **132**, 17343.

[11] J. Cao, T. Kako, P. Li, S. Ouyang, j. Ye, *Electrochem. Comm.* 2011, **13**, 275.

[12] C. R. Morales-Guio, S. D. Tilley, H. Vrubel, M. Gratzel, X. Hu, *Nat. Comm.* 2014, 5, 3059.

[13] K. Iwashina, A. Kudo, *J. Am. Chem. Soc.* 2011, **133**, 13272.

[14] J. Cao, Y. Zhang, L. Liu, J. Ye, *Chem. Comm.* 2013, **49**, 3440.

[15] Y. Lin, Y. Xu, M. T. Mayer, Z. I. Simpson, G. McMahon, S. Zhou D., Wang, *J. Am. Chem. Soc.* 2012, **134**, 5508.

[16] X. Qi, G. She, M. Wang, L. Mu, W. Shi, *Chem. Comm.* 2013, **49**, 5724.

[17] J. Gu, Y. Yan, J. W. Krizan, Q. D. Gibson, Z. M. Detweiler, R. J. Cava, A. B. Bocarsly, *J. Am. Chem. Soc.* 2014, **136**, 830.

[18] M. Yoshida, K. Takanabe, K. Maeda, A. Ishikawa, J. Kubota, Y. Sakata, Y. Ikezawa, K. Domen, *J. Phys. Chem. C* 2009, **113**, 10151.

[19] P. Reunchan, S. Ouyang, N. Umezawa, H. Xu, Y. Zhang, J. Ye, *J. Mater. Chem. A* 2013, **1**, 4221.

[20] S. Ouyang, H. Tong, N. Umezawa, J. Cao, P. Li, Y. Bi, Y. Zhang, J. Ye *J. Am. Chem. Soc.* 2012, **134**, 1974.

[21] P. Li, S. Ouyang, G. Xi, T. Kako, J. Ye *J. Phys. Chem. C* 2012, **116**, 7621.

[22] W. Ji, K. Yao, Y. Lim, Y. C. Liang, A. Suwardi, *Appl. Phys. Lett.* 2013, **103**, 062901.

[23] Hu, R.; Li, C.; Wang, X.; Sun, Y.; Jia, H.; Su, H.; Zhang Y.; Catal. Comm. 2012, 29, 35.

[24] R. Hu, C. Li, X. Wang, Y. Sun, H. Jia, H. Su, Y. Zhang, *Catal. Comm.* 2012, **29**, 3517.

[25] S. Thirumalairajan, K. Girija, N. Y. Hebalkar, D. Mangalaraj, C. Viswanathan, N. Ponpandian, *RSC Adv.*, 2013,**3**, 7549.

[26] R. Abazari, S. Sanati, L. A. Saghatforoush, *Mater. Sci. Semiconductor. Processing.* 2014, **25**, 301.

[27] Tang, P., Tong, Y., Chen, H., Cao, F., Pan, G, *Current Applied Physics*, 2013, **13**, 340.

[28] I. N. Sora, F. Fontana, R. Passalacqua, C. Ampelli, S. Perathoner, G. Centi, F. Parrino, L. Palmisano, *Electrochim. Acta* 2013, **109**, 710.

[29] V. Celorrio, K. Bradley, O. J. Weber, S. R. Hall, D. J. Fermin, *ChemElectroChem*, 2014, **1**, 1667.

[30] Waernhus, I.; Vullum, P.E.; Holmestad, R.; Grande, T.; Wiik, K. Solid State Ionics 2005, 176, 2783.

[31] Sora, I. N.; Fontana, F.; Passalacqua, R.; Ampelli, C.; Perathoner, S.; Centi, G.; Parrino, F.; Palmisano, L. Electrochimica Acta, 2013, 109, 710

[32] Q. Ding, F. Meng, C. R. English, M. Caban-Acevedo. M. J. Shearer, D. Liang, A. S. Daniel, R. J. Hamers, S. Jin, *J. Am. Chem. Soc.* 2014, **136**, 8504.

[33] Cao, J.; Kako, T.; Li, P.; Ouyang, S.; Ye, J. Electrochem. Comm. 2011, 13, 275

[34] Matsumoto, Y. J. Solid State Chem. 1996, 126, 227. (b) Duret, A.; Gra¨tzel, M. J. Phys. Chem. B 2005, 109, 17184.

[35] K. Maeda, M. Higashi, B. Siritanaratkul, R. Abe, K. Domen, *J. Am. Chem. Soc.* 2011, **133**, 12334.

[36] M. Higashi, K. Domen, R. Abe, *J. Am. Chem. Soc.* 2013, **135**, 10238.

[37] T. Yamashita, P. Hayes, *Appl. Surf. Sci.* 2008, **254**, 2441.

# Chapter 5 General conclusions and future prospects

## 5.1 General conclusions

Photoelectrochemical (PEC) water splitting has been widely researched for many years as it is a promising method for solar energy conversion. Among various semiconductors, iron-based photoelectrodes especially hematite are widely studied as photoanodes. This thesis is aimed at improving the photoelectrochemical water splitting performances of normal hematite based systems ($Fe_2O_3$-Pt system) by designing an all-iron based tandem cell, p-$LaFeO_3$/n-$Fe_2O_3$. In order to achieve this goal, three strategies were used. Superior solar water splitting activity of hematite photoanodes was realized by forming homojunction which increased the charge separation efficiency in hematite. Then, FeO(OH) nanosheets were loaded on the surface of hematite to improve the charge transfer kinetics of anode/electrolyte interface. Finally, p-type $LaFeO_3$ were obtained as photocathodes for water reduction and an all-iron-based tandem cell is realized.

The first strategy tried to increase the charge separation efficiency of photoanode by constructing bilayer hematite homojunctions. As is commonly known, the Fermi level of an n-type oxide semiconductor can be modulated nearer to conduction band by increasing the donor concentration in it. This makes it possible to construct homojunction photoelectrodes within hematite by combining two layers with different carrier concentrations. In this work, two types of hematite layers with different carrier

concentrations can be easily obtained by introducing artificial oxygen vacancies in them. After combining two hematite layers with different Fermi levels, a homojunction formed between them which made the hole-electron separate more efficiently in photoanodes. The PEC performances of hematite were greatly improved after homojunction formation. The onset potential decreased more than 0.2 mV while the photocurrent density increased to nearly 5 times (1.1 $mA/cm^2$) at 1.23 V vs. RHE under AM 1.5 G illumination. And with this homojuction configuration, the hematite homojunctions showed 15 times higher stability compared with the high-vacancy (high-donor-concentration) $Fe_2O_3$ phtoelectrodes for oxygen evolution. Open-circuit-potential study proved that the photovoltage generated by hematite homojunction is more than two times of single layer hematite films and indicated the charge separation efficiency is successfully increased due to the formation of homojunction.

The second strategy was intended to decrease the charge transfer kinetics between the photoanode/electrolyte interfaces by loading nanostructured FeO(OH) on the surface of hematite as cocatalyst. FeO(OH) nanosheet with thickness only ~15 nm was loaded on the surface of hematite successfully by electrodepostion. The photocurrent onset potential shifted negatively by 140 mV, and the photocurrent density increased to nearly 4 times at 1.23 V vs. RHE compared to pure hematite photoanodes. Water splitting activity showed that gases generation rates of $H_2$ and $O_2$ for the $Fe_2O_3$/FeO(OH)-Pt PEC device was nearly 2:1, indicating pure water splitting was really occurred in this system.

Moreover, the oxygen evolution rate for such prepared $Fe_2O_3$/FeO(OH) photoanode was as high as 10.1 μmol·$h^{-1}$·$cm^{-2}$. And it showed much higher stability (>70 hours) compared with previous photoanodes. EIS study proved that the existence of FeO(OH) reduced the charge transfer kinetics significantly on the FeO(OH)/electrolyte interface and served as cocatalyst to lower the activation energy for water oxidation. Furthermore, due to the nanosheet morphology of FeO(OH), the reaction area was dramatically increased compared with the previously flat surface of hematite.

Finally, p-type $LaFeO_3$ films were prepared by pulsed laser deposition and used as photocathodes for the first time for water reduction. The photo current density of 100 nm $LaFeO_3$ photocathodes was about 54.5 μA $cm^{-2}$ at 0 V vs. RHE under AM 1.5G irradiation. The gases evolution rates for this photocathode were ~7.0 μmol $h^{-1}$ for hydrogen and ~3.8 μmol $h^{-1}$ for oxygen respectively. By using $LaFeO_3$ as photocathode instead of Pt, a low-cost and all iron-based photoelectrochemical cells, p-$LaFeO_3$/n-$Fe_2O_3$ was designed. The rates for hydrogen and oxygen evolution of this photocell was nearly 2:1, and can keep the high rate at 11.5 μmol $h^{-1}$ for water reduction and 5.7 μmol $h^{-1}$ for water oxidation respectively under visible light irradiation even after 120 hours.

In summary, the first example of n-$Fe_2O_3$/p-$LaFeO_3$ tandem cell for overall solar water splitting was obtained with superior photoelectrochemical performances. Hematite homojunction is firstly and successfully prepared with enhanced activity by controlling the oxygen vacancies in different layers. This example offered a new

approach to obtain metal oxide semiconductor homojunctions without foreign element doping with superior PEC activity. Then, FeO(OH) with morphology of nanosheet was obtained on the surface of hematite for the first time. The improvement in PEC performances of FeO(OH)/$Fe_2O_3$ proved that FeO(OH) is a promising candidate as cocatalyst for metal oxide photoanodes. Finally, our results also revealled a promising prospect of $LaFeO_3$ photocathodes as PEC devices for solar energy conversion.

## 5.2 Future prospects

Photoelectrochemical water splitting has been studied for many years. Although many developments have been realized, the efficiency of PEC devices is still far from required. In my opinion, if PEC water splitting could be applied in the industry in the future, unbiased solar water splitting must be realized with a photo-to-hydrogen efficiency above 10%.

Although $Fe_2O_3$-$LaFeO_3$ tandem cell is designed in this thesis, unbiased solar water splitting still cannot be realized. The onset for hematite photoanode is more positive than 0.8 V vs. RHE, while that for $LaFeO_3$ photocathode is more negative than 0.5 V vs. RHE. As a result, the total photo-voltage between this tandem cell is not big enough for water splitting and an over 0.3 V external bias is needed.

In order to realize unbiased solar water splitting using iron-based photocells, an overlap of onset potential between photoanode and photocathode need to be existed. Besides, the photocurrent density of the tandem cell is primarily depended on the

electrode with lower activities. Based on this theory, two directions still need to be further studied.

1. Try to decrease the onset potential of hematite photoanode. As discussed previously, the onset potential for temporary hematite photoanode is still very high, about 0.7 V vs. RHE. New preparation methods need to be researched. If nanostructured hematite is prepared with high crystal quality and reaction area, the onset potential of hematite will be decreased.

2. Try to increase the light absorption property and decrease the charge recombination efficiency of photocathodes. In my opinion, this is the biggest challenge not only in my work but also in other researches. As discussed in chapter 4, although $LaFeO_3$ has solar response and can be used as photocathodes, there are still two limitations for the $LaFeO_3$ film obtained in this thesis. On one hand, the $LaFeO_3$ film cannot absorb visible light efficiently. On the other hand, the photocurrent density is still very low, <0.1 $mA/cm^2$. This will greatly limit the solar-to-electricity efficiency of the whole photocells. As a result, new preparation methods need to be found for $LaFeO_3$. Or new kinds of p-type semiconductors with much higher photocurrent density need to be explored as photocathodes for water reduction in the future.

# Acknowledgement

Firstly, I want to express my deep and sincere gratitude to my supervisor, Professor Jinhua Ye, who supported my work a lot and encouraged me to understand what is research and how to do research work with a rigorous attitude. Besides, her brilliant management for our research group produces a kind of creative and helpful academic atmosphere, which makes my life here enjoyable and favoring.

I'm also very grateful to Dr. Tetsuya Kako, Prof. Mukai, Dr. Masuda who has taught me a lot for experiments, characterizations, presentations and rigorous attitude of research and inspired me to further improve my work during discussions.

Besides, I would like to give special thanks to Aya-san and Haruna-san, because without their help and arrangement in our labs, we cannot do our experiments joyfully. And they also do a lot for my daily life.

I also want to thank Dr. Naoto Umezawa, Dr. Hideki Abe, Tsubada-san, Aki-san gave me many support during my Ph.D course.

Then I appreciate Dr. Meng Xianguang, Dr. Wang Tao, Dr. Chang Kun, Dr. Liu Lequan, Dr. Ouyang Shuxin, Dr. Kang Qing, Dr. Zhang Huabin, Dr. Liu Huimin, Dr. Zhao Guixia, Mr. Shi Li, Mr. Liu Guigao, Mrs. Jiang Haiying, Mr. Li Mu, Ms. Pang Hong, Mr. Hai Xiao, Mr. Lu Hao, Ms. Yang Liuqing and Ms. Wang Hongmei for the help both in academics and life.

# Acknowledgement

I appreciate the financial support from the Japanese Government (Monbukagakusho: MEXT) Scholarship. I'm really enjoying my work and daily life here and learned a lot from my life in Japan.

At last, I would like to express my regards and blessings to all of my friends, my relatives and the people who supported me during my Ph. D course to have happy life the bright future.

# Academic Activities

## Papers

1. Hematite Homojunctions without Foreign Element Doping for Efficient and Stable Overall Water Splitting, **Q. Yu**, X. Meng, L. Shi, G. Liu, P. Li, J. Ye, RSC Adv. 2016, 6, 62263.
2. Hematite Films Decorated with Nanostructured Ferric Oxyhydroxide as Photoanodes for Efficient and Stable Photoelectrochemical Water Splitting, **Q. Yu**, X. Meng, T. Wang, P. Li, J. Ye, Adv. Funct. Mater. 2015, 25, 2686.
3. A highly durable p-$LaFeO_3$/n-$Fe_2O_3$ photocell for effective water splitting under visible light, **Q. Yu**, X. Meng, T. Wang, P. Li, L. Liu, K. Chang, J. Ye, Chem. Commun. 2015, 51, 3630.
4. Exceptional enhancement of $H_2$ production in alkaline environment over plasmonic Au/$TiO_2$ photocatalyst under visible light, X. Meng, **Q. Yu**, T. Wang, G. Liu, K. Chang, P. Li, APL Mater. 2015, 3, 104401.
5. Modulation of Sulfur Partial Pressure in Sulfurization to Significantly Improve the Photoelectrochemical Performance over the $Cu_2ZnSnS_4$ Photocathode, Y. Zhang, S. Ouyang, **Q. Yu**, P. Li, J. Ye, Chem. Commun. 2015, 51, 14057.
6. Band-Structure-Controlled BiO(ClBr)(1-x)/2Ix Solid Solutions for Visible-Light Photocatalysis, G. Liu, T. Wang, S. Ouyang, L. Liu, H .Jiang, **Q. Yu**, T. Kako, J. Ye, J. Mater. Chem. A 2015, 3, 8123.

7. Photocatalytic $CO_2$ conversion over alkali modified $TiO_2$ without loading noble metal cocatalyst, X. Meng, S. Ouyang, T. Kako, P. Li, **Q. Yu**, T. Wang, J. Ye, Chem. Commun. 2014, 50, 11517.

## Presentations

1. Hematite Films Decorated with Nanostructured Ferric Oxyhydroxide as Photoanodes for Efficient and Stable Photoelectrochemical Water Splitting, **Q. Yu**, X. Meng, T. Wang, P. Li, J. Ye, Mar. 25-28, 2015, Oral presentation, 2015 年日本化学会年会
2. Hematite Films Decorated with Nanostructured Ferric Oxyhydroxide as Photoanodes for Efficient and Stable Photoelectrochemical Water Splitting, **Q. Yu**, X. Meng, T. Wang, P. Li, J. Ye, Dec. 3, 2015, Poster, 2015, 第 22 回シンポジウム「光触媒反応の最近の展開」
3. Hematite Homojunctions without Foreign Element Doping for Efficient and Stable Overall Water Splitting, **Q. Yu**, X. Meng, L. Shi, G. Liu, P. Li, J. Ye, Mar. 24-27, Oral presentation, 2016 年日本化学会年会